CHARACTERIZATION AND OXIDATIVE ADDITION OF DIFFERENT RHODIUM(I) CARBONYL DIPHENYL-2-PYRIDYLPHOSPHINE COMPLEXES

M.P. COETZEE

CHARACTERIZATION AND OXIDATIVE ADDITION OF DIFFERENT RHODIUM(I) CARBONYL DIPHENYL-2-PYRIDYLPHOSPHINE COMPLEXES

A thesis submitted to meet the requirements for the degree of

Magister Scientiae

in the

FACULTY OF NATURAL AND AGRICULTURAL SCIENCES

DEPARTMENT OF CHEMISTRY

at the

UNIVERSITY OF THE FREE STATE

BLOEMFONTEIN

by

MICHAEL PIERRE COETZEE

Promotor

Prof. W. Purcell

Co-promotor

Dr. J.A. Venter

November 2008

Dankbetuigings

Hiermee wil ek my opregte dank en waardering uitspreek teenoor Prof. W. Purcell, my studieleier, vir sy eindelose geduld, opoffering en kundige leiding tydens hierdie studie. Vervolgens wil ek ook my dank en waardering uitspreek teenoor Dr. J.A. Venter, my mede-studieleier, vir sy waardevolle bydrae en leiding wat die studie aansienlik vergemaklik het. Ook ’n blyk van waardering aan Prof. S.S. Basson wat betrokke was aan die begin van my studie.

Dan wil ek ook graag my waardering uitspreek teenoor almal verbonde aan die Chemie Departement vir die ondersteuning wat hulle gegee het op die een of ander manier tydens die verhandeling.

’n Besonderse dank gaan aan my ouers vir hulle motivering, opoffering en aanmoediging gedurende die studie. Ek dra dan ook die verhandeling aan hulle op as ’n geringe blyk van waardering.

Laastens wil ek my Hemelse Vader bedank vir die genade en talente wat ek ontvang het.

Contents

Page

List of Tables

Table **Page**

List of Schemes

Scheme **Page**

List of Figures

Figures **Page**

Figures **Page**

Figures **Page**

List of Abbreviations

Ligands

acac	acetyl acetone/2,4 pentanedione
ba	N-butyl acetate
COD	*cis,cis*-1,5-cyclopentadiene
CN^-	cyanide
cupf	N-phenyl-N-nitrosohydroxylamine, cupferron
Cy	cyclohexyl
CH_3I	methyl iodide[a]
dbm	1,3-diphenyl-1,3-propanedione, dibenzoylmethane
dmavk	2-aminovinyl-4-pentanonato
DMF	N,N-dimethylformamide
DMSO	dimethylsulfoxide
DPP	diphenyl-2-pyridylphosphine
Et	ethyl
hacsm	methyl(2-amino-1-cyclopentene-1-dithiocarboxylato)
hfaa	1,1,1,5,5,5-hexafluoro-2,4-pentane, hexafluoroacetylacetone
hpt	1-hydroxy-2-pyridinethione
LL'-Bid	mono anionic bidentate ligand
L	one of the donor atoms of the bidentate ligand
L'	second donor atom of the bidentate ligand
neocupf	N-naphthyl-N- nitrosohydroxylamine, neocupferron
ox	8-hydroxyquinoline
pic	2-picolinic acid

[a] When CH_3I is between brackets, [CH_3I], it indicates the concentration of methyl iodide. All metal complexes are also given between brackets, for example, [Rh(cupf)(CO)(DPP)].

PPh_3	triphenylphosphine
PX_3	tertiary phosphine with substituents X
sacac	thioacethylacetone
tfaa	1,1,1-trifluoro-2,4-pentadione
tfdmaa	1,1,1-trifluoro-5-methyl-2,4-hexanedione
Tol	tolyl

General

A	absorption
δ	chemical shift in NMR spectra
Dn	solvent donicity
$\Delta G°$	standard free energy
ΔH^*	activation enthalpy
IR	infrared
NMR	nuclear magnetic resonance spectroscopy
ΔS^*	activation entropy
T	temperature in Kelvin
θ	Tolman cone angle of tertiary phospines
UV	ultraviolet
ν_{CO}	infrared carbonyl stretching frequency

Constants

ε	dielectric constant
h	Planck constant
k_b	Boltzman constant

K	equilibrium constant
k	rate constant
k_{obs}	observed rate constant
R	universal gas constant

Key words

Synthesis

Characterization

Oxidative addition

Rhodium

DPP (Diphenyl-2-pyridylphosphine)

cupf (N-Phenyl-N-nitrosohydroxylamine ammonium salt)

acac (2,4-pentadione)

methyl iodide

alkyl

acyl

Summary

The aim of the study was to synthesize different [Rh(LL')(CO)(DPP)] complexes [LL' = cupf (N-phenyl-N-nitrosohydroxylamine ammonium salt, acac (2,4-pentanedione) and DPP (diphenyl-2-pyridylphosphine)] and to characterize the complexes by means of IR, NMR and crystallographic data. A comparison between the IR spectra of the rhodium dicarbonyl complex and that of the substituted carbonyl complex clearly showed the disappearance of one of the carbonyl stretching frequencies, confirming thus the displacement of one of the carbonyl ligands by the phosphine ligand. In both cases the stretching frequency of the mono substituted carbonyl shifted to a lower wavelength. The ^{1}H-NMR results for the mono carbonyl complexes obtained in this study clearly show an down-field shift of new peaks compared to the dicarbonyl complexes and confirm a change in the chemical environment in the metal complex which correlates with the substitution of one of the carbonyl ligands by a phosphine ligand. [Rh(acac)(CO)(DPP)] crystallized into a monoclinic ($P2_1/n$) and triclinic ($P\bar{1}$) space group with final R values of 2.81 and 3.08% respectively. The triclinic space group showed two isomorphic species.

Secondly, the oxidative addition of methyl iodide to [Rh(cupf)(CO)(DPP)] in different solvents and at different temperatures was studied to determine a possible mechanism for this reaction.

[Rh(cupf)(CO)(DPP)] undergoes oxidative addition by methyl iodide, forming a Rh(I)*- intermediate species *via* a very fast equilibrium, followed by the formation of a Rh(III)-alkyl species and finally the formation of a Rh(III)-acyl species as was observed for acetonitrile, acetone and chloroform. Only one reaction was observed for ethyl acetate as solvent with only the formation of the alkyl complex as final product. The results obtained show that the increase in nucleophilicity of rhodium caused by the DPP ligand led to an increase in the rate of formation of the alkyl and acyl in the [Rh(cupf)(CO)(DPP)] complex.

Opsomming

The doel van die ondersoek was om veskillende [Rh(LL')(CO)(DPP)] komplekse [LL' = cupf (N-feniel-N-nitrosohidrosielamien ammoniumsout, asas (2,4-pentaandioon) and DPP (difeniel-2-piridielfosfien)] te sintetiseer en m.b.v infrarooi, KMR and kristallografiese tegnieke te karakteriseer. 'n Vergelyking tussen the infrarooi data van die rhodium dikarbonielkompleks en die gesubstitueerde karbonielkompleks wys duidelik die verdwyning van die een karboniel strekkingsfrekwens wat op die substitusie van een van die karbonielligande deur die fosfienligand dui. In beide gevalle het die strekkingsfrekwens na 'n laer golflengte beweeg. Die ^{1}H-KMR resultate vir die monokarbonielkompleks toon duidelik die verskuiwing van nuwe pieke na 'n laer veld as dit vergelyk word met die dikarbonielkompleks en dui op 'n verandering in die chemiese omgewing van die metaalkompleks wat ooreenstem met die substitusie van een van die karbonielligande deur die fosfienligand. Die [Rh(asas)(CO)(DPP)] kompleks kristalliseer in monokliniese ($P2_1/n$) en trikliniese ($P\bar{1}$) ruimtegroepe met finale R-waardes van 2.81 en 3.08% onderskeidelik. Die trikliniese ruimtegroep toon ook dat daar twee verskillende isomere in die kristal teenwoordig is.

Tweedens is die oksidatiewe addisie van metieljodied aan [Rh(cupf)(CO)(DPP)] in verskillende oplosmiddels en by verskillende temperature ondersoek om 'n moontlike meganisme vir die reaksie voor te stel.

Die [Rh(cupf)(CO)(DPP)] kompleks ondergaan oksidatiewe addisie deur metieljodied met die vorming van 'n Rh(I)* intermediêr, gevolg deur die vorming van 'n Rh(III) alkiel spesie en laastens die vorming van 'n Rh(III) asiel spesie soos waargeneem vir asetonitriel, asetoon en chloroform. Slegs een reaksie is waargeneem met etielasetaat as oplosmiddel en slegs die alkielkompleks is in hierdie oplosmiddel as finale produk gevorm. Die waargenome resultate dui daarop dat die verhoging in nukleofiliteit van rodium a.g.v. die DPP ligand tot 'n versnelling in alkiel- en asielvorming in die [Rh(cupf)(CO)(DPP)] kompleks lei.

Chapter 1

Introduction

Organometallic chemistry, which involves metal complexes containing direct metal-to-carbon bonds, has grown since the early 1950's at an almost exponential rate, mostly owing to the development of an impressive array of highly sophisticated apparatus of which in particular NMR and single-crystal X-ray equipments have been invaluable.[1]

Theoretical studies of the bonding in metal compounds as well as the reaction pathways have not only contributed to new knowledge, but also to the purposeful design of complexes and their use in stoichiometric and catalytic reactions. This theoretical knowledge has increased to a level that a deep insight into the steric and electronic properties of ligands and of their complexes have been gained. This allowed research to design new ligands and react them with the metal centers, which allowed for the chemical control of the reaction rates as well as product selectivity.

The current study was concerned with the preparation and properties of Rh(I) complexes containing a new phosphine ligand in order to determine its influence on oxidative addition reactions. This chapter will deal with some historical aspects of carbonylation reactions as well as recent developments in the carbonylation of methanol and will be followed by an overview of the research that was done by this laboratory on the oxidative addition of Rh(I). Finally, the different aims of this project will be highlighted.

1.1 Historical aspects of carbonylation reactions

Homogeneous carbonylation catalysis is concerned with the transition-metal assisted addition of carbon monoxide to organic compounds and involves a carbon-carbon coupling process to give higher molecular weight carbonyl-containing products.

[1] P. W. N. M. van Leeuwen, K. Morokuma, J. H. van Lenthe, *Theoritical Aspects of Homogeneous Catalysis:* Kluwer Academic Publishers, (1995).

Carbonylation chemistry was pioneered by Otto Roelen (Ruhrcchemie) and Walther Reppe (IG Farben, later BASF) in the late 1930's.[2] Since then it has developed worldwide into the highest volume and most important industrial process based on homogeneous catalysis.

The first thirty years of industrial carbonylation catalysis implied the use of simple metal carbonyl catalysts, high reaction temperatures and pressures, and only low product selectivity. Significant cost advantages resulted from the use of carbon monoxide (derived from natural gas) and of low-priced methanol (from synthesis gas) as feedstocks. A first methanol-to-acetic acid carbonylation process was commercialized in 1960 by BASF. It used an iodide-promoted cobalt catalyst, and required very high pressures (600 atm) as well as high temperatures (230°C), but only yielded acetic acid in *ca.* 90% selectivity.[2]

The situation changed in the mid-sixties with the discovery that organophosphine-substituted rhodium and palladium complexes are active catalysts for carbonylation reactions under milder reaction conditions. The serendipitous discovery of $[Rh(PPh_3)_3Cl]$ by Osborn and Wilkinson,[3, 4] which was used as a catalyst for the hydroformylation of alkenes but also for the hydrogenation of alkenes,[5] has stimulated a tremendous amount of fundamental and applied research in this area.

A major advance came in 1966 with the discovery of rhodium-iodide catalysts for the carbonylation of methanol by Monsanto, which led to the start-up of the first commercial unit in 1970. The advantages over the cobalt-catalyzed BASF process consist in significantly milder conditions (30-60 atm pressure and 150-200°C), allowing substantial savings in construction costs and hence in capital expenditure, as well as

[2] W.A. Herrmann and B. Cornils, *Applied Homogeneous Catalysis with Oraganometallic Compounds*, VCH Weinheim, (1999).

[3] J. F. Young, J. A. Osborn, F. H. Jardine and G. Wilkinson, *Chem. Comm.*, (1965), 131.

[4] J. A. Osborn, F. H. Jardine, J. F. Young and G. Wilkinson, *J. Chem. Soc. A.*, (1966), 1711.

[5] R. S. Dickson, *Organometallic Chemistry of Rhodium and Iridium*; Academic Press, London, (1983), p. 277.

obtaining higher selectivity for acetic acid, making further savings on both running and capital costs. The disadvantage of using rhodium, a costly precious metal is counter-balanced by lower operating costs, especially as milder reaction conditions decrease the corrosion risk due to the aggressive reaction medium (acetic acid, iodic acid).[6]

$$CH_3OH + CO \xrightarrow{[Rh(CO)_2I_2]^-} CH_3COOH$$

In 1986, the ownership of the Monsanto technology was acquired by BP Chemicals who further developed the process and licensed it around the world. In 1996, a new catalytic process for the carbonylation of methanol to acetic acid, named Cativa, was announced by BP Chemicals. This process is based on a catalyst system composed of iridium complexes with ruthenium activators.

1.2 Electronic influence

Over the past few decades our group has been interested in the manipulation of the reactivity of the Rh(I) center in [Rh(BID)(CO)(PX_3)] complexes towards iodomethane oxidative addition (BID = monoanionic bidentate ligands containing different donor atoms such as O, N and S, and PX_3 = tertiary phosphine or phosphite). The utilization of the aforementioned model complexes may give insight into mechanistic aspects of homogeneous catalysis, such as the well known Monsanto process, where the oxidative addition was identified as the rate determining step in the methanol carbonylation cycle.

Square planar Rh(I) complexes, being coordinatively unsaturated, undergo oxidative addition reactions with various organic and inorganic molecules. Research have shown that oxidative addition reactions can proceed *via* different reaction pathways and since

[6] K. Kobayashi, *Chem. Econ. Eng. Rev.*, **16,** (1984), 32.

the addition can either be *cis* or *trans*, it is imperative to know the molecular structures of the reactants and products, as well as the nature of intermediates, in order to propose suitable reaction mechanisms. The importance for these investigations has been the desire to gain a greater understanding of the electronic and steric factors influencing the oxidative addition reactions, which are vital steps in the functioning of many of these compounds in homogeneous catalysis.[7, 8] Based on kinetic studies,[9, 10, 11, 12] the proposed mechanism of the oxidative addition of CH_3I to Rh(I) carbonyl phosphine complexes is a nucleophilic attack by the rhodium atom on the carbon atom of the methyl iodide where a linear polar transition state is formed which leads to *trans* addition.

Results obtained from these studies of this laboratory indicated that the electronic properties, and therefore the reactivity of the square planar complex can be controlled, not only by the donor atoms of the bidentate ligands bonded to the metal center, but also by the different groups bonded to these ligands. It was found that the order of reactivity of the different donor atoms are N,S > S,O > O,O while it was found that electron withdrawing groups bonded to the bidentate ligand also decreases the rate of oxidative addition reaction with acac > ba > dbm > tfaa > hfaa (where acac = acetylacetone, ba = n-buthyl acetate, dbm = dibenzoylmethane, tfaa = 1,1,1-trifluoro-2,4-pentadione, hfaa = hexafluoroacetylacetone). In addition to these results it was found that the reactivity of the oxidative addition reaction is also influenced by the groups bonded to the phosphine ligands, or in some cases also to the donicity of the solvent.

Any change in the metal complex that leads to an increase in the electron density around the central metal atom and thus to an increase in the nucleophility of the metal atom, will lead to an increase in reactivity. The kinetics of oxidative addition is thus a function of

7 D. Foster, *Adv Organomet Chem*., **17**, (1979), 255.

8 D. Foster and T.D. Singleton, *J Mol Catal*., **17**, (1982), 299.

9 G.J. Lamprecht and J.H. Beetge, *S Afr J Chem*., **40**, (1987), 131.

10 G.J. van Zyl, G.J. Lamprecht and J.G. Leipoldt, *Inorg Chim Acta*, **122**, (1986), 75.

11 J.G. Leipoldt, S.S. Basson and L.J. Botha, *Inorg Chim Acta*, **168**, (1990), 215.

12 J.A. Venter, J.G. Leipoldt and R. van Eldik, *Inorg Chem*., **30**, (1991), 2207.

the σ- and π-bonding capability of the ligands. Ligands with good σ-bonding capability will increase the electron density of the metal center and increase the rate of oxidative addition. Ligands with strong π-acceptor capability will decrease the density and will lead to a slower reaction. Previous studies that contained bidentate donor atoms (L,L'-Bid) showed that both *cis*- and *trans*-addition may occur at the rhodium center. Studies regarding phosphine ligands however, confirmed a mechanism that consist of a rapid oxidative addition step followed by the slower acyl formation, with a negligible solvent pathway for the first step.

1.3 Steric influence

The steric influence of the phosphine ligand on oxidative addition reactions was also studied in detail. The Tolman cone angle was used as an indication of the steric influence of the different phosphine ligands and a decrease in oxidative addition rate was observed for phoshine ligands with large cone angles. These results can be contributed by the steric hindrance and groups bonded to the phosphine ligand that leads to an increase or decrease in Rh-P bond distance.

Phosphorus ligands associated with bulky groups leads to the formation of a Rh(I)-carbonyl complex that decreases slowly with a simultaneous increase in the formation of a Rh(III)-alkyl complex. In contrast to the relative fast oxidative addition step, the migratory insertion step that leads to the formation of the Rh(III)-acyl species, is much slower.

1.4 Aims of this work

In the light of the previous discussion, the following goals were set for this investigation.

The ligand used during the study was diphenyl-2-pyridylphosphine. Diphenyl-2-pyridylphosphine (DPP) has been used in other studies as a multidentate ligand to coordinate transition metals. The labile nitrogen-metal bond of the pyridyl-coordinated

metal center is a useful property in various catalytic reactions involving diphenyl-2-pyridylphosphine as mono- or bidentate ligand.

- To synthesize different [Rh(LL')(CO)(DPP)] complexes (LL' = cupf (N-phenyl-N-nitrosohydroxylamine ammonium salt, acac (2,4-pentanedione) and DPP (diphenyl-2-pyridylphosphine) and to characterize the complexes by means of IR, NMR and crystallographic data.
- To study the oxidative addition of iodomethane to the complexes in different solvents and at different temperatures to determine a possible mechanism for these reactions.

Chapter 2

The catalytic carbonylation of methanol

Carbonylation catalysis encompasses a large and important area of organometallic chemistry. Homogeneous carbonylation reactions form the majority of these catalytic processes due to their higher reaction rates and selectivity compared to heterogeneous systems. Important catalytic carbonylation reactions include the hydroformylation of olefins to give aldehydes and alcohols, which is the most important homogeneous catalytic process industry,[1] the synthesis of ketones from olefins and the synthesis of lactones and lactams from olefins or halide-containing alcohols.[2] The production of carboxylic acids, carboxylic esters and acyl halides from methanol is the second most important industrial homogeneous catalytic process.[3, 4]

2.1 Transition metal catalyzed carbonylation of methanol

Acetic acid is an important industrial commodity chemical with a number of different applications. The world demand for this versatile compound is about 6 million tons per year. Since the 1950's novel production processes and different catalysts have been introduced and improved methods were commercialized. The objective of the development of new acetic acid processes has been to reduce raw material consumption, energy requirements, and investment costs.

[1] W. A. Herrmann and B. Cornils, *Applied Homogeneous Catalysis with Organometallic Compound*s, VCH Weinheim, (1999).

[2] G. W. Parshall and S. D. Ittel, *Homogeneous Catalysis*, 2nd Edition, Wiley-Interscience, New York, (1992), p. 96.

[3] K. Weissermel and H. J. Arpe, *Industrial Organic Chemistry*, 3rd Edition, VCH, Weinheim, (1997).

[4] H. M. Colquhoun, D. J. Thompson and M. V. Twigg, *Carbonylation: Direct Synthesis of Carbonyl Compounds*, Plenum Press, New York, (1991).

At present, industrial processes for the production of acetic acid are dominated by methanol carbonylation. Approximately 60 per cent of the total world acetic acid manufacturing capacity is accounted for by the carbonylation of methanol. From an industrial point of view this production method is one of the major achievements of applied homogeneous catalysis. These methanol-to-acetic-acid processes *via* the carbonylation of methanol are not only highly selective, but also allow the use of methanol as a cheaper feedstock as compared to ethylene. Results have shown that the carbonylation of methanol is mainly catalysed by Group VIII transition metal complexes, especially by rhodium, iridium, cobalt, and nickel.[5, 6, 7, 8, 9] All known methanol carbonylation processes need iodine compounds as essential co-catalysts since the reaction proceeds *via* the methyl iodide pathway as it alkylates the transition metal involved. Apart from acetic acid, the carbonylation of methanol (**Reaction 2.1**) also gives, according to **Reaction 2.2**, rise to the formation of methyl acetate, which is also used as a solvent in the Cativa processes.

$$CH_3OH + CO \longrightarrow CH_3COOH \qquad \textbf{2.1}$$

$$CH_3COOH + CH_3OH \longrightarrow CH_3COOCH_3 + H_2O \qquad \textbf{2.2}$$

The cobalt-catalyzed BASF process was introduced in the late 1950s while the rhodium-based Monsanto process followed in the early seventies. It was found that the rhodium catalysts operated at milder conditions and with increased selectivity, compared to cobalt

[5] A. Mullen, N*ew Syntheses with Carbon Monoxide*; Springer Verlag, Berlin, (1980), p.243.

[6] J. Falbe, *Synthesen mit Kohlenmonoxid*; Springer Verlag, Berlin, (1977).

[7] J. Falbe, *Methodicum Chimicum*, Georg Thieme Verlag, Stuttgart, **5**, (1975).

[8] N. V. Kutepow and W. Himmele, *Ullmanns Encyclopädie der technischen Chemie*, 4th edition, Verlag Chemie, Weinheim, **9**, (1975), p. 155.

[9] D. Forster, *Adv. Organometal. Chem*., 17, (1979), 255.

or nickel catalysts. It is therefore not surprising that most commercial plants now use the rhodium-based Monsanto process.

2.1.1 The rhodium-based Monsanto catalyst

The production of acetic acid by the Monsanto process is based on a rhodium catalyst and operates at a pressure of 30 to 60 bar and at temperatures of 150 to 200ºC. The process gives selectivity of over 99 per cent based on methanol. The catalytic cycle of this classic example of a homogeneous catalytic reaction consists of six steps (**Scheme 2.1**).[10] The cycle includes several of the main reaction types known in organometallic chemistry,[11] such as oxidative addition, ligand migration, CO insertion, and reductive elimination. These types of elementary steps have been examined separately in a number of experimental and theoretical studies.[12, 13, 14, 15] Systematic studies including a detailed inspection of full catalytic cycles are much rarer.[16, 17, 18] The proposal of the different steps in the catalytic cycle of methanol carbonylation[10] was based upon results obtained from characterization of reactants, intermediates and products by X-ray crystallography,[9] infrared and NMR spectroscopy (**Scheme 2.1**).[19]

[10] D. Forster, *J. Am. Chem. Soc.*, **98**, (1976), 846.

[11] B. C. Gates, *Catalytic Chemistr*y; Wiley: New York, (1992).

[12] N. Koga and K. Morokuma, *J. Am. Chem. Soc.*, **115**, (1993), 6883.

[13] S. Sakaki, Y. Ujino and M. Sugimoto, *Bull. Chem. Soc. Jpn.*, **69**, (1996), 3047.

[14] S. Sakaki and M. Ieki, *J. Am. Chem. Soc*.,**115**, (1993), 2373.

[15] K. Albert, P. Gisdakis and N. Rösch, *Organometallics*, **17**, (1998), 1608.

[16] T. Matsubara, N. Koga, Y. Ding, D. G. Musaev and K. Morokuma, *Organometallics*, **16**, (1997), 1065.

[17] A. Dedieu, *Inorg. Chem.*, **19**, (1980), 375.

[18] P. Margl, T. Ziegler and P. E. Blöchl, *J. Am. Chem. Soc.*, **118**, (1996), 5412.

[19] A. Haynes, B. E. Mann, G. E. Morris and P. M. Maitlis, *J. Am. Chem. Soc.*, **115**, (1993), 4093.

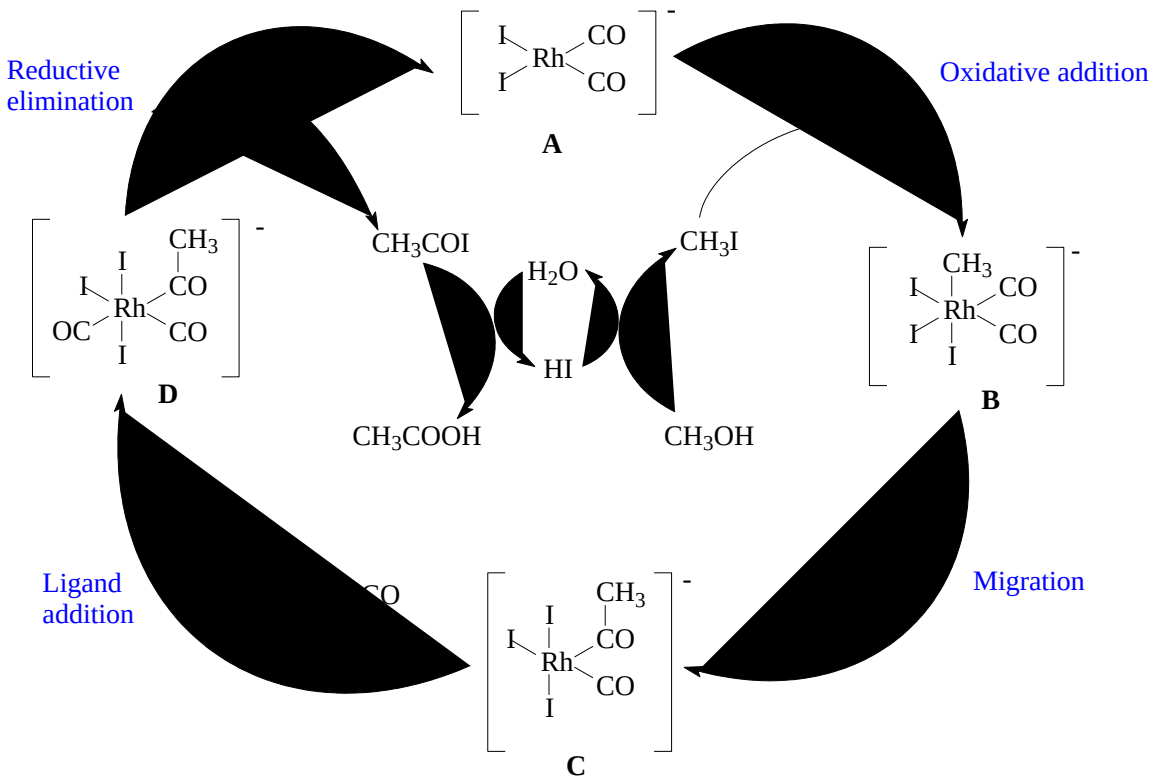

Scheme 2.1: Catalytic cycle of the rhodium-catalyzed methanol carbonylation (Monsanto process) [24]

The *cis*-$[Rh(CO)_2I_2]^-$ (**A**) anion was found to be the initial catalytically active species.[10] The interaction of this rhodium complex with the CH_3I substrate results in the formation of the hexa-coordinated $[(CH_3)Rh(CO)_2I_3]^-$ complex (**B**).[19] Results have shown that the complex is kinetically unstable and transforms into the isomeric penta-coordinated acetyl complex $[(CH_3CO)Rh(CO)I_3]^-$ (**C**) as a result of the migration of the methyl group to the CO ligand.[20] The rhodium acetyl anion **C** was found to form dimers through a very weak Rh-I-Rh bridge (with a rhodium-iodine distance of 3.0 Å, as compared to 2.7 Å commonly found for Rh-I bonds).[21] Complex **C** reacts rapidly with CO to form the six-

[20] M. Bassetti, D. Monti, A. Haynes, J. M. Pearson, I. A. Stanbridge and P. M. Maitlis, *Gaz. Chim. Ital.*, **122**, (1992), 391.

[21] H. Adams, N. A. Bailey, B. E. Mann, C. P. Manuel, C. M. Spencer and A. G. Kent, *J. Chem. Soc., Dalton Trans.*, (1988), 489.

coordinated dicarbonyl complex **D** with terminal CO.[21] This species has been characterized by IR and NMR spectroscopy as a *mer* isomer.[22]

Isomerization to a *fac* isomer was proposed to facilitate the subsequent elimination of CH_3COI.[22] The *fac* isomer decomposes at room temperature to yield acetyl iodide, CH_3COI, and $[Rh(CO)_2I_2]^-$. The latter species starts the next catalytic cycle. Finally, acetic acid is formed by acetyl iodide hydrolysis.

2.1.2 Mechanistic studies of the rhodium-catalyzed process

Different kinetic investigations have confirmed the possible steps in the catalytic cycle depicted in **Scheme 2.1**. These studies have indicated that the rate of methanol carbonylation depends on the concentrations of both the rhodium complex and methyl iodide.[22] These results also indicated that the reaction rate is independent of the methanol concentration and the carbon monoxide pressure, while the rate-determining step is the oxidative addition of methyl iodide to the rhodium center in complex **A.** These deductions were made since the reaction rate was essentially first order in both catalyst and methyl iodide concentrations under normal reaction conditions.

These results also indicated that a substantial amount of water (14 - 15 wt.%) is required to achieve high catalyst activity and also to maintain good catalyst stability.[16, 17, 18, 19] In fact, if the water content is less than 14-15 wt.%, the rate-determining step becomes the reductive elimination of the acetyl species (complex **D)**. However, as rhodium also catalyzes the water-gas shift reaction (**Scheme 2.2**), the side reaction leading to CO_2 and H_2 is significantly affected by water and hydrogen iodide concentration in the reaction mixture.[23, 24]

[22] L. A. Howe and E. E. Bunel, *Polyhedron*, 14, (1995), 167.

[23] D. Forster and T. W. Dekleva, *J. Chem. Edu.*, 63, (1986), 204.

[24] D.J. Watson, *Catalysis of Organic reactions*, Marcel Dekker, New York, (1998), p. 369.

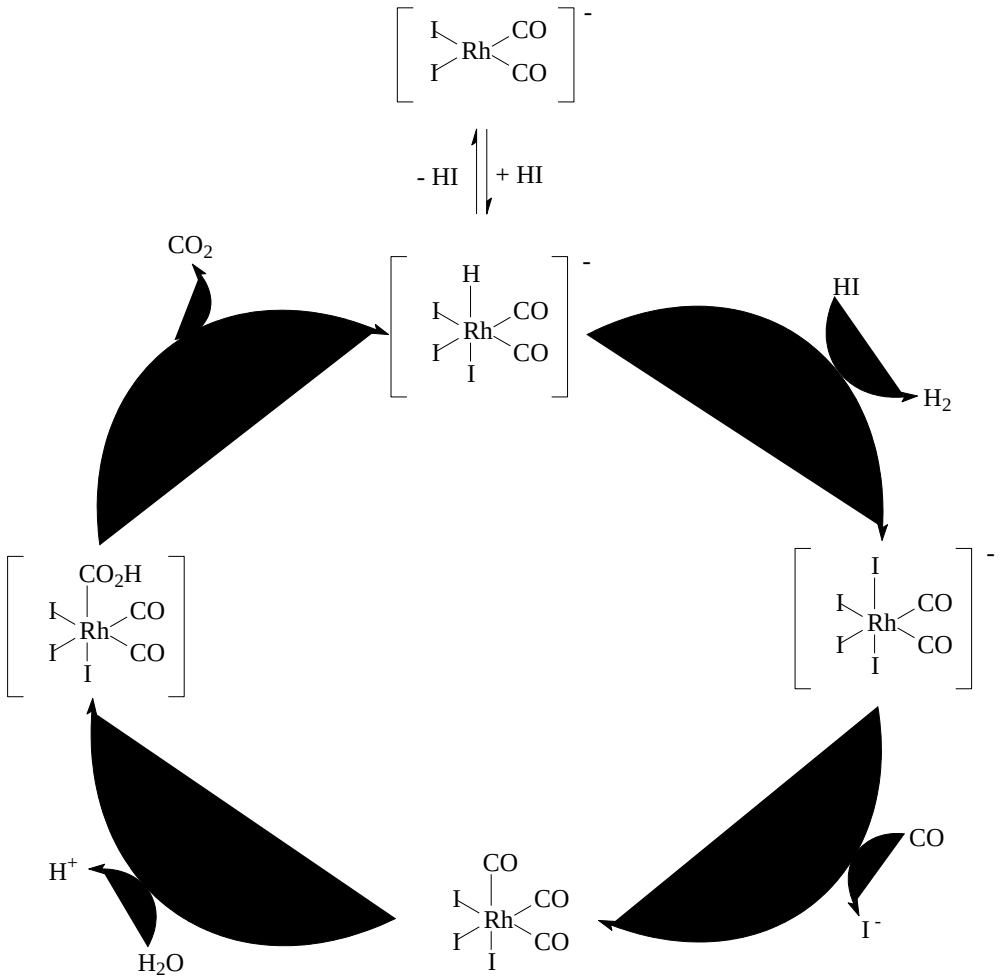

Scheme 2.2: Catalytic cycle of the water-gas shift reaction as side-reaction in the rhodium-catalyzed methanol carbonylation [24]

Another interesting result obtained from these studies indicates that propionic acid is obtained as the major liquid by-product in this process. It is produced by the carbonylation of ethanol which is often present as a minor impurity in the methanol feed. However, alternative routes to propionic acid must also be operating in this system since more propionic acid is observed than what can be accounted for by ethanol contamination of the feedstock. A possible reaction pathway is that the rhodium catalyst can also generate acetaldehyde, which is supposed to undergo reduction by hydrogen to give ethanol, which subsequently yields propionic acid.

One possible precursor for the generation of acetaldehyde is the rhodium-acetyl species, **D**, shown in **Scheme 2.1**[24] which can react with hydrogen iodide to yield acetaldehyde and $[Rh(CO)I_4]^-$. The latter species is well known in this system and is postulated as the principal cause of catalyst loss by precipitation of inactive rhodium triiodide.[24] However, under the commercial operating conditions of the original Monsanto process, these trace compounds did not present a problem to either product yield or product purity.

2.1.3 The Cativa iridium catalyst for methanol carbonylation

The potential use of iridium instead of rhodium was identified in earlier work done by Monsanto.[9] Results at that stage indicated that the reaction rates exhibited by the rhodium catalyst were superior to that of iridium system. Recently, it was disclosed that an improved iridium catalyst, in combination with a promotor metal such as ruthenium, had higher activity and selectivity than reported in previous iridium systems.[25] The production of acetic acid using the iridium catalyst system has been commercialized in 1996 by BP-Amoco in two large-scale plants and has received wide publicity as the "Cativa" process. Although much more iridium is required to achieve an activity comparable to the rhodium catalyst-based processes, the catalyst system is able to operate for example at reduced water levels (less than 8 wt.% for the Cativa process versus 14-15 wt.% for the conventional Monsanto process). Added to the lower by-product formation improved carbon monoxide efficiency was achieved. Until the early 1990's another driving force for the use of iridium was the price difference between rhodium (17 $/g) and iridium (2 $/g), but since early 1996 this difference decreased, minimizing the advantage in catalyst price.

One of the major advantages of the iridium-based process was the high stability of the iridium catalyst species.[26] Its robustness at low water concentrations (0.5 wt.%) was particularly significant and ideal for optimization of the methanol carbonylation process.

[25] *Japanese Patent Koukai* to Poulenc, (1994), 06-340573.

[26] C. J. E. Vercauteren, K. E. Clode and D. J. Watson, *European Patent*, (1994), 616,997.

The iridium catalyst was also found to remain stable under a wide range of conditions that would cause the rhodium analogues to decompose completely too inactive and largely unrecoverable rhodium salts. Besides this stability, iridium is also much more soluble than rhodium in the reaction medium, which meant that higher catalyst concentrations can be obtained and thereby increasing reaction rates.

Fundamental research was used to determine the unique differences between the rhodium and iridium catalytic cycles in methanol carbonylation.[27] The anionic iridium cycle, shown in **Scheme 2.3**, is similar to the rhodium cycle, but contains several differences which may be responsible for the advantages of the Cativa over the Monsanto process. Kinetic studies have shown that the slowest step in the iridium cycle is not the oxidation addition, but the subsequent migratory insertion of CO to form the iridium-acyl species, **G**, which involves the elimination of ionic iodide and the coordination of an additional CO ligand. The studies have also shown that the reaction inversely depend upon the concentration of ionic iodide, which implies that very higher reaction rates should be achievable by operating at low iodide concentrations. Results suggest that the inclusion of species capable of assisting in removing iodide should promote the rate-limiting step. Promotors for this system fall within two distinct groups: simple iodide complexes of zinc, cadmium, mercury, gallium and indium,[28] and carbonyl-iodo complexes of tungsten, rhenium, ruthenium and osmium.[29, 30]

[27] P. M. Maitlis, A. Haynes, G. J. Sunley and M. J. Howard, *J. Chem. Soc., Dalton Trans.*, (1996), 2187.

[28] M. J. Baker, M. F. Giles, C. S. Garland and G. Rafeletos, *European Patent*, (1995), 749,948.

[29] J. G. Sunley, M. F. Giles and C. S. Garland, *European Patent*, (1994), 643,034.

[30] C. S. Garland, M. F. Giles, A. D. Poole and J. G. Sunley, *European Patent*, (1994), 728,726.

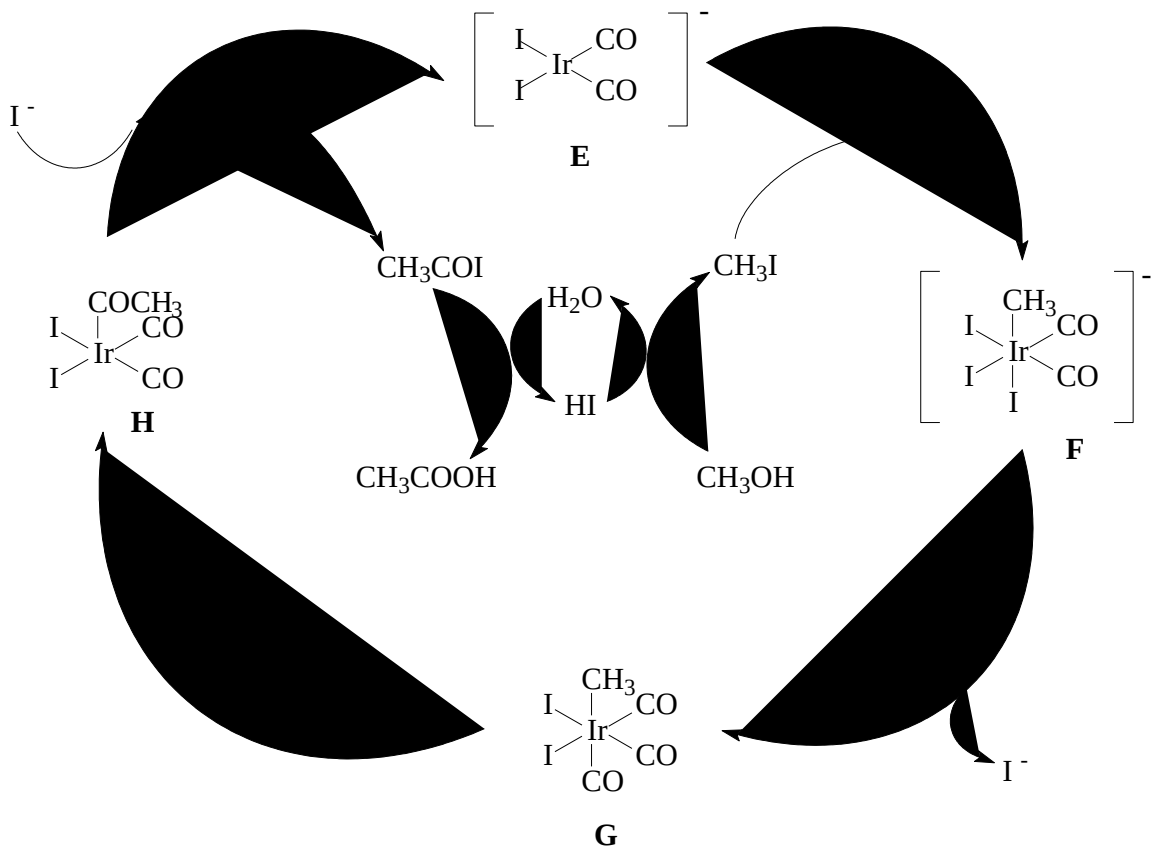

Scheme 2.3: Catalytic cycle of the iridium-catalyzed methanol carbonylation (Cativa process) [27]

2.1.4 Mechanistic studies of the iridium-catalyzed process

Research has shown that the kinetics of the Cativa process is in accordance with the mechanism shown in **Scheme 2.3**. A combination of promoters may also be used. None of these metals are effective as carbonylation catalysts in their own right, but all are effective when used in conjunction with an iridium complex. The presence of a promoter leads to a substantial increase in the proportion of the "active anionic" species $[(CH_3)Ir(CO)_2I_3]^-$, **F**, and a substantial decrease in the loss of iridium by the formation of inactive $[Ir(CO)_3I_3]$ and $[Ir(CO)_2I_4]^-$ species, which are intermediates in the water-gas shift reaction (**Reaction 2.3** and **2.4**).

A proposed mechanism for the promotion of iridium catalysis by a metal promoter $M(CO)_xI_y$, is given in **Scheme 2.4** (where M = Transition metals like Co and Ni).

$$[Ir(CO)_2I_2] + 2HI \longrightarrow [Ir(CO)_2I_4] + H_2 \quad \textbf{2.3}$$

$$[Ir(CO)_2I_4] + CO \longrightarrow [Ir(CO)_3I_3]^+ + I^- \quad \textbf{2.4}$$

The promotion is thought to occur *via* direct interaction of promoter and iridium species as shown. The rate of reaction is dependent upon the loss of iodide from $[(CH_3)Ir(CO)_2I_4]^-$. These metal promoters are believed to reduce the standing concentration of I^-, thus facilitating the loss of iodide from the catalytic species. It is also postulated that carbonyl-based promoters may then go on to donate CO in further steps of the catalytic cycle.

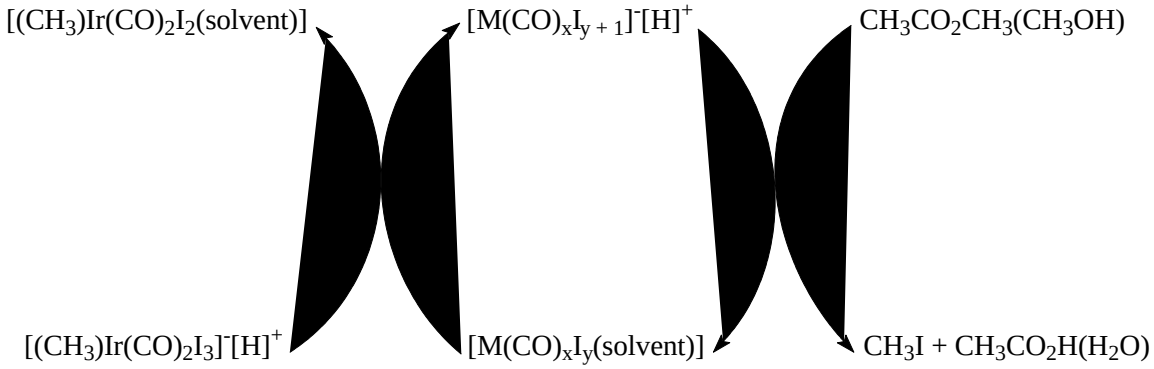

Scheme 2.4: Implication of metal promoters such as $[Ru(CO)_4I_2]$ in the iridium-catalyzed methanol carbonylation (Cativa process) [27]

2.2 Ligand-accelerated catalysis

The migratory insertion reaction of CO into metal-alkyl bonds is a fundamental step in the metal-iodide catalyzed carbonylation of methanol to acetic acid (and also in hydroformylation reactions).[31] The original $[Rh(CO)_2I_2]^-$ catalyst, developed at the Monsanto laboratories[9, 32] and studied in detail by Forster and co-workers,[9, 10] is largely used for the industrial production of acetic acid and anhydride. However, the conditions used industrially (30-60 bar and 150-200°C)[30] have spurred the search for new catalysts, which could operate under milder conditions.[19, 27, 33, 34, 35, 36, 37, 38, 39, 40] The rate-determining step of the rhodium-based catalytic cycle is the oxidative addition of CH_3I, causing catalyst design to be focused on the improvement of this reaction.

The basic idea was that ligands which increase the electron density at the metal should promote oxidative addition, and consequently increase the overall rate of the reaction. For this purpose, other rhodium complexes have been synthesized lately, and they have been shown to be active catalysts of comparable or better performance compared to the Monsanto catalyst.[33, 37, 41, 42]

---

[31] J. P. Collman, L. S. Hegedus, J. R. Norton and R. G. Finke, *Principles and Applications of Organotransition Metal Chemistry*, University Science Books: Mill Valley, CA, (1987).

[32] K. K. Robinson, A. Hershman, J. H. Craddock and J. F. Roth, *J. Mol. Catal.*, **27**, (1972), 389.

[33] J. R. Dilworth, J. R. Miller, N. Wheatley, M. J. Baker and J. G. Sunley, *J. Chem. Soc., Chem. Commun.*, (1995), 1579.

[34] T. Ghaffar, H. Adams, P. M. Maitlis, A. Haynes, G. J. Sunley and M. J. Baker, *Chem. Commun.*, (1998), 1359.

[35] R. W. Wegman, A. G. Abatjoglou and A. M. Harrison, *J. Chem. Soc., Chem.Commun.*, (1987), 1891.

[36] K. G. Moloy and R. W. Wegman, *Organometallics*, **8**, (1989), 2883.

[37] J. Rankin, A. D. Poole, A. C. Benyei and D. J. Cole-Hamilton, *Chem. Commun.*, (1997), 1835.

[38] J. Rankin, A. C. Benyei, A. D. Poole and D. J. Cole-Hamilton, *J. Chem. Soc., Dalton Trans.*, (1999), 3771.

[39] J. Yang, A. Haynes and P. M. Maitlis, *Chem. Commun.*, (1999), 179.

[40] L. Gonsalvi, H. Adams, G. J. Sunley, E. Ditzel and A. Haynes, *J. Am. Chem. Soc.*, **121**, (1999), 11233.

[41] K. V. Katti, B. D. Santarsiero, A. A. Pinkerton and R. G. Cavell, *Inorg. Chem.*, **32**, (1993), 5919.

The most important class of these rhodium complexes are those containing simple phosphine ligands such as PEt_3,[38] or diphosphine ligands of the type PPh_2-CH_2-CH_2-PPh_2.[36]

Cole-Hamilton *et al*. have investigated the use of trialkylphosphines as promoters for rhodium-based carbonylation catalysts, because they are strongly electron-donating and thus increase the electron density on the metal center. Complexes of the type $[Rh(PEt_3)_2(CO)X]$ (X = Cl^-, Br^- or I^-) have a ν(CO) absorption centered around 1960 cm^{-1}, as compared to 1988 and 2059 cm^{-1} for $[Rh(CO)_2I_2]^-$, suggesting that the rhodium center is more electron-rich in the triethylphosphine complexes. $[Rh(PEt_3)_2(CO)Cl]$ turned out to be a very active catalyst precursor for acetic acid production.

It was found that in the presence of 17.1 wt.% H_2O at 120 to 150 °C and 27 bar pressure, $[Rh(PEt_3)_2(CO)I]$ catalyses the carbonylation of methanol at a rate nearly twice as high as that of $[Rh(CO)_2I_2]^-$. Thus, the water acts to maintain the catalyst in its active form [as a rhodium(I) complex] and decreases the formation of inactive rhodium(III) complexes such as $[Rh(CO)_2I_4]^-$ or $[Rh(PEt_3)_2(CO)I_3]$.

The addition of methyl iodide to $[Rh(PEt_3)_2(CO)I]$ in CH_2Cl_2 was shown to result in the formation of $[(CH_3)Rh(PEt_3)_2(CO)I_2]$ (**Scheme 2.5**).[37] The methyl group coordinated *cis* with respect to the carbonyl ligand, as required for migratory insertion. There are no X-ray crystal structure analyses for complexes of the type $[(CH_3)Rh(PR_3)_2(CO)X_2]$, however other six-coordinate rhodium(III) complexes resulting from oxidative addition of CH_3I, most of them with iodide and methyl ligands in mutually *trans* positions, were

[42] M. J. Baker, M. F. Giles, A. G. Orpen, M. J. Taylor and R. J. Watt, *J. Chem. Soc., Chem. Commun.*, (1995), 197.

isolated and structurally characterised.[41, 42, 43] The isolation of the methyl complex from a catalytically active system is rather unlikely, since the insertion of carbon monoxide into the Rh-C bond is thought to be extremely rapid. For $[Rh(CO)_2I_2]^-$ the methyl complex has a very short lifetime and was only detected as a intermediate by IR spectroscopy in neat methyl iodide,[19] while for the related $[Rh(PPh_3)_2(CO)Cl]$ complex the oxidative addition of methyl iodide gives the six-coordinate complex $[(CH_3)Rh(PPh_3)_2(CO)(Cl)I]$ in equilibrium with the five-coordinate insertion product, $[(CH_3CO)Rh(PPh_3)_2(Cl)I]$.[43] In the case of the triethylphosphine analogue, the higher electron density on the metal is responsible for the less facile methyl migration in $[(CH_3)Rh(PEt_3)_2(CO)I_2]$. Despite the stability of the methylrhodium(III) complex, preliminary kinetic studies suggested that oxidative addition of CH_3I was still rate-determining.

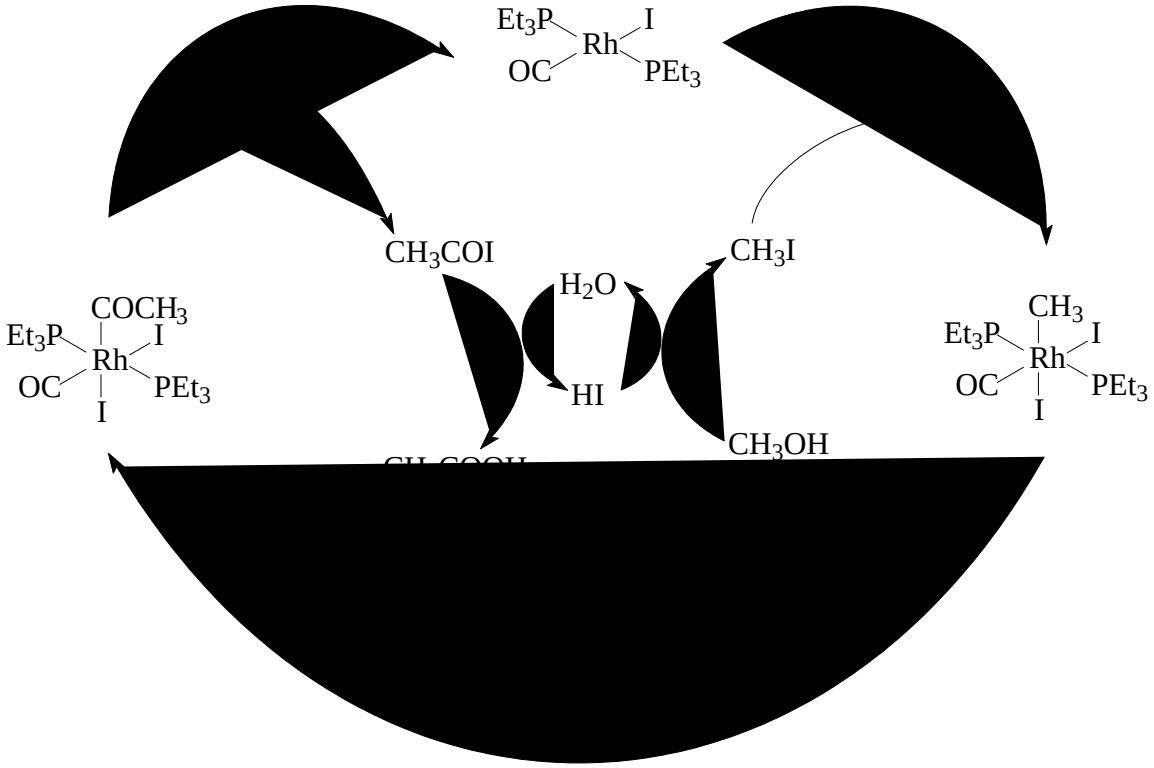

Scheme 2.5: Catalytic cycle of methanol carbonylation catalyzed by the neutral complex $Rh(PEt_3)_2(CO)I$[37]

[43] T. G. Schenck, C. R. C. Milne, J. F. Sawyer and B. Bosnich, *Inorg. Chem.*, **24**, (1985), 2338.

Mixed bidentate ligands such as PPh_2-CH_2-$P(O)Ph_2$,[35] PPh_2-CH_2-$P(NPh)Ph_2$[41] and PPh_2-CH_2-$P(S)Ph_2$[42] have been shown to be effective in rhodium-catalyzed carbonylation of methanol. Wegman *et al.*[35] have found that *cis*-[Rh{$Ph_2P(CH_2)_2P(O)Ph_2$}(CO)Cl] is a precursor to a very active catalyst for the carbonylation of methanol under mild reaction conditions.[35] The reaction of *cis*-[Rh{$Ph_2P(CH_2)_2P(O)Ph_2$}(CO)Cl] with CO resulted in the displacement of the rhodium-oxygen bond and the formation of a new species according to the equilibrium shown in **Scheme 2.6**.

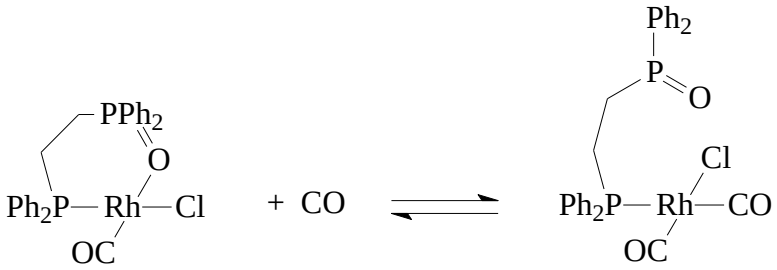

Scheme 2.6: Equilibrium between [Rh{η^2-$Ph_2P(CH_2)_2P(O)Ph_2$}(CO)Cl] and [Rh{η^1-$Ph_2P(CH_2)_2P(O)Ph_2$}$(CO)_2$Cl] [35]

Results obtained by infrared spectroscopy from this study indicated that the ratio of the η^2- and the η^1-complexes was approximately 1 : 1 (at 22°C and 1 bar CO). Infrared spectroscopic studies carried out under catalytic conditions at 80 °C and 3.5 bar CO (turnover frequency 400 h^{-1}) reveal only the η^1-coordinated phosphine oxide species. There is also no indication of $[Rh(CO)_2I_2]^-$, which is the principal rhodium species present during catalysis with the Rh-I catalyst.[10] In addition, there is no induction period as might be expected if dissociation of $Ph_2P(CH_2)_2P(O)Ph_2$ and subsequent formation of $[Rh(CO)_2I_2]^-$ is important.[9]

Baker *et al.*[42] have found that the use of the diphosphinesulfide $Ph_2PCH_2P(S)Ph_2$ as a bidentate phosphine ligand for the rhodium catalysed carbonylation of methanol allows a substantial rate increase under industrially feasible conditions (180°C, 70 bar CO).[42]

The initial experiments were carried out using a ligand/rhodium ratio of 4 : 1, but the optimum rate enhancement was observed when the discrete *cis*-[Rh{η^2-$Ph_2PCH_2P(S)Ph_2$}(CO)Cl] complex was used as pre-catalyst. These authors showed that any additional phosphine quaternizes with CH_3I, and that the addition of iodide also inhibits the catalytic reaction (**Scheme 2.7**). Addition of three equivalents of $[(CH_3)PPh_3]I$ causes a similar retardation in rate. [Rh{$Ph_2PCH_2P(S)Ph_2$}(CO)Cl] is readily formed upon mixing $[Rh(CO)_2Cl]_2$ with two equivalents of $Ph_2PCH_2P(S)Ph_2$ in CH_3OH, and there is no evidence for the formation of dinuclear complexes in this reaction.[44]

The X-ray crystal structure analysis of [Rh{$Ph_2PCH_2P(S)Ph_2$}(CO)Cl] confirmed the stereochemistry at rhodium, in which the phosphorus atom is *trans* with respect to the chloro ligand, while the sulfur atom is *trans* with respect to the carbonyl ligand. The structure also showed no unusual features to explain the unexpected stability of the catalyst at high temperatures in the case for [Rh{$Ph_2PCH_2P(S)Ph_2$}(CO)Cl]. There is no evidence for a hemilabile behavior of the P-S ligand for [Rh{$Ph_2PCH_2P(S)Ph_2$}(CO)Cl], while it has been assumed to be important for catalysis employing mixed-donor ligands.[45] These results showed for the first time that a discrete rhodium-phosphine complex can give a significant improvement in carbonylation activity over $[Rh(CO)_2I_2]^-$ under industrial conditions.

[44] T. C. Blagborough, R. Davis and I. Ivison, *J. Organomet. Chem.*, **467**, (1994), 85.

[45] A. Bader and E. Lindner, *Coord. Chem. Rev.*, **108**, (1991), 27.

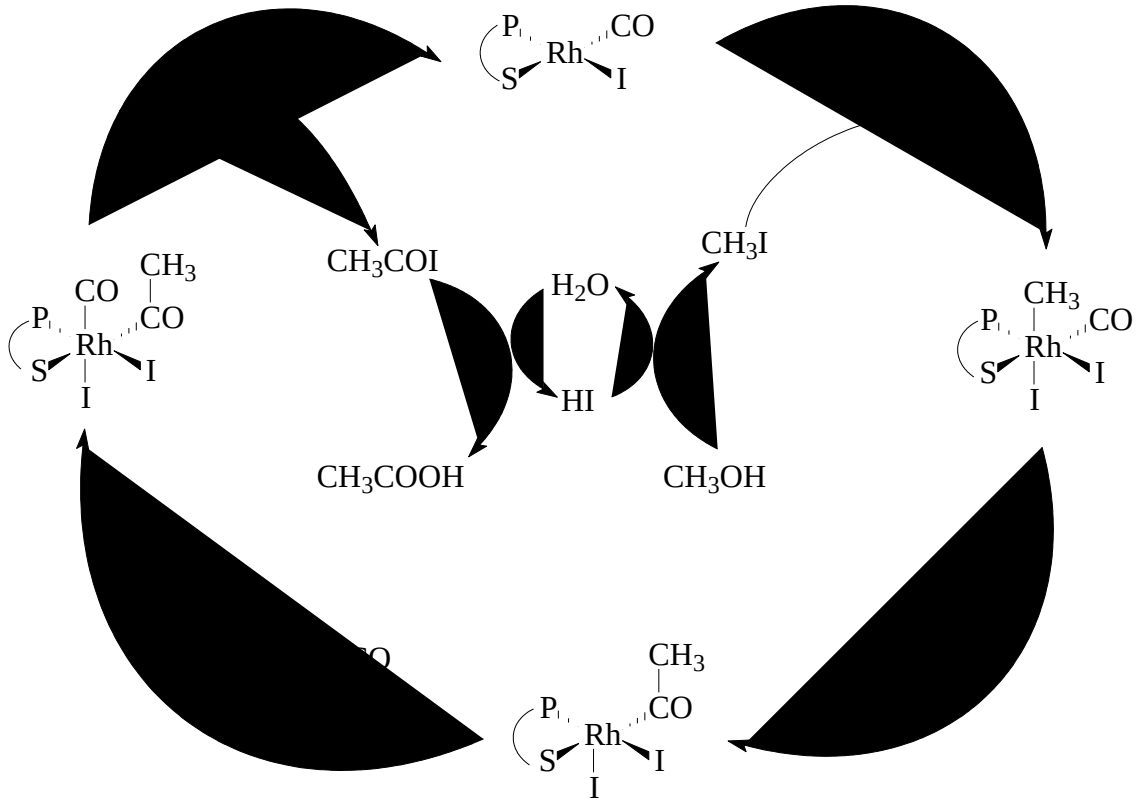

Scheme 2.7: Catalytic cycle of the methanol carbonylation catalyzed by the neutral complex [Rh{$Ph_2PCH_2P(S)Ph_2$}(CO)I] [42]

Dilworth *et al.*[33] described other methanol carbonylation catalysts which showed significant improvements in absolute rates over those obtained with $[Rh(CO)_2I_2]^-$.[33] Both the dinuclear phosphinothiolate complex and the mononuclear phosphinothioether complex synthesized according to **Scheme 2.8** efficiently catalyze the carbonylation of methanol with comparable rate. The authors proposed a mechanism similar to the cycle proposed for [Rh{$Ph_2PCH_2P(S)Ph_2$}(CO)I (**Scheme 2.8**).[42]

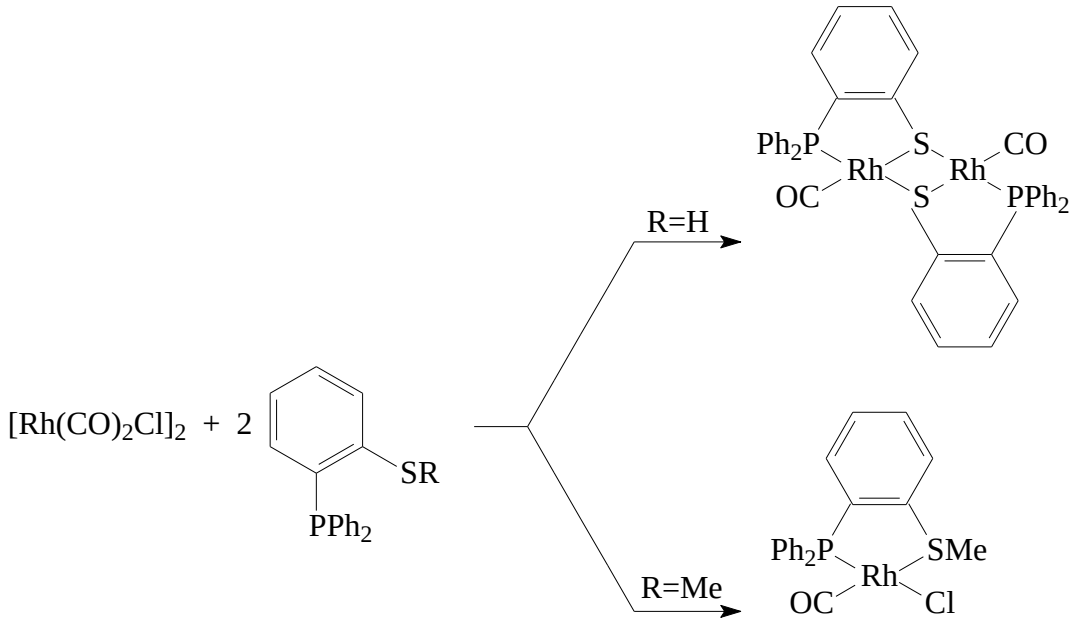

Scheme 2.8: Synthesis of rhodium phosphinothiolate and phosphinothioether complexes [42]

Pringle *et al.*[46] reported that rhodium complexes of unsymmetrical ethylene diphosphine ligands are more efficient catalysts than the symmetrical dppe analogues for methanol carbonylation and longer-lived than any other reported ligand-modified catalysts under industrial conditions.[46, 47, 48, 49] The catalysts were prepared by addition of diphosphines to $[Rh(CO)_2Cl]_2$ in methanol (**Scheme 2.9**).

[46] C. A. Carraz, E. J. Ditzel, A. G. Orpen, D. D. Ellis, P. G. Pringle and G. J. Sunley, *Chem. Commun.*, (2000), 1277.

[47] C. P. Casey, E. L. Paulsen, E. W. Beuttenmueller, B. R. Proft, B. A. Matter and D. R. Powell, *J. Am. Chem. Soc.*, **121**, (1999), 63.

[48] H. Brunner and A. Stumpf, *J. Organomet. Chem.*, **459**, (1993), 139.

[49] P. N. Kapoor, D. D. Pathak, G. Gaur and M. Kutty, *J. Organomet. Chem.*, **276**, (1984), 167.

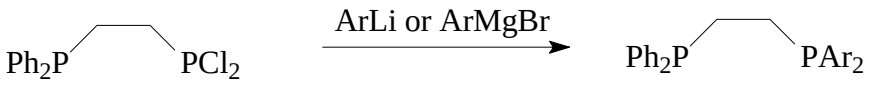

Ar = 4-C_6H_4OMe or 3,5-$C_6H_3F_2$ or 3,4,5-$C_6H_2F_3$

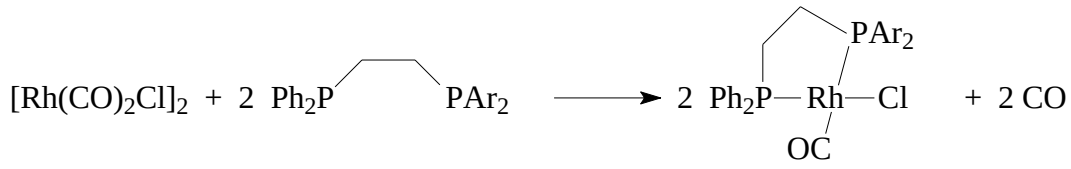

Scheme 2.9: Synthesis of rhodium complexes with unsymmetrical diphosphine ligands [48]

The results obtained from this study indicated that in each case the conversion of methanol was greater than 98%, and the selectivity for acetic acid was greater than 99%. However, the carbonylation rates are lower for these diphosphine complexes than for the $[Rh(CO)_2I_2]^-$ catalyst. Different observations by means of infrared and ^{31}P-NMR spectra suggested that the catalyst is indeed a diphosphine-rhodium complex throughout the catalytic reaction and not $[Rh(CO)_2I_2]^-$. Infrared spectra obtained *in situ* during a reaction with $Ph_2PCH_2CH_2P(3,4,5\text{-}C_6H_2F_3)_2$ showed the absence of the intense ν(CO) bands of $[Rh(CO)_2I_2]^-$ at 2059 and 1988 cm^{-1}. At the end of the catalytic reaction, P NMR and IR spectra showed the presence of a mixture of diphosphine rhodium(III) carbonyl complexes. The product *fac*-$[Rh\{Ph_2PCH_2CH_2P(3,4,5\text{-}C_6H_2F_3)_2\}(CO)I_3]$ was isolated from the reaction mixture, using the $[Rh\{Ph_2PCH_2CH_2P(3,4,5\text{-}C_6H_2F_3)_2\}(CO)Cl]$ catalyst.[46] The rate of catalysis was constant throughout a catalytic run and the acetylation of a second aliquot of methanol lead to the consumption of the first volume of methanol. The rate was identical as in the first run.

The above mentioned observation confirmed the longevity of the catalyst to be greater than any previous rhodium-phosphine catalyst since every diphosphine complex executes over 500 turnovers without noticeable diminution of activity.

The results also indicated that the amount of propionic acid reported (formed during the water-gas shift reaction) for these diphosphine catalysts is significantly less than that with $[Rh(CO)_2I_2]^-$ as catalyst under the same conditions.

The asymmetry of the diphosphine is also crucial. Casey *et al.*[47] showed that unsymmetrical diphosphines are superior to the symmetrical analogues for hydroformylation catalysis and associated this with a preference of the better σ-donor for the axial site in the trigonal bipyramidal intermediates. It is noteworthy that P,O-,[35] P,N-[41] and P,S-donor[42] ligands used for methanol carbonylation are all unsymmetrical with one strong and one medium or weak donor atom.

Indeed, all these new ligands enhanced the oxidative addition step, but as a consequence they usually retard the subsequent CO insertion step, because the increased electron density at the metal also leads to stronger Rh-CO bonds. Optimal parameters are required to achieve the delicate balance between these two factors which will afford highly efficient catalysts.

Chapter 3

Theoretical aspects of oxidative addition reactions

The term “oxidative addition” is used to designate a widespread class of reactions, generally of low-spin transition metal complexes. The term “low spin” (or “spin paired”) refers to those transition metal complexes in which the ligand field splittings are sufficiently large that the d-electrons first fill up (with pairing if necessary) all the available stable (bonding and nonbonding) orbitals before beginning to populate the antibonding orbitals. In general the metal complex serves as both a Lewis acid and base during oxidative addition. The formal oxidation state of the central metal atom increases by two units and two new groups/ligands bond to the metal center. The incoming groups are reduced during this process while the metal atom itself is oxidized. The following equilibrium represents an oxidative addition reaction:[1]

$$L_nM^m + XY \rightleftharpoons L_nM^{m+2}(X)(Y)$$

where L represents the ligands; n the number of ligands; M the metal atom and m the oxidation state. The forward reaction is known as oxidative addition and the reverse reaction as reductive elimination. The position or extent of the equilibrium is determined by the type of metal and bound ligands, the type of addendum molecule XY, the bonds M-X and M-Y that are formed as well as the medium or solvent in which the reaction takes place. Illustrative of the above-mentioned reaction are a few examples given below:[2]

[1] F.A. Cotton and G. Wilkinson, *Basic Inorganic chemistry,* John Wiley & Sons, Inc., New York (1976).

[2] J. Halpern, *Acc. Chem.Res.*, **3**, (1970), 386.

$2\ [Co^{II}(CN)_5]^{3-} + CH_3I \longrightarrow [Co^{III}(CN)_5I]^{3-} + [Co^{III}(CN)_5CH_3]^{3-}$

$[Ir^{I}(CO)\{P(C_6H_5)_3\}_2Cl] + H_2 \longrightarrow [Ir^{III}(CO)\{P(C_6H_5)_3\}_2(H)_2Cl]$

$[Pt^{0}\{P(C_6H_5)_3\}_2] + [(C_6H_5)_3SnCl] \longrightarrow [Pt^{II}\{P(C_6H_5)_3\}_2\{Sn(C_6H_5)_3\}Cl\}]$

The occurrence of oxidative-addition reactions are related to the characteristic coordination numbers of low-spin transition metal complexes given in **Table 3.1**.[2]

Table 3.1: Characteristic Coordination Numbers of Low-Spin Complexes

Coordination no .	**Examples**	**Electron configuration**	**Total no. of valence electrons**
8	$[Mo(CN)_8]^{2-}$, $[Mo(CN)_8]^{4-}$	d^1, d^2	17, 18
6	$[M(CN)_6]^{2-}$ (M = Cr, Mn, Fe, Co)	d^3, d^4, d^5, d^6	15-18
5	$[Co(CN)_5]^{3-}$, $[Ni(CN)_5]^{3-}$	d^7, d^8	17, 18
4(square planar)	$[Ni(CN)_4]^{2-}$	d^8	16
4(tetrahedral)	$[Cu(CN)_4]^{3-}$, $[Ni(CO)_4]$, $[Pt\{P(C_6H_5)_3\}_4]$	d^{10}	18
3	$[Pt\{P(C_6H_5)_3\}_3]$	d^{10}	16
2	$[Ag(CN)_2]^-$	d^{10}	14

As can been seen from **Table 3.1** there is an inverse dependence of the preferred coordination number on the d-electron population of the transition metal atom, a trend which becomes especially pronounced as the filling of the d subshell approaches completion. This trend reflects the constraints of the well-known "18-electron" (or "noble gas") rule. According to this rule the stable configurations in such complexes are restricted to those in which the total number of valence electrons (comprising the d-electrons of the metal and the σ-bonding electron pairs donated by each of the ligands) does not exceed 18. Three such classes of reactions are illustrated in a few examples given below (**Reaction 3.1-3.3**).[2] They are the oxidative-addition reactions of five-coordinate d^7, four-coordinate d^8, and two-coordinate d^{10} complexes.

$$ML_5 \xrightarrow[+\,L]{-\,e} ML_6$$

d^7 (17) d^6 (18)

$$2\,[Co^{II}(CN)_5]^{3-} + X\text{-}Y \longrightarrow [Co^{III}(CN)_5X]^{3-} + [Co^{III}(CN)_5Y]^{3-}$$

X-Y = H_2, Br_2, HOH, HOOH, CH_3I, ICN, etc. **3.1**

$$ML_4 \xrightarrow[+\,2L]{-2e} ML_6$$

d^8 (16) d^6 (18)

$$[Ir^{I}(CO)\{P(C_6H_5)_3\}_2Cl] + X\text{-}Y \longrightarrow [Ir^{III}(X)(Y)(CO)\{P(C_6H_5)_3\}_2Cl]$$

X-Y = H_2, Cl_2, HCl, CH_3I, RSO_2-Cl, RHg-Cl, R_2Si-H, etc. **3.2**

$$ML_2 \xrightarrow[+\,2L]{-2e} ML_4 \xrightarrow[+\,2L]{-2e} ML_6$$

d^{10} (14) d^8 (16) d^6 (18)

$$[Pt^{0}\{P(C_6H_5)_3\}_2] \xrightarrow{X\text{-}Y} [Pt^{II}\{P(C_6H_5)_3\}_2(X)(Y)] \xrightarrow{X\text{-}Y} [Pt^{IV}\{P(C_6H_5)_3\}_2(X)_2(Y)_2]$$

X-Y = CH_3I, $C_6H_5CH_2$-Br, $(C_6H_5)_3$Sn-Cl, etc. **3.3**

The driving force for each reaction is associated with the increase in stability in going from the initial open shell configuration (containing 17, 16, and 14 valence electrons, respectively) to the closed shell configuration of the product.

Research has shown that low spin d^8- and d^{10}-complexes often react with covalent molecules in order to increase the coordination number by means of oxidative addition reactions. The prototype of the above mentioned type of reaction was observed in 1962 by Vaska and Diluzio,[3] when hydrogen was added to a square planar iridium complex (**Figure 3.1**).

[3] L. Vaska and J.W. Diluzio, *J.Am.Chem. Soc*. **84**, (1962), 679.

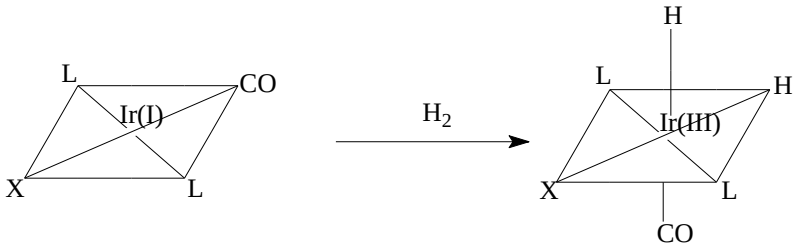

[X = Cl, Br, I; L = $P(C_6H_5)_3$]

Figure 3.1: Addition of hydrogen to a square planar iridium complex.

The influence of the above-mentioned factors (increase in stability of product, increase in coordination number etc.) will be discussed in more detail in this chapter.

3.1 Requirements for oxidative addition

A number of prerequisites have to be fulfilled before oxidative addition reactions can take place.[1, 4] The prerequisites include that (a) there has to be non-bonding electron density on the metal atom, (b) the availability of two vacant coordinating positions in the complex coordination sphere to ensure the formation of two new bonds with the ligands X and Y, and (c) the oxidation state of the metal atom has to be two units lower than the most stable oxidation state.

In general, the oxidative addition of coordinatively unsaturated square-planar 16-electron d^8-complexes of Rh(I) and Ir(I) produces six-coordinated 18 electron d^6-complexes of Rh(III) and Ir(III).[4] Some examples are given in the following reaction (**Reaction 3.4 - 3.6**). Milstein and Stille[5] as well as Stieger and Kelm[6] substantiated that in most cases the loss of ligands of square-planar molecules does not take place before the occurrence of oxidative addition.

[4] I.C. Douek and G. Wilkinson, *J. Chem. Soc*., **A**, (1969), 2604.

[5] D. Milstein and J.K. Stille, *J. Am. Chem. Soc*., **101**, (1979), 4992.

[6] H. Stieger and K. Kelm, *J. Phys. Chem*., (1973), 290.

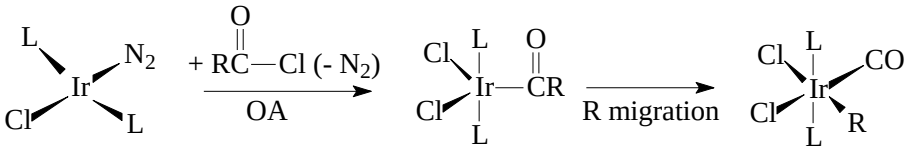

NVE = 16
OS = +1

NVE = 16
OS = +3

NVE = 18
OS = +3

3.4

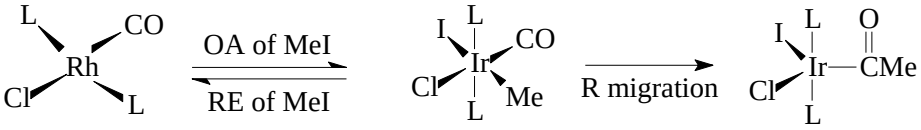

NVE = 16
OS = +1

NVE = 18
OS = +3

NVE = 16
OS = +3

3.5

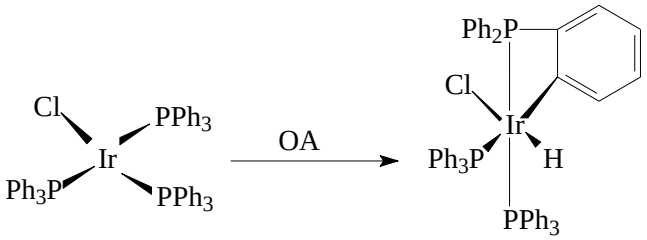

NVE = 16
OS = +1

NVE = 18
OS = +3

3.6

Before oxidative addition can occur it becomes necessary at times for the complex to dissociate some of its bound ligands to establish a vacant coordination position. An example of the above mentioned criteria is the complexes $[M(PPh_3)_4]$, with M = Ni(0), Pd(0), Pt(0), which are all coordinatively saturated and have d^{10}-electron configurations.[6] The first step in the oxidative addition of these complexes are the dissociation of some of the phosphine ligands in solution to yield three- and two-coordinated complexes that are coordinatively unsaturated and are thus reactive towards oxidative addition.[6]

Another example where dissociation of bound ligands from square planar (tetra-coordinated) complexes prelude the oxidative addition reaction is illustrated by the oxidative addition of H_2 with $[RhClL_3]$[7] or $[IrX(CO)L_2]$.[8] This ligand dissociation is

[7] Y. Ohtani, M. Fujimoto and A. Yamagishi, *Bull. Chem. Soc. Japan*, **50**, (1977), 1453.

most probably catalyzed by the solvent. The solvated species which are formed in this manner undergo oxidative addition according to the same mechanism as usual, but only at different rates.[7, 9] Results have shown in certain cases that oxidative addition can only occur when there is dissociation from five-coordinated complexes to reactive four-coordinated 16-electron complexes.[10, 11, 12] During the addition of H_2 to the five-coordinated 18-electron d^8-Ir(I) complex, $[Ir(CO)(PMe_2Ph)_3Cl]$, Chen and Halpern[13] found that the reaction progressed more rapidly than the corresponding reaction in which the four-coordinate $[Ir(CO)(PMe_2Ph)_2Cl]$ complex was used. These results are in contrast to that found for the five-coordinated d^8-complexes like $[Ni(CN)_5]^{3-}$, that are non-reactive to substrates such as H_2. According to the general prerequisite, $[Ni(CN)_5]^{3-}$ is expected to be more reactive due to a vacant bonding site.

In case of the 18-electron penta-coordinated complex such as $[Os(CO)_3L_2]$, oxidative addition leads to a six-coordinated, 18-electron, d^6-complex as final product (**Reaction 3.7**)[14] that can be isolated and can lead through nucleophilic substitution of a neutral ligand to species of greater stability.

[8] R.J. Cross, *Chem. Soc. Rev*., **14**, (1985), 197.

[9] R.J. Mureinik, M. Weitzberg and J. Blum, *Inorg. Chem*., **18**, (1979), 915.

[10] J.F. Harrod and C.A. Smith, *Can. J. Chem*., **48**, (1970), 870.

[11] M.J. Chuch, M.J. Mays, R.N.F. Simpson and F.P. Stefanini, *J. Chem. Soc*., **A**, (1970), 2909.

[12] M.G. Burnett and R.J. Morrison, *J. Chem. Soc*., **A**, (1971), 2325.

[13] J. Chen and J. Halpern, *J. Am. Chem. Soc*., **93**, (1971), 4939.

[14] J.P. Collman and W.R. Roper, *J.Am. Chem. Soc*., **88**, (1966), 3504.

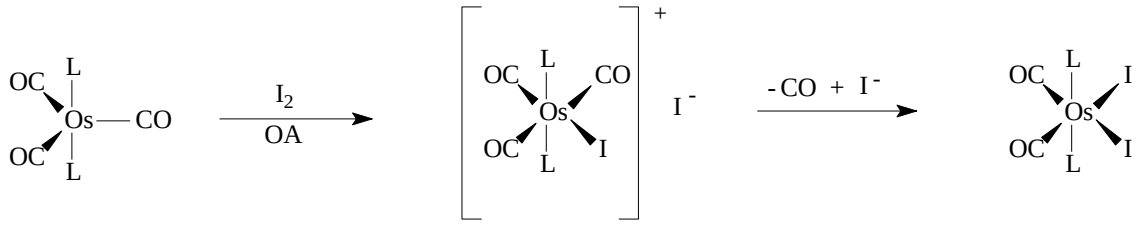

OS = 0 OS = 2+ OS = 2+

3.7[14]

3.2 Mechanisms of oxidative addition

Extensive research has been done on the mechanisms whereby oxidative addition reactions proceed. However, in certain cases conclusions regarding the mechanism according to which the reaction takes place are debatable. The reason for this is that a delicate balance exists between certain mechanisms and each case should therefore be thoroughly investigated so as to ascertain the predominate mechanism. Certain factors like the formal charge of the complex, the nature of the metal, bound and incoming ligands (or most likely the addendum), as well as the experimental conditions (solvent, temperature and the presence of impurities) influence the final reaction rate as well as the final product that is formed by the reaction.

Criteria used for determining the dominant mechanism include the following: (a) stereochemistry of both the metal and the addendum (b) interpretation of polar- or radical intermediates (c) rearrangement of the radical intermediates (d) the formulation of the rate law and the nature of the activation parameters as well as (e) the effect of the solvent polarity and radical scavengers on the rate of the oxidative addition reaction.

On the above mentioned basis the following division can be used to summarize the representative mechanisms that were found in literature:

1. Concerted one-step mechanism
2. Two-step S_N2-type mechanism
3. Free radical mechanism
4. Ionic mechanism

There is an increase in the number of possible reaction pathways that in turn impedes exact classification or allocation of a mechanism to a reaction if there is a crossover between mechanisms.

3.2.1 Concerted one-step mechanism

According to the mechanism, oxidative addition occurs when the reaction takes place under non-polar conditions and is typified by H_2-addition to Vaska's complex, $[IrCl(CO)(PPh_3)_2]$ (**Reaction 3.8**).[3]

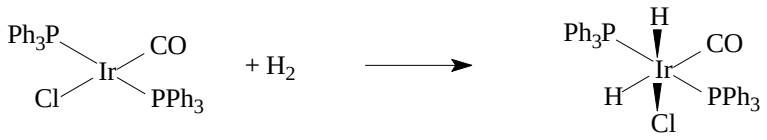

3.8[3]

The addendum in this type of mechanism is a homonuclear molecule or another molecule with little or no polarity, for example H_2, O_2, Cl_2, C_2H_4, etc. while the concerted *trans*-addition remains a symmetry-prohibited process.[15, 16] The mechanism also leads to a *cis*-arrangement of the addendum if no rearrangement has taken place. The reaction pathway is essentially an electrophilic attack on the metal. This type of reaction is described in terms of the overlap of filled d_{xz}- or d_{yz}-metal orbitals with a vacant σ*-antibonding orbital of the added molecule,[16] representing a cyclic transition state (**Figure 3.2**).

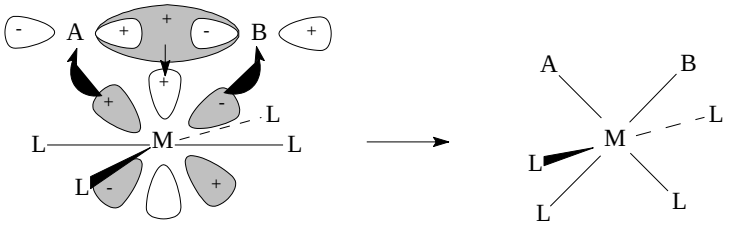

Figure 3.2: Orbital overlap in the concerted *cis*-addition of a molecule AB.[16]

[15] P.S. Braterman and R.J. Cross, *Chem. soc. Rev*., **2**, (1973), 271.

[16] R.G. Pearson, *Symmetry rules for chemical reactions*, Wiley interscience, New York, (1976).

Saillard and Hoffmann[17] however pointed out that overlap of a filled σ-orbital of AB, with a vacant metal acceptor-orbital, also has to be involved. This overlap is represented by a charge transfer in another direction, that of AB to the metal. What might be of greater significance than the reverse, and as a result of the coordinative unsaturation requirement, is the initial flow of electron density from AB to M. The above mentioned interactions impair the A-B bond, while M-A and M-B bonds are strengthened. According to this description, nucleophilic attack on the metal is the starting phase of the concerted oxidative addition of, for example H_2 to a square-planar molecule. Furthermore, the type of ligands also have a role to play in the characterization of the mechanism of the reaction and is illustrated by the stereo specific *cis*-addition of H_2 to [IrX(CO)(dppe)] with the additional interaction of $\sigma(H_2)$ with π^*(CO) orbitals.[18]

3.2.2 Two-step S_N2-type mechanism

In contrast to the concerted mechanism, this mechanism involves an electrophilic attack on the metal atom.[16, 19, 20] The two-step mechanism can be applied to the addition of dipolar molecules such as CH_3I and HCl (**Figure 3.3**) to different metal complexes.

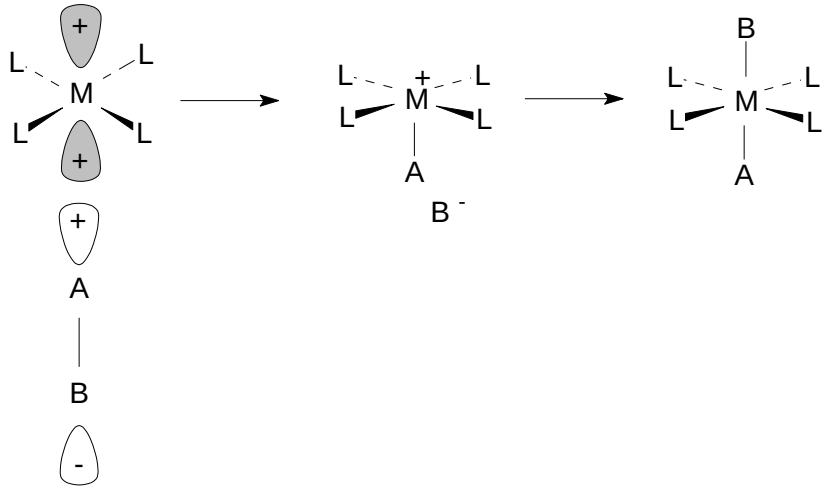

Figure 3.3: Presentation of the addition of dipolar molecules.[19]

[17] J.Y. Saillard and R. Hoffmann, *J.Am. Chem. Soc*., **106**, (1984), 2006.

[18] C.E. Johnson and R. Eisenberg, *J.Am. Chem. Soc*., **107**, (1985), 3148.

[19] J.P. Collman and W.R. Roper, *Adv. Organomet. Chem*., **14**, (1976), 345.

[20] J. Halpern, *Acc. Chem. Res*., **3**, (1970), 386.

Square-planar molecules can be differentiated from other systems through the donor orbital (filled d_z^2) and the acceptor orbital (p_z) by virtue of having the same symmetry in relation to the incoming group in the direction of the z-axis. Conclusions can be made about the nature of the attack on the metal and the substantial polarity of the two- or three-centered transition state from observations such as the dependence of the rate on the nucleophilicity of the metal complex as well as first-order relationships for both reactants, the large negative values of the activation entropies and the dependence of activation parameters on the solvent polarity.

Results have shown that oxidative addition *via* a two-centered transition state leads to stereochemical inversion of the configuration at the carbon center of the alkyl group, as seen in many S_N2 processes.[21] In contrast to the above-mentioned reactions, a three-centered transition state leads to retention or inversion of configuration at the carbon and is dependent upon the degree of the metal-halogen bond formation during the transition state.[22]

Criteria used to distinguish between two- and three-centered transition states seems problematic at times. Activation enthalpy- and activation entropy values for certain addition reactions have indicated that no distinction can be made between two- and three-centered transition states.[23] Results have shown that the sensitivity of different addenda towards polar effects of different solvents during oxidative addition can be measured by the variation of the donor properties of the triarylphosphine ligands, L = (*p*-$(C_6H_4)_3P$, in $[IrCl(CO)L_2]$.[22] The large variation in activation enthalpy- and activation entropy values between methyl iodide and benzyl chloride indicates that polar effects cannot be used to draw a distinction.[23]

[21] J.A. Labinger, R.J. Braus, D. Dolphin and J.A. Osborn, *J. Chem. Soc., Chem. Comm*., (2002), 612.

[22] R. Ugo, A. Pasini, A. Fusi and S. Cenini, *J. Am. Chem. Soc.*, **94**, (1972), 7364.

[23] J. Burgess, M.J. Macker and R.D.W. Kemmit, *J. Organomet. Chem*., **72**, (1974), 121.

Research has shown that the oxidative addition reactions of organic halides and similar molecules occur *via* a nucleophilic attack on the carbon. Reactions of tertiary amines and alkyl halides proceed *via* a linear S_N2-displacement at the carbon molecule (**Figure 3.4**).[24]

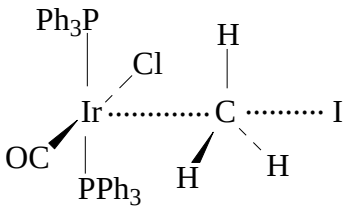

Figure 3.4: Linear S_N2-displacement[24]

Later studies of the above-mentioned oxidative addition reaction have shown that an asymmetrical transition state (**Figure 3.5**)[24] is more probable than a linear geometry thus explaining the electronic effects observed during the reaction.

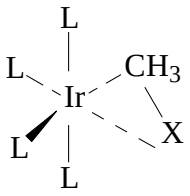

Figure 3.5: Asymmetrical transition state[24]

Measurements of the volume of activation, in various solvents, of the addition of CH_3I or O_2 to Vaska's complex, $[IrCl(CO)(PPh_3)_2]$, provided more information with regard to the reaction mechanism.[6] The authors considered a linear transition state (**Figure 3.3**) to better explain the rate determining bond-forming associative step that correlates with the negative ΔV^*-value, rather than the simultaneous formation of two bonds (**Figure 3.4**).

During a nucleophilic reaction, even through solvent coordination, the species attacked by the electrophile are an 18-electron five coordinated molecule and not the 16-electron

[24] P.B. Chock and J. Halpern, *J. Am. Chem. Soc*., **88**, (1966), 3511.

square-planar complex. There are various examples of electrophilic attack on 18-electron species and the process is considered as well-established.[25, 26, 27]

The S_N2-type transition state for oxidative addition is also supported by the effect of structural change of alkyl halides. A number of oxidative addition reactions[28, 29] follow the classic pattern for the rate of S_N2-substitution, namely methyl- > ethyl- > isopropyl halides and methyl iodide > -bromide > -chloride[30] that concurred with organic substitution processes. These studies have shown that changing the halide in the addendum, RX, have a relative small influence,[22, 23] but a change in the aryl groups with electron-withdrawing substitutes enhanced the rate more profoundly.[5, 9, 28] These results were also used as prove for electrophilic attack by the carbon on the metal with the retainment of a three-centered transition state (**Figure 3.4**) at the metal center.[9]

3.2.3 Free radical mechanism

A comparative study of several oxidative addition processes indicates that free radical processes are virtually in competition with other routes.[31, 32]

Research has shown that it is sometimes difficult in practice to distinguish between S_N2-type and free radical mechanisms.[16] Both mechanisms are partially dependent upon the oxidation-reduction characteristics of the metal-complex and the bound ligands. An important criterion for participation or non-participation of a free radical mechanism is

[25] A.J. Deeming and B.L. Shaw, *J. Chem. Soc*., **A**, (1970), 3356.

[26] A.J. Hart-Davis and W.A.G. Graham, *Inorg. Chem*., **9**, (1970), 2658.

[27] A.J. Oliver and W.A.G. Graham, *Inorg. Chem*., **9**, (1970), 243.

[28] J.P. Collman and M.R. MacLaury, *J. Am. Chem. Soc*., **96**, (1974), 3019.

[29] G.N. Schrauzer and E. Deutsch, *J. Am. Chem. Soc*., **91**, (1969), 3341.

[30] J.K. Kochi, *Organometallic mechanisms and catalysis,* Academic Press, London, (1978).

[31] J. Blum, M. Weitzberg and J. Mureinik, *J. Organomet. Chem*., **122**, (1976), 261.

[32] A.V. Kramer and J.A. Osborn, *J. Am. Chem. Soc*., **96**, (1974), 7832.

that the X-Y bond breaking of the added molecule XY should occur first, before interaction with the metal center, as compared to the S_N2-mechanism where bond formation and bond breaking take place at the same time.

The free radical mechanism can occur in two types of reactions pathways[30] and is summarized as follows:

a) Radical chain reaction (propagating succession)

$$RX + RM\cdot \longrightarrow RMX + R\cdot$$

$$R\cdot + M \longrightarrow RM\cdot$$

b) Radical non-chain reaction (electron-transfer)

$$RX + M \longrightarrow [R\cdot M X\cdot]$$

$$[R\cdot MX\cdot] \longrightarrow RMX$$

where RX = alkyl halide and M = metal

The radical chain reaction has been observed in oxidative addition reactions of Ir(I), Rh(I) and Pt(0) with alkyl halides. Research has shown that the reaction of $[IrCl(CO)(PMe_3)_2]$ with $PhCHFCH_2Br$ is initiated through radical sources like O_2 or benzoyl peroxide and inhibited by radical scavengers like hydroquinone, galvinoxyl or duroquinone.[33]

Oxidative addition of alkyl halides, like CH_3I, CH_3OCH_2Cl, benzyl chloride, etc., to $[IrCl(CO)(PMe_3)_2]$ are not effected by suppressants and the reaction occurs according to a radical chain reaction with the formation of a free radical. Oxidative addition of alkyl halides to the rhodium(I)-complex, $[RhCl(CO)(PEt_3)_2]$, occurred *via* a radical non-chain reaction and is not affected by radical scavengers.[30] Simultaneous involvement of both chain- and non-chain reactions are dependent upon the reactivity and structure of the alkyl halides. Distinctions are mainly based on the effect of radical scavengers and initiators.[30]

[33] C.K. Brown, D Georgian and Wilkinson, G.; *J. Chem. Soc., Dalton Trans*., (1973), 929.

3.2.4 Ionic mechanism

Research has shown that this mechanism proceeds *via* the protonation of a square planar complex to form a five-coordinated intermediate. The five-coordinated intermediate undergoes intramolecular isomerization where the halide ion coordinates to form the final product.[34]

$$[MXL_3] + H^+ \longrightarrow [MHXL_3]^+$$

$$[MHXL_3]^+ + Cl^- \longrightarrow [MHClXL_3]$$

There are two types of ionic mechanisms and both are initiated by polar solvents like dimethyl formamide and substrates like HCl and HBr. In the first mechanism the complex is protonated and then the anion coordinates to form the final product. The metal ion has a low oxidation state (**Reaction 3.9**).[35]

$$[Pt(PPh_3)_4] + H^+ + Cl^- \longrightarrow [PtH(PPh_3)_3]^+Cl^- + PPh_3$$

$$[PtH(PPh_3)_3]^+Cl^- \longrightarrow [PtHCl(PPh_3)_2] + PPh_3$$

3.9

The second type involves the attack of the halide on the metal ion followed by the protonation of the intermediate to form the final product. The mechanism is initiated by a net positive charge on the metal ion and electron acceptor ligands (**Reaction 3.10**).[36]

$$[Ir(cod)L_2]^+ + Cl^- + H^+ \rightleftharpoons [IrCl(cod)L_2] + H^+$$

$$[IrCl(cod)L_2] + H^+ \rightleftharpoons [IrHCl(cod)L_2]^+$$

3.10

[34] F.A. Cotton, P.L. Gaus and G. Wilkinson, *Basic Inorganic Chemistry*; John Wiley and Sons: New York, (1987).

[35] W.J. Louw, D.J.A. De Waal and T.V. Ashworth, *J. Chem. Soc. Dalton Trans*., (1978), 340.

[36] R.H. Crabtree and D.F. Chodosh, *J. Organomet. Chem*., **181**, (1979), 203.

An important criterion of an ionic mechanism is the formation of the five-coordinated intermediate during oxidative addition. The geometry of the five-coordinated intermediate, usually square-pyramidal, shows *trans*-addition, but intramolecular rearrangement of the intermediate leads to the formation of both a *cis*- and *trans*-addition product (**Scheme 3.1**):[30]

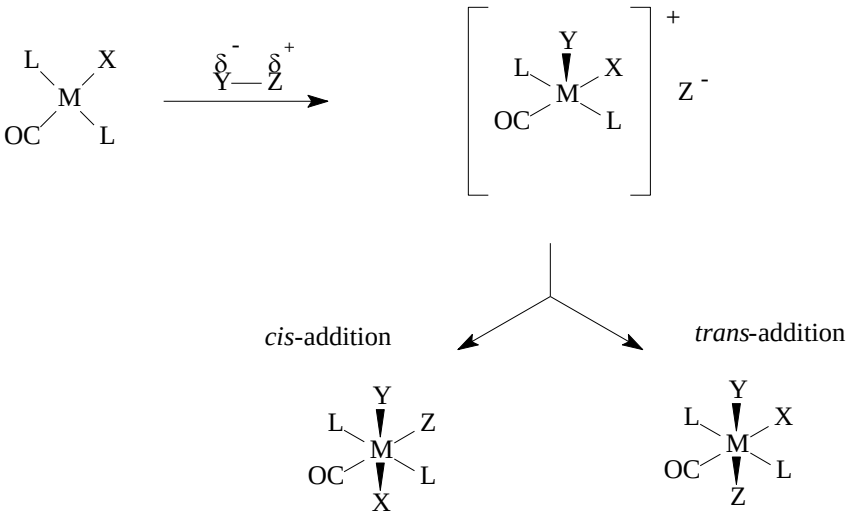

Scheme 3.1: Ionic mechanism of a five-coordinated cationic intermediate[30]

3.3 Factors influencing oxidative addition

Research has shown that various factors may influence the reaction rate and final reaction products of oxidative addition reactions. These include the type of metal center, steric and electronic properties of the bound ligands, the addendum, the reaction medium and the possibility of catalysis. It appears that all these factors influence the nucleophilic character of the metal complex and that any change in the nucleophilicity of the metal will determine the outcome of the reactions.[37, 38]

[37] C.K. Brown, D. Georgian and G. Wilkinson, *J. Chem. Soc., Dalton Trans*., (1973), 929.

[38] A.J. Deeming and B.L. Shaw, *J. Chem. soc*., **A**, (1969), 1802.

3.3.1 The metal

The metal center and more specific its ability to act as nucleophile plays a pivotal role in the final rate as well as the type of product that is formed during oxidative addition reactions. Results that were obtained from numerous studies indicate that the heavier low valent transitions metals are more nucleophilic/basic than the metals in the earlier transition series. A well-known example is the comparison of the oxidative addition of CH_3I to the Vaska complexes of Ir(I) and Rh(I). The iridium complex, $[IrCl(CO)\{P(C_6H_5)_3\}_2]$ (heavier, more basic), reacts fully and irreversibly with CH_3I, while the reaction with the corresponding rhodium complex is reversible[39, 40] (**Reaction 3.11**) illustrating the weaker nucleophilicity of the lighter element.

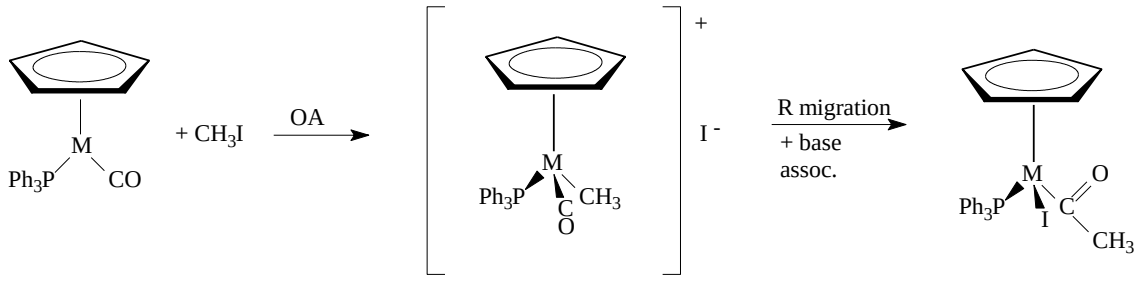

M = Ir(I) or Rh(I)

3.11[39]

In general, the later transition metals with the lowest oxidation states demonstrate the greatest tendency towards oxidative addition. This tendency is adequately demonstrated by **Figure 3.6**[39] which summarize the results for d^8 elements and can be used as an estimate when different metals are studied for oxidative addition reactions.

[39] R.S. Nyholm and K. Vrieze, *J.Chem.Soc*., (1965), 5337.

[40] M. Kubota, D.M. Blake and S.A. Smith, *Inorg. Chem*., (1971), 1430.

The general requirements for a metal to undergo oxidative addition reactions are as follows:

- The availability of non-bonding electron density in the metal
- The availability of two vacant coordination positions on the metal to allow for the formation of two new bonds
- The ability to form a product with an oxidation state two units higher than the starting complex

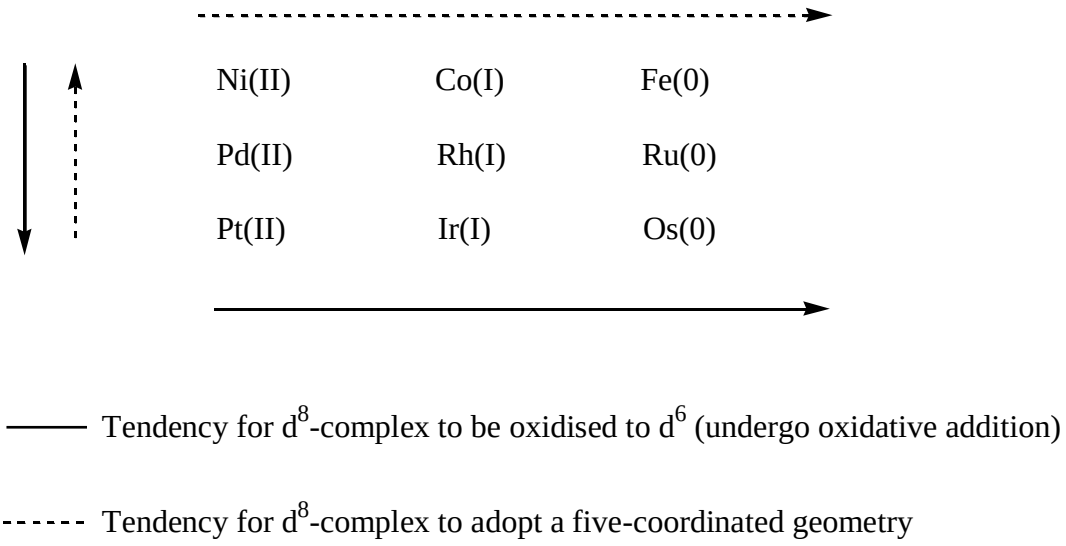

Figure 3.6: Ability of d^8 metals to undergo oxidative addition reactions.[39]

A full and comprehensive comparison which encompasses three members of a particular sub-group or between metals of neighbouring sub-groups is not possible due to a lack of iso-structural complexes for a whole series. Comparisons are further hampered by the characteristic tendency of d^8-complexes to become coordinatively unsaturated as sub-groups are ascended or one moves from right to the left in group VIII.

It is therefore easy to understand that any factor that affects or changes the nucleophilicity of the metal center such as the bound ligands will eventually influences the final outcome of the reaction.

3.3.2 Bound ligands

The ability of existing groups within the coordination sphere to change or control the electron density on the metal ion also plays a very important role in oxidative addition reactions. It is mainly the σ- and π- bonding properties of the bound ligands[41] which affect the electron density on the metal center, which in turn render the metal center more or less nucleophilic. Ligands with good σ-donor properties will increase the electron density on the central atom and this increase in nucleophilicity will lead to more rapid reaction rates. On the other hand, ligands with strong π-acceptor properties will lower the electron density on the central metal atom resulting in slower reaction rates. Examples of ligands with good σ-donor properties include the trivalent phosphorous ligands of the type PX_3, but also include the AsX_3, SX_3 and SeX_2 ligands. The donor ability of these ligands can also be manipulated by the addition of electron withdrawing groups such OR, Cl or F to the ring structure.

The order of Lewis basisity for aryl-, alkyl- and mixed aryl-alkylphosphines may be summarized as follows:[32, 38]

$$PPh_3 < P(Ph)_2CH_3 < P(Ph)(CH_3)_2 < P(CH_3)_3$$

Increase in Lewis basisity

Carbonyl ligands on the other hand are good examples of strong π-acceptor ligands. These ligands cause a decrease in nucleophilicity of the metal center as a result of metal-to-carbon electron back-donation.

[41] I. Vaska, L. Chen and W.V. Miller, *J. Am. Chem. Soc*., **93**, (1971), 6671.

Another study which highlighted the influence of the bound ligands on nucleophilicity of the metal center was done by Basson, Leipoldt and Nel.[42] In this study they investigated the influence of different β-diketones with different electron donor abilities on the rate of oxidative addition reactions as seen in the reaction below.

$$[Rh(\beta\text{-diketone})(PPh_3)(CO)] + CH_3I \longrightarrow [Rh(\beta\text{-diketone})(PPh_3)(CO)(CH_3)(I)]$$

These ligands were influenced by the type and number of electron withdrawing groups attached to the ligands. The order of their reactivity followed the same trend as that of their nucleophilicities and can be presented as follows:

ACAC (1.0) > TFAA (0.24) ~TFDMAA (0.22) >> HFAA (0.02)

The steric demand of ligands already bound to the metal center also plays a very important role in the rate of these reactions, as well as the final products that are obtained. Results obtained from two different studies underlines the importance of bulkiness (steric demand) on the rate of reactions. Brown[43] studied the influence of size/bulkiness on the nucleophilic substitution in alkyl halides using substituted pyridines, while Hart-Davis and Graham[26] studied the nucleophilic addition of methyl iodide to different $[C_5H_5Co(CO)L]$ complexes with a variation of the bulkiness of the L ligand. The relative reaction rates are given in **Figure 3.7.**

[42] S.S. Basson, J.G. Leipoldt and J.T. Nel, *Inorg. Chim. Acta*., **84**, (1984), 167.

[43] H.C. Brown, *J. Chem. Soc*., (1956), 1249.

The relative reaction rates are as follows:

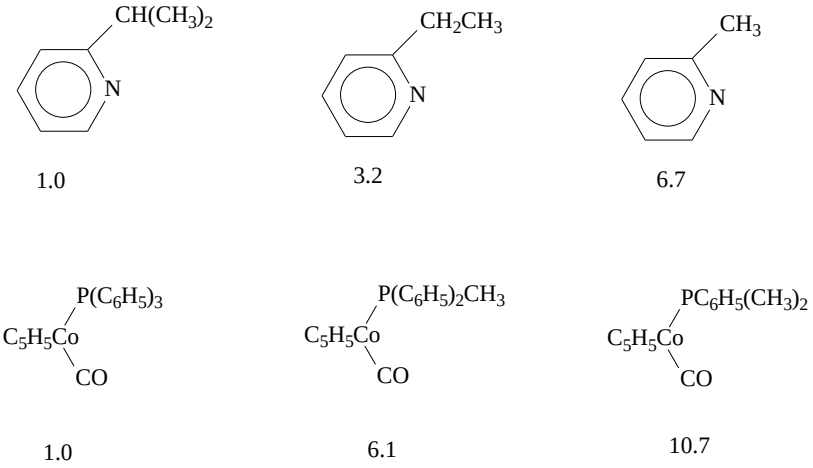

Figure 3.7: Relative reaction rates of the nucleophilic addition of methyl iodide to $[C_5H_5Co(CO)L]$.[26]

Both these studies demonstrated a decrease in reaction rate with an increase in bulkiness.

The contribution of phosphine ligands to either the nucleophilicity of the metal complex or to the steric demand within the complex is so intertwined that deductions from research results should be made with care. The Lewis basicity of tertiary phosphines as indicated by their respective pK_a values are normally used to indicate their relative nucleophilic contribution as indicated by **Table 3.2**.

These results clearly show a very good correlation between the rate of oxidative addition and the pK_a values of the different phosphine ligands. The results in the table also highlight the degree of π-back-donation which is prevalent in the complexes. A high degree of σ-donation (high electron donating ability) result in strong back-donation with weaker CO bonds and the resulting low carbonyl stretching frequency as indicated for PCy_3.

Electron withdrawing groups decrease the σ-donation ability of the phosphine, less π-back-donation and thus higher carbonyl stretching frequencies as demonstrated by P(*p*-$C_6H_4Cl)_3$.

Table 3.2: Rate of oxidative addition of $PhCH_2Cl$ to tertiary phosphines.[44]

Tertiary phosphine	**k (10^4) /$M^{-1}s^{-1}$**	**pK_a**	**ν(CO)/cm^{-1}**
PCy_3		9.65	2056.4
P(*p*-$C_6H_4OCH_3)_3$	3.3	4.57	2066.1
P(*p*-$C_6H_4CH_3)_3$		3.84	2066.7
PPh_3	1.2	2.73	2068.9
P(*p*-$C_6H_4F)_3$		1.97	2071.3
P(*p*-$C_6H_4Cl)_3$	0.2	1.03	2072.8

A measure of the bulkiness of phosphine ligands can be expressed in terms of the Tolman cone angle.[45] The cone angle θ, (Tolman angle) is defined as the angle of the cone formed by the three substituents, with the M-P bond distance equal to 2.28Å (**Figure 3.8**). Tolman chose the distance to represent the distance between the centers of P and Ni, since he developed his measurement of cone angles while studying Ni-P complexes.

[44] G. Wilkinson, *Comprehensive Coordination Chemistry in syntheses, reaction properties and application, Oxford Press*, (1987), 458.

[45] C.A. Tolman, *Chem. Rev*., **77**, (1977), 313.

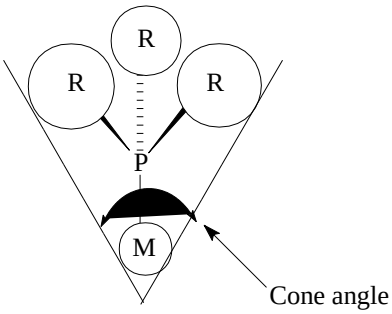

M = metal; R = alkyl, aryl

Figure 3.8: Tolman cone angle.[45]

A measure of the cone angle for a large number of phosphine ligands are given in **Table 3.3**.

Table 3.3: Cone angles and electronic parameters for selected phosphine ligands.[45]

Phosphine ligand	**θ (degrees)**	**ν(CO)/ cm^{-1}**
$P(Bu^t)_3$	182	2056.1
PCy_3	170	2056.4
$P(p\text{-}MeOC_6H_4)_3$	145	2066.1
$P(o\text{-}Tol)_3$	194	2066.7
$P(p\text{-}Tol)_3$	145	2066.7
PPh_2Me	136	2067.0
PPh_3	145	2068.9
$P(p\text{-}ClC_6H_4)_3$	145	2072.8
$PPh_2C_6F_5$	158	2074.8
$P(OPh_3)_3$	128	2085.3
PF_3	104	2110.8

The PCy_3 ligand which has the largest σ-donating capability (according to pK_a values) is also one of the bulkier ligands and these properties are working in direct opposition with one another which complicates the interpretation of results. Different models however exists which attempt to separate the steric and electronic effects of these phosphine ligands.

3.3.3 The addend

The addend molecule not only influences the mechanism of the reaction, but also the stereochemistry and the nature of the products during oxidative addition reactions. Addenda can be divided into three classes according to Collman and Hegeman;[46] (a) polar electrophilic reactants, (b) molecules that remain bound in the adduct and (c) non-polar addenda.

Examples of the addenda belonging to the different classes are as follows: (R = alkyl)[47]

Class A: X_2 (halogens), H-Y (Brönsted acids), R-X (alkylating reactants), RCOX (acylating reactants), $SnCl_4$, HgX_2, RSCl, etc.
Class B: O_2, S_2, Se_2, $RCON_3$, RN_3, RN=NR, RCH=CHR, S=C=S, H_2C=O, etc.
Class C: H_2, R_3SiH, R_3Ge-H, R_3Sn-H, RSH, RCHO, RH, etc.

Results have shown that the addition of Class A addenda normally yields *cis*- or *trans*-products while the unsaturated reagents belonging to Class B normally retain at least one bond in the adduct which results in the formation of *cis*-products. Class C addenda on the other hand almost always yield a stereo specific *cis*-addition.

[46] J.P. Collman and L.S. Hegedus, *Principles and applications of organotransition metal chemistry*, University Science Books, Mill Valley, California., (1980).

[47] J.P. Collman, L.S. Hegedus, J.R. Norton and R.G. Finke, *Principles and Applications of Organotransition Metal Chemistry*; University Science Boks: Mill Valley, (1987).

For this class of molecule the addition of C-H bonds is restricted mainly to intramolecular oxidative additions of activated C-H groups.

It is important to consider various factors when determining and allocating the role of alkyl halides, RX, in oxidative addition. The reactivity of an alkyl halide for example depends upon the dissociation energy of the R-X bond as well as the electron donating ability of the halogen. Research by Douek and Wilkinson[4] indicated that methyl iodide reacted considerably faster than methyl bromide at room temperature and established the order of reactivity for different halogens which are bound to the same alkyl-group as I > Br > Cl.[3, 26, 47] This order is also in accordance with the order of effectivity of the leaving group in S_N2 reactions.

The ease of nucleophilic attack by the metal complex on the α-carbon of an alkyl halide will depend a great deal upon the electrophilic nature of the α-carbon and thus also on the inductive effect of the halogen. This is in accordance with the inability of ethyl- and butyl iodide to react with $[RhCl(CO)(PPh_3)_2]$, while methyl iodide readily undergoes oxidative addition.[4] The central carbon atoms of ethyl- and butyl iodide are less positive in spite of greater dipole moments and thus less prone to nucleophilic attack. The steric effect of the butyl substituent is another important factor that exerts an influence on these reactions. The butyl group obstructs access to the metal, for example rhodium, thus retarding the reaction. The order of reactivity of alkyl halides for different alkyl groups bound to the same halide can be regarded as CH_3 > CH_3CH_2 > secondary > cyclohexyl.[3, 26, 47]

The alkyl halide (e.g. methyl iodide) has to be the reacting species unless the mechanism is purely ionic. It is anticipated that a nucleophilic attack by the rhodium electron pair on the methyl group takes place during one of the stages, with the corresponding transfer of the iodine atom to the metal (**Figure 3.9**).

During such an attack, the methyl iodide molecule can either be free (A), coordinated to the attacking rhodium via iodine (B), or coordinated to a rhodium atom in another molecule (C).[48]

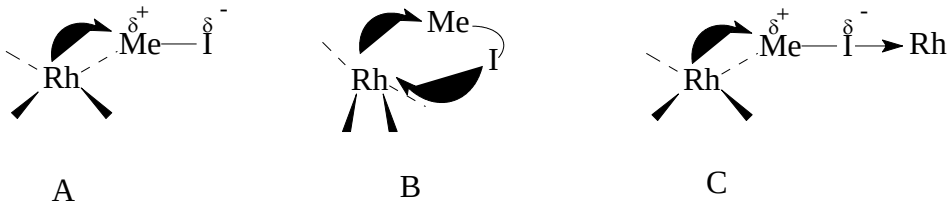

A B C

Figure 3.9: Nucleophilic attack of the rhodium electron pair on the methyl group with corresponding transfer of the iodine atom to the metal.[48]

3.3.4 The solvent

Results obtained from different studies also indicated that the medium in which the oxidative addition reaction occurs plays a vital role in the total progress of the reaction. It was found that not only influence the solvent the reaction rate of the reaction,[3, 26, 42] but also the mechanism of the reaction,[49] the stereochemistry of the intermediates and the products,[50] as well as the composition and the ratio of products.[26, 51] Distinguishing between effects or identifying the exact influence of the solvent is not self-evident because the choice of solvent may simply affect the progress of the reaction by differentially changing the rates of competing pathways and can only be traced back to fundamental physical or chemical properties of solvents.

Protic solvents such as water, methanol, formamide, hydrogen fluoride and ammonia have the ability to form strong hydrogen bonds. Dipolar aprotic solvents such as

[48] J.P. Collman, D.W. Murohy and G. Dolcetti, *J. Am. Chem. Soc*., **95**, (1973), 2687.
[49] R.G. Pearson and Rajaram, *Inorg. Chem*., **13**, (1974), 246.

[50] D.M. Blake and M. Kubota, *Inorg. Chem*., **9**, (1970), 989.

[51] J.P. Collman, , M. Kubota, F.D. Vastine, J.Y. Sun and J.W. Wang, *J. Am. Chem. Soc*., **90**, (1968), 5430.

dimethyl formamide (DMF), dimethyl sulphoxide (DMSO), acetone, acetonitrile and nitromethane are highly polar in nature, but can only be regarded as very weak hydrogen bond donors. The phenomenon of hydrogen bonding may be regarded as an important interaction during the reaction in determining the protic/dipolar aprotic solvent effects on reaction rates according to this classification.[52]

Another important property of a solvent is its donicity which is a measure of the kinetic concept of nucleophilicity. Donicity can be regarded as the ability of a Lewis base to act as an incoming ligand to influence the rate of a nucleophilic substitution reaction. Essentially donicity can be used as a qualitative value, like electronegativity. Donicity values,[53] together with dielectric constants of a number of known solvents are given in **Table 3.4**.

Table 3.4: Donicity values and dielectric constants of a number of known solvents.[53]

Solvent	**Dn**	**ε**
1,2-Dicloroethane	0	10.1
Benzene	0.1	2.28
Nitromethane	2.7	38.9
Acetonitrile	14.1	38.0
Ethyl acetate	17.1	6.0
Methanol	19	32.6
Dimethylforamide	26.6	36.1
Dimethylsulphoxide	29.8	45.0

Generally speaking, the ionization ability of a solvent increases with an increase in donicity and dielectric constant and leads to an increase in oxidative addition reactions.

[52] A.J. Parker, *Chem. Rev*., 69, (1969), 1.
[53] U. Mayer and V. Gutmann, *Adv. Inorg. Chem. Radiochem*., **17**, (1975), 189.

Ugo[22] *et al* observed large ΔS*-values and solvent effects for oxidative addition of *trans*-[IrCl(CO){P(Et_nPh_{3-n})$_3$}$_2$] with alkyl halides. These observations could not only be attributed to the significant dipolar interaction between the addend and the metal complex (S_N2-type), but also to the large degree of transformation postulated for the three-centered transition state that leads to retention or inversion of configuration at the carbon.

Large negative ΔS*-values will indicate significant solvent dependency for reactions which proceeds *via* dipolar intermediates according to Haga, Kawakami and Tanaka.[54] These large ΔS*-values for polar solvents, like acetone or acetonitrile, is attributed to the presence of strongly orientated solvent molecules which surrounds the cationic complex during charge separation induced by the formation of a dipolar intermediate or activated complex.

A negative value for ΔS* and a small ΔH*-value should be observed under these conditions for a polar solvent as the dipolar intermediate are stabilized through solvation.

In spite of the above-mentioned explanation, it is not always possible to determine the exact role of the solvent during oxidative addition since the reaction between the solvent and the transition metal complexes can also destabilize the metal complex.[54] The role of the solvent during the above mentioned reactions are further complicated by the reaction of the solvent with the addenda.

3.3.5 Catalysis

Research has shown that the catalysis by iodide ions plays an important role in oxidative addition. Results obtained from a study involving the iodide-catalyzed methyl iodide

[54] M. Haga, K. Kawakami and T. Tanaka, *Inorg. Chim. Acta*, **12**, (1975), 93.

addition to $[RhI(CO)L_2]$[55] (L = $AsPh_3$ or $SbPh_3$, but not PPh_3), it was found that L is substituted by an iodide ion (**Reaction 3.12**). These results also indicated that the newly formed anionic complex then reacts much more rapidly with CH_3I than the neutral starting complex if the reaction proceeds *via* an electrophilic attack at the metal as expected.

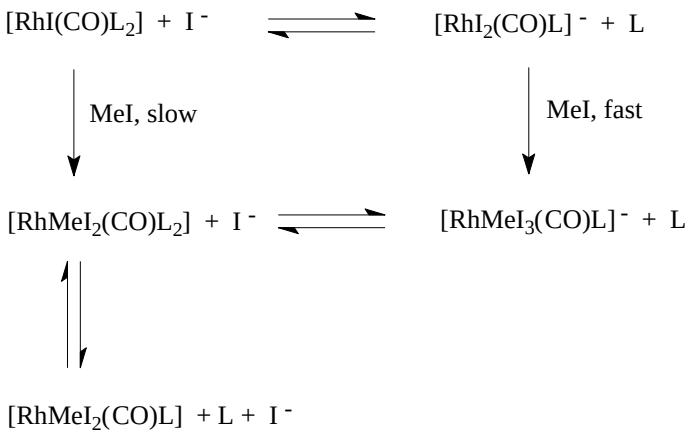

3.12[55]

These systems are quite uncommon, and the operation thereof can have interesting outcomes. The dissociation of triarylphosphine, resulting from the reaction between $[RhI(CO)L_2]$ and CH_3I can react to form $[PAr_3Me]^+I^-$. This iodide ion can in turn coordinates with rhodium to form $[RhClI_2(CO)L]^-$, that reacts more rapidly than the original complex.[56] Characteristic of these kind of reactions are the presence of induction periods at the start of the reaction.[4, 56]

Iodide ion catalysis of a different kind was found with $[Ir(COD)(phen)]^+$.[57] In this study it was found that I^- does not substitute another ligand, but adds to the $[Ir(COD)(phen)]^+$ complex to form the five-coordinated [IrI(COD)(phen)] which in turn undergoes a more rapid addition reaction with CH_3I than the square-planar complex (**Reaction 3.13**).

[55] D. Forster, *J. Am. Chem. Soc*., 97, (1975), 951.
[56] S. Franks, F.R. Hartley and J.R. Chipperfield, *Inorg. Chem*., **20**, (1981), 3238.

[57] D.J.A. De Waal, T.I.A. Gerber and W.J. Louw, *Inorg. Chem*., **21**, (1982), 1259.

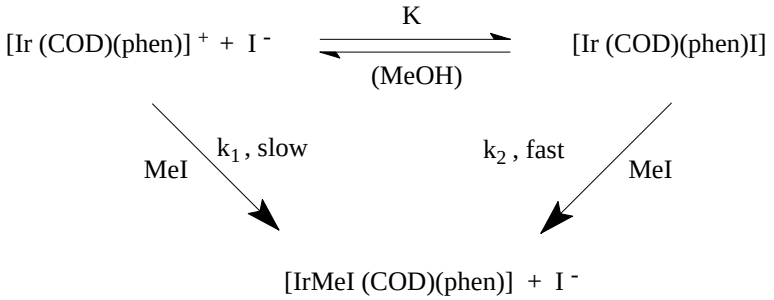

3.13[57]

Results obtained from the oxidative addition reaction between [Rh(cupf)(CO)(PX_3)][58] and CH_3I, indicated a reaction mechanism where the reaction proceeds through two competing rate-determining steps. The k_1 path implied a nucleophilic attack on CH_3I, giving a 16 electron five–coordinated intermediate, whereas the solvent-assisted k_2 path proceeds *via* a solvent-stabilized trigonal bipyrimidal intermediate. The solvent-assisted k_2 path was also viewed as an oxidative addition catalysis phenomenon similar to the solvent effects in the migratory insertion of CO into transition metal alkyl bonds.

The fast dissociative trapping of the solvent-stabilized trigonal bipyrimidal intermediate by CH_3I during its conversion to the ionic intermediate of the k_1 path was proposed. This solvent-stabilized intermediate, being still a Rh(I) complex, is also expected to be much more reactive towards CH_3I, since the stereo chemical transformation, similar to that of the ionic intermediate, has already been taken care of during the k_2 step.

In conclusion, research results and examples have shown that various factors like the metal, bound ligands, addenda and the solvent influenced the reaction rate and product formation during oxidative addition. During oxidative addition the driving force is associated with the increase in stability of the complex. There were also a few requirements before oxidative addition reactions could take place. These results also indicated or confirmed that a number of prerequisites are necessary for oxidative addition to take place, such as the availability of two vacant positions in the coordination sphere of the complex to ensure the formation of two new bonds with the ligands X and Y.

[58] S.S. Basson, J.G. Leipoldt, A. Roodt and J.A. Venter, *Inorg. Chim. Acta*, **128**, (1987), 31.

Chapter 4

Synthesis and characterization of [Rh(LL')(CO)(DPP)] complexes

It is well known that $RhCl_3.3H_2O$ can be used as reagent in die synthesis of rhodium(I) complexes. The tetracarbonyl-μ-dichlorodirhodium(I) dimer, $[RhCl(CO)_2]_2$, that forms after reduction and substitution of $RhCl_3.3H_2O$ can be prepared according to the method described by Varsharski and Cherkasova.[1] The method results in the reduction of rhodium(III) in N,N-dimethylformamide to form the dimer as product. The dimer can then be used *in situ* to react with a bidentate ligand that acts as a precursor in the formation of different rhodium(I) phoshine complexes.

The Lewis basicity of tertiary phosphines as indicated by their respective pK_a values are normally used to indicate their relative nucleophilic contribution and was discussed in detail in **Chapter 3**. The results highlighted the degree of π-back-donation which is prevalent in the complexes. A high degree of σ-donation (high electron donating ability) from phosphorus to rhodium resulted in strong back-donation from rhodium to carbon with weaker CO bonds and a lower carbonyl stretching frequency. Electron withdrawing groups on phosphorus decrease the σ-donation ability of the phosphine which leads to less π-back-donation to carbon and thus higher carbonyl stretching frequencies.

The bulkiness of phosphine ligands (cone angle) also plays a very important role during coordination chemistry and is illustrated in **Figure 4.1.**[2] A phosphine ligand which has the largest σ-donating capability (according to pK_a values) is also one of the bulkier ligands and these properties are working in direct opposition with one another which complicates the interpretation of results.

[1] Y.S. Varsharski, T.G. Cherkasova and J. Russ, *Inorg. Chem*., **12**, (1967)**,** 899.

[2] C.A. Tolman, *Chem. Rev*., **77**, (1977), 313.

This chapter deals with the synthesis and characterization of a number of square planar Rh(I) complexes. IR spectrophotometry and NMR spectrometry were mainly used to identify the different complexes while X-ray crystallography was also employed on one of the starting complexes during the process.

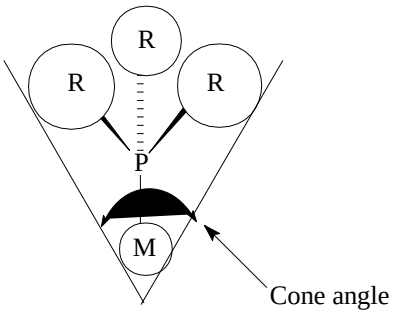

M = metal; R = alkyl, aryl

Figure 4.1: Tolman cone angle.[2]

4.1 Experimental

4.1.1 General experimental conditions

All chemicals used during the synthesis were of reagent grade and were used without further purification. The $RhCl_3.3H_2O$ and diphenyl-2-pyridylphosphine were purchased from Sigma-Aldrich. Solvents were purified and dried prior to use by standard procedures.[3] Material safety data sheets for chemicals used during the synthesis is given in **Appendix B**. IR spectra were recorded with a Digilab FTS 2000 spectrophotometer while the NMR spectra were obtained at 293 K on Bruker 300 and 600 MHz spectrometers.

[3] A.J. Gordon and R.A. Ford, *The Chemist Companion: A Handbook of Practical Data, Techniques and References, John Wiley and Sons, New York,* (1972).

Intensity data were collected at –100 °C on a Bruker APEX(II) CCD area detector diffractometer with graphite monochromated Mo K_α radiation (50kV, 30mA). The collection method involved ϕ and ω-scans of width 0.5°. Data reduction was carried out using the program *SAINT+*[4] and face indexed absorption corrections were made using the program *XPREP*. The crystal structure was solved by direct methods using *SHELXTL*.[5] Non-hydrogen atoms were first refined isotropically followed by anisotropic refinement by full matrix least-squares calculations based on F^2 using *SHELXTL*. Hydrogen atoms were first located in the difference map then positioned geometrically and allowed to ride on their respective parent atoms. Diagrams and publication material were generated using SHELXTL and PLATON.[6]

4.1.2 Synthesis of [Rh(cupf)(CO)$_2$]

A few drops of water were added to 0.5002 g (1.90 mmol) $RhCl_3.3H_2O$. 10 cm^3 N,N-dimethylformamide (DMF) was added and the solution was refluxed until die solution changed colour from red brown to light orange. The solution was filtered and allowed to cool before adding an equivalent amount (0.2947 g, 1.90 mmol) N-phenyl-N-nitrosohydroxylamine ammonium salt (cupf).

$$RhCl_3.3H_2O \xrightarrow[DMF]{\text{reflux}} [RhCl(CO)_2]_2 \xrightarrow{\text{cupferron}} [Rh(cupf)(CO)_2]$$

Subsequently 100 cm^3 water were added to the resulting solution which allowed for the precipitation of the product. The product was filtered and dried in the fume cupboard.

[4] Bruker *SAINT+*, Version 6.02 (includes XPREP and SADABS). *Bruker AXS Inc., Madison, Wisconsin, USA,* (1999).

[5] Bruker SHELXTL, Version 5.1. (includes XS, XL, XP, XSHELL) *Bruker AXS Inc., Madison, Wisconsin, USA,* (1999).

[6] A. L. Spek, *J. Appl. Cryst.***, 36**, (2003), 7-13.

The resulting product was purified by dissolving it in 40 cm^3 acetone, adding charcoal and allowed it to boil for 2 minutes. The solution was then filtered through celite and water was added to the resulting solution to precipitate the final product.

The resulting yellow product was filtered and dried over phosphorus pentoxide over night in a vacuum desiccator. The IR spectrum of $[Rh(cupf)(CO)_2]$ complex is given in **Figure 4.2** while the NMR spectrum is given in **Figure 4.3**.

Results:

Yield: 70 %

IR data: $\nu_{(CO)}$ = 2064 and 2013 cm^{-1}.

^1H NMR($CDCl_3$): δ 7.81(s; CH), 7.50(s; CH), 2.15(s; NH) ppm (s = singlet, d = doublet, t = triplet)

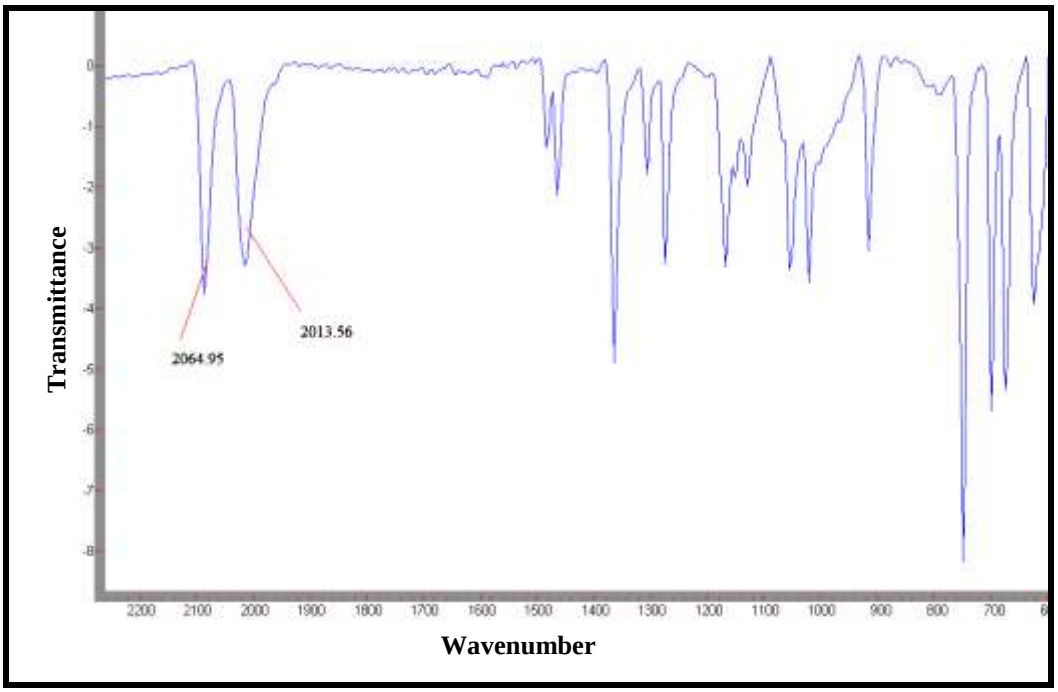

Figure 4.2: IR spectrum of pure $[Rh(cupf)(CO)_2]$.

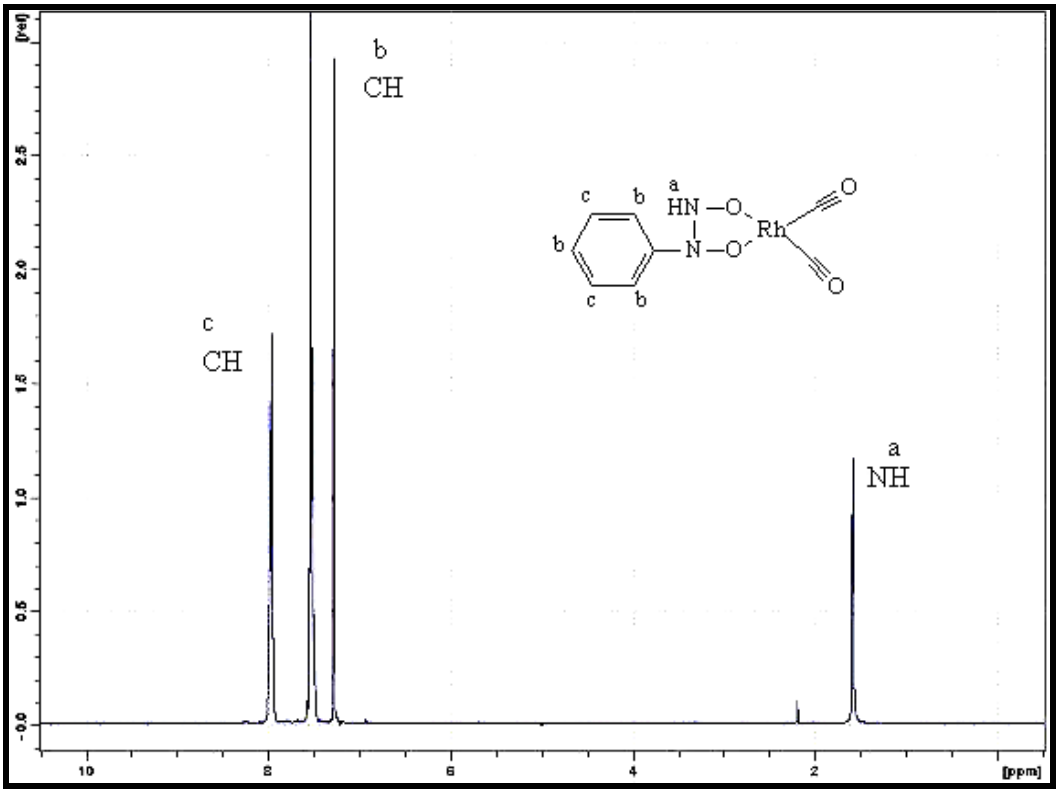

Figure 4.3: ^{1}H-NMR spectrum of [Rh(cupf)$(CO)_2$] in $CDCl_3$.

4.1.3 Synthesis of [Rh(cupf)(CO)(DPP)]

0.2001 g (0.64 mmol) [Rh(cupf)$(CO)_2$] was dissolved in 10 cm^3 methanol. To this solution 1.2 equivalent (0.2013 g, 0.76 mmol) diphenyl-2-pyridylphoshine was added and heated slightly to 30 °C for 5 minutes. The colour of the solution changed from yellow to red and a yellow [Rh(cupf)(CO)(DPP)] product started precipitating immediately.

$$[Rh(cupf)(CO)_2] + 1.2 \text{ eq DPP} \xrightarrow{\text{MeOH}} [\text{ Rh(cupf)(CO)(DPP)}]$$

The solution was filtered, washed with methanol and then dried in the fume cupboard. The IR spectrum of [Rh(cupf)(CO)(DPP)] complex is given in **Figure 4.4** while the NMR spectrum is given in **Figure 4.5** and **Figure 4.6**.

Results:

Yield: 60 %

IR data: $\nu_{(CO)}$ = 1981 cm^{-1}.

^{1}H NMR($CDCl_3$): δ 8.81(s; CH), 8.05(s; CH), 7.81(s; CH), 7.50(s; CH), 7.36(s; CH), 3.51 (s; CH), 2.15(s; NH) ppm (s = singlet, d = doublet, t = triplet)

^{31}P NMR ($CDCl_3$, p.p.m..): [δ, ^{1}J(Rh–P) = 170.19 Hz]

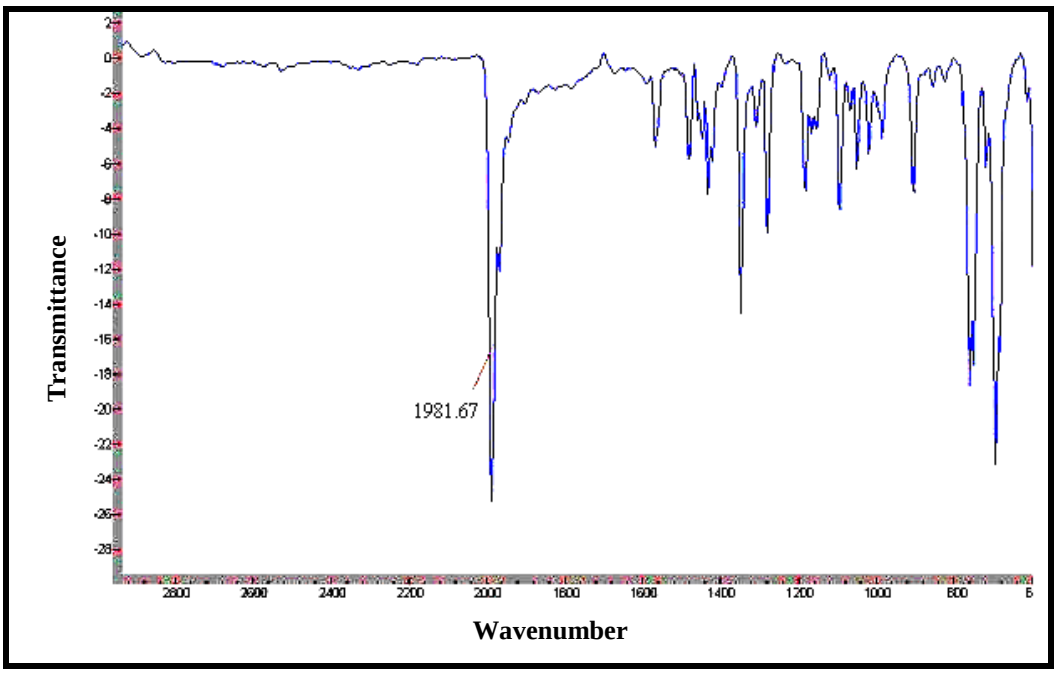

Figure 4.4: IR spectrum of pure [Rh(cupf)(CO)(DPP)]

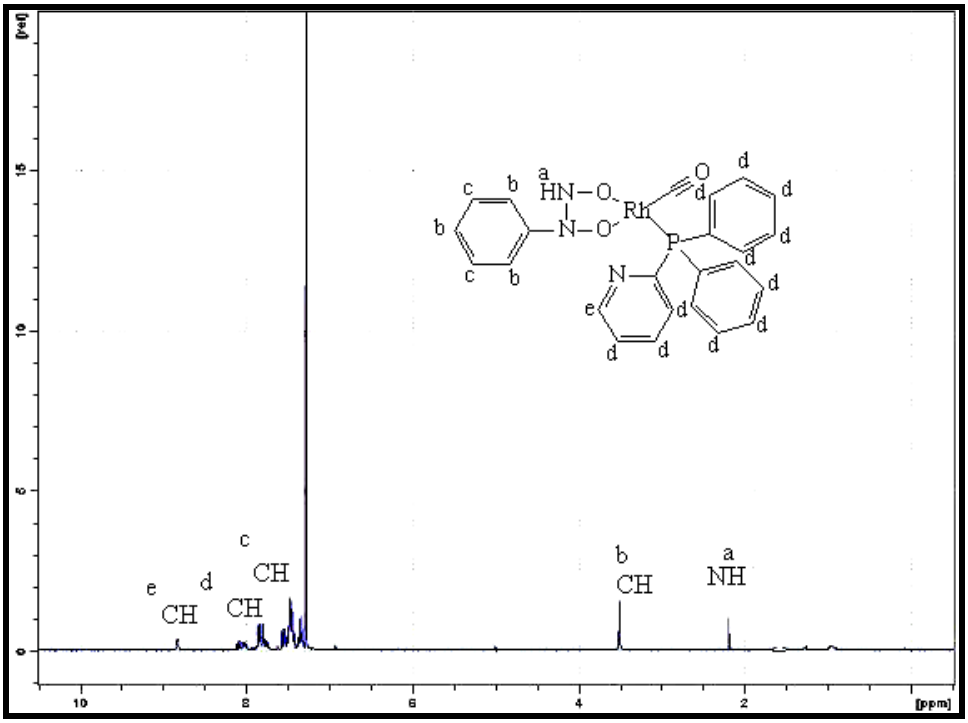

Figure 4.5: ^{1}H-NMR spectrum of [Rh(cupf)(CO)(DPP)] in $CDCl_3$.

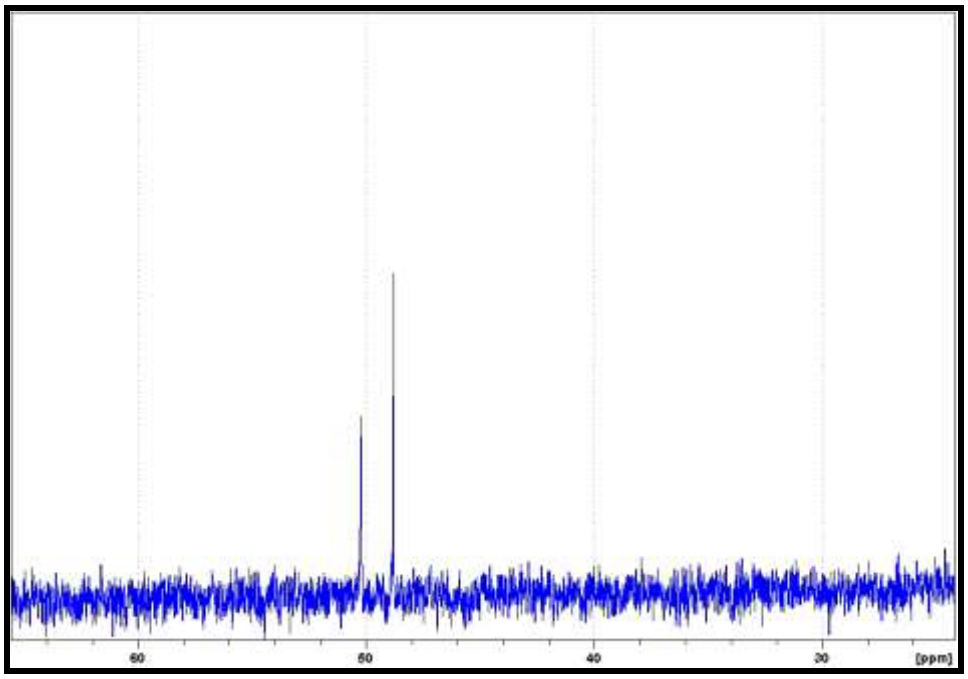

Figure 4.6: ^{31}P-NMR spectrum of [Rh(cupf)(CO)(DPP)] in $CDCl_3$

4.1.4 Synthesis of [Rh(cupf)(CH_3)(CO)(DPP)(I)]

0.2501 g (0.46 mmol) [Rh(cupf)(CO)(DPP)] was dissolved in 5 cm^3 chloroform. To this solution 0.28 cm^3 (4.55 mmol, 0.64 g) CH_3I (10 x excess) was added. The solution was closed for 20 minutes and the colour of the solution changed from orange to red brown. After completion of the reaction the solvent was allowed to evaporate to form [Rh(cupf)(CH_3)(CO)(DPP)(I)] as final product.

$$[Rh(cupf)(CO)(DPP)] + CH_3I \longrightarrow [Rh(cupf)(CH_3)(CO)(DPP)(I)]$$

The IR spectrum of [Rh(cupf)(CH_3)(CO)(DPP)(I)] complex is given in **Figure 4.7** while the NMR spectrum is given in **Figure 4.8**.

Results:

IR data: $\nu_{(CO)}$ = 2060 cm^{-1}.

^{1}H NMR($CDCl_3$): δ 8.81(s; CH), 8.05(s; CH), 7.81(s; CH), 7.50(s; CH), 7.36(s; CH), 3.51 (s; CH), 2.15(s; NH), 1.60(s; CH_3) ppm (s = singlet, d = doublet, t = triplet)

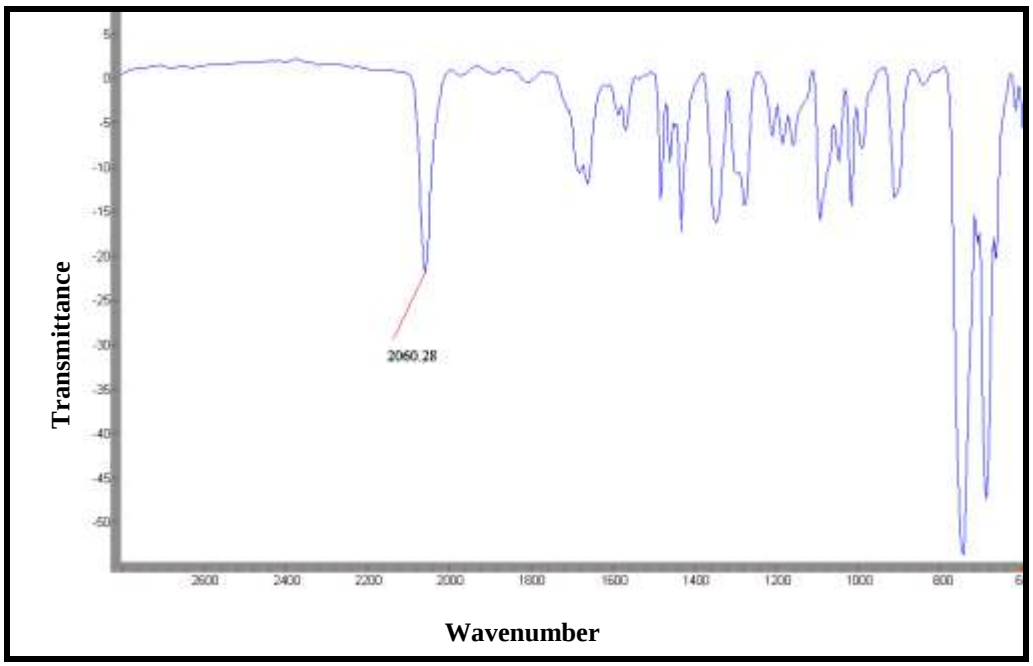

Figure 4.7: IR spectrum of pure [Rh(cupf)(CH_3)(CO)(DPP)(I)]

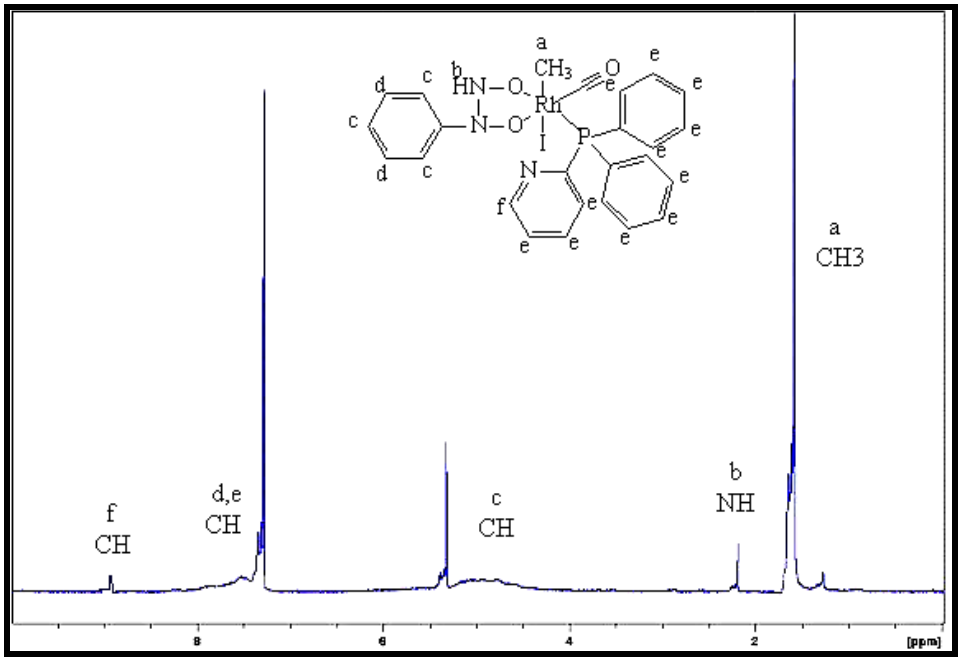

Figure 4.8: ^{1}H-NMR spectrum of [Rh(cupf)(CH_3)(CO)(DPP)(I)] in $CDCl_3$.

4.1.5 Synthesis of [Rh(acac)$(CO)_2$]

A few drops of water were added to 0.5135 g (1.95 mmol) $RhCl_3.3H_2O$. 10 cm^3 N,N-dimethylformamide (DMF) was added and the solution was refluxed until die solution turned from red brown to light orange. The solution was then filtered and allowed to cool before adding an equivalent amount (0.20 cm^3, 1.95 mmol) of acetyl acetone (acac).

$$RhCl_3.3H_2O \xrightarrow[DMF]{\text{reflux}} [RhCl(CO)_2]_2 \xrightarrow{\text{acac}} [Rh(acac)(CO)_2]$$

Water (100 cm^3) was added to this solution which allowed for the precipitation of the product. The reddish/purple product was centrifuged and washed several times with water. The resulting product was purified by recrystallization in acetone.

The IR spectrum of [Rh(acac)$(CO)_2$] complex is given in **Figure 4.9** while the NMR spectrum is given in **Figure 4.10**.

Results:

Yield: 69 %

IR data: $\nu_{(CO)}$ = 2063 and 2001 cm^{-1}.

^1H NMR($CDCl_3$): δ 3.38(d; CH), 2.05(s; CH), 1.54(s; CH_3), 1.21(d;CH_3) ppm (s = singlet, d = doublet, t = triplet)

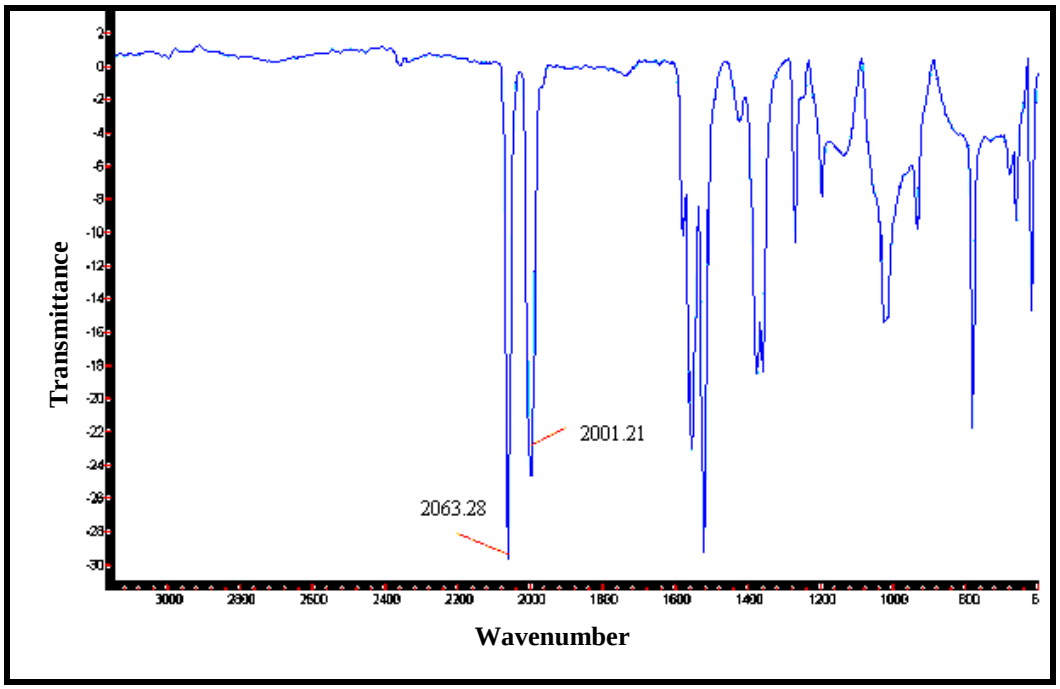

Figure 4.9: IR spectrum of pure [Rh(acac)$(CO)_2$].

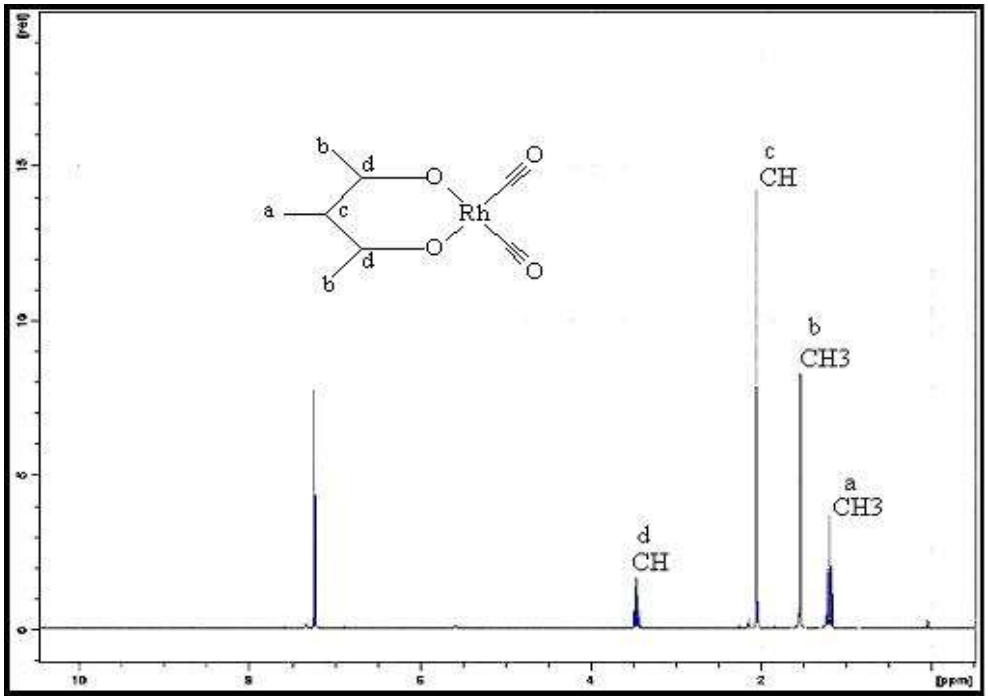

Figure 4.10: ^{1}H-NMR spectrum of [Rh(acac)$(CO)_2$] in $CDCl_3$.

4.1.6 Synthesis of [Rh(acac)(CO)(DPP)]

0.1968 g (0.76 mmol) [Rh(acac)$(CO)_2$] was dissolved in 10 cm^3 methanol. To this solution an equivalent amount of diphenyl-2-pyridylphoshine (0.2000 g, 0.76 mmol) was added and heated slightly to 30 °C for 5 minutes. The colour of the solution changed from yellow to red and the yellow [Rh(acac)(CO)(DPP)] product precipitated from the solution.

$$[Rh(acac)(CO)_2] + \text{eq DPP} \xrightarrow{\text{MeOH}} [\text{Rh(acac)(CO)(DPP)}]$$

The product was filtered, washed with methanol and dried in the fume cupboard.

The IR spectrum of [Rh(acac)(CO)(DPP)] complex is given in **Figure 4.11** while the NMR spectra is given in **Figure 4.12** and **Figure 4.13**.

Results:

Yield: 60 %

IR data: $\nu_{(CO)}$ = 1976 cm^{-1}.

^{1}H NMR($CDCl_3$): δ 7.81(d; CH), 7.31(t; CH), 3.38(d; CH), 2.05(s; CH), 1.54(s; CH_3), 1.21(d;CH_3) ppm (s = singlet, d = doublet, t = triplet)

^{31}P NMR ($CDCl_3$, p.p.m..): [δ, ^{1}J(Rh–P) = 175.42 Hz]

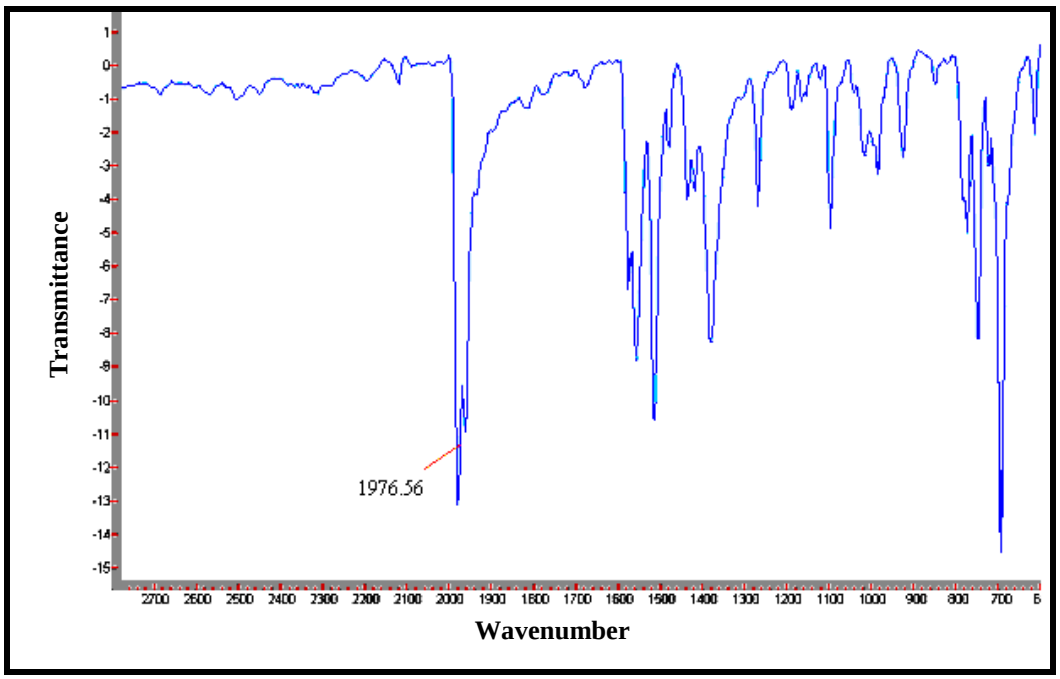

Figure 4.11: IR spectrum of pure [Rh(acac)(CO)(DPP)].

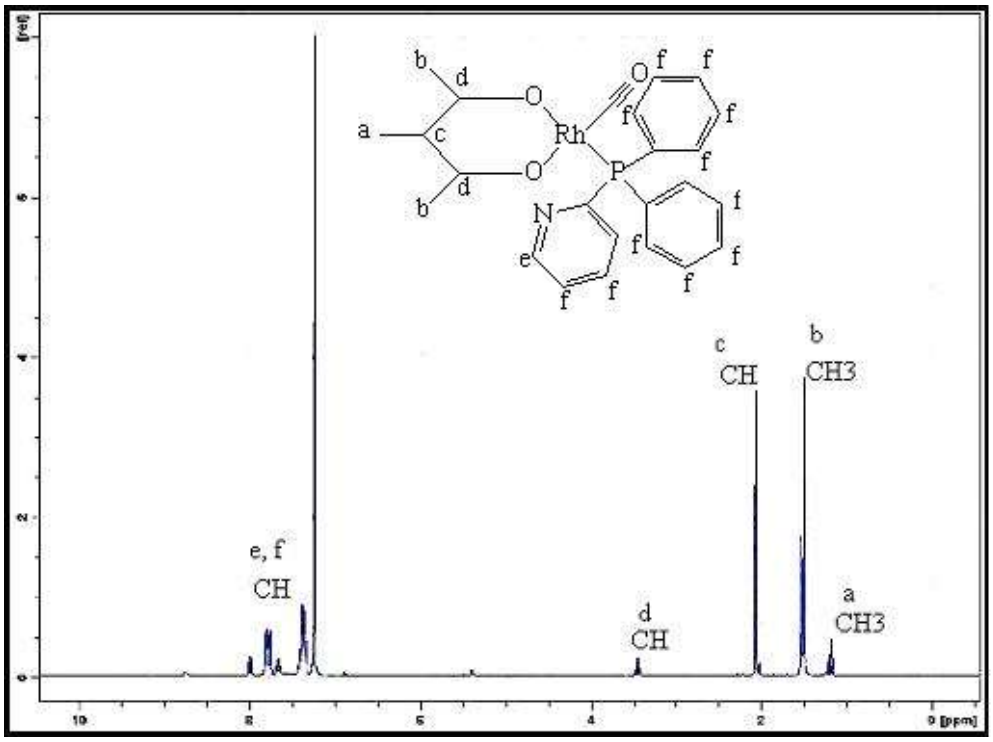

Figure 4.12: ^{1}H-NMR spectrum of [Rh(acac)(CO)(DPP)] in $CDCl_3$.

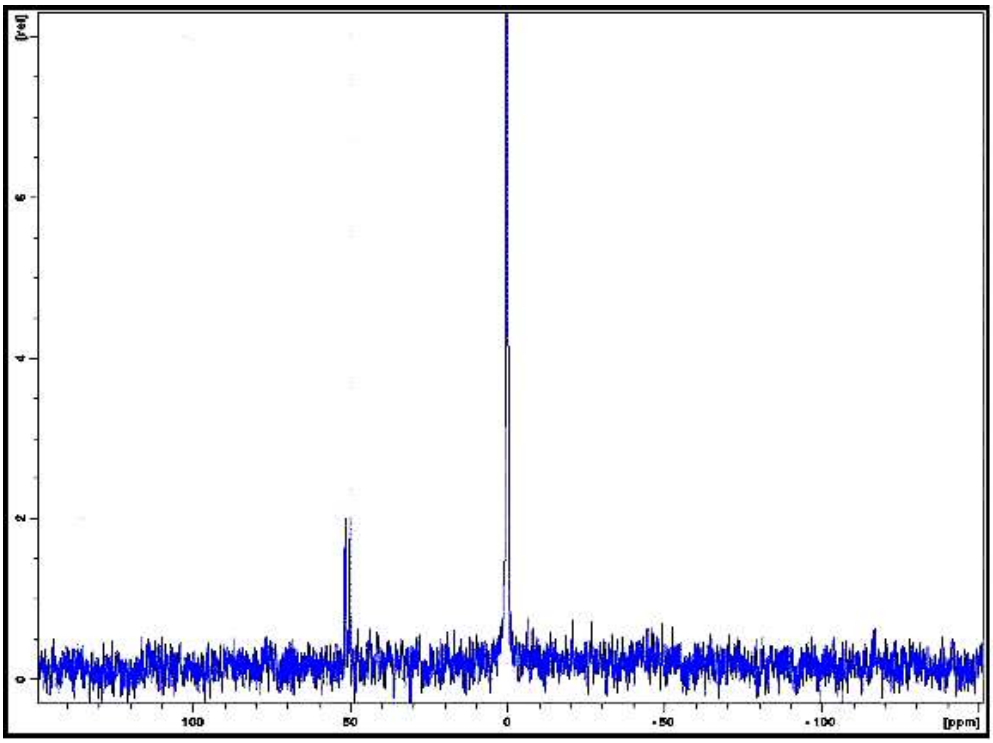

Figure 4.13: ^{31}P-NMR spectrum of [Rh(acac)(CO)(DPP)] in $CDCl_3$.

Table 4.1: Summary of IR data for the different rhodium(I) complexes synthesized.

Complex	**ν(CO) (cm $^{-1}$)**
[Rh(cupf)$(CO)_2$]	2064, 2013
[Rh(cupf)(CO)(DPP)]	1981
[Rh(cupf)(CH_3)(CO)(DPP)(I)]	2060
[Rh(acac)$(CO)_2$]	2060, 2001
[Rh(acac)(CO)(DPP)]	1976

Table 4.2: Summary of ^{1}H-NMR data for the different rhodium(I) complexes synthesized.

Complex	**δ ppm**.
[Rh(cupf)$(CO)_2$]	7.81(s; CH), 7.50(s; CH), 2.15(s; NH) ppm
[Rh(cupf)(CO)(DPP)]	8.81(s; CH), 8.05(s; CH), 7.81(s; CH), 7.50(s; CH), 7.36(s; CH), 2.15(s; NH)
[Rh(cupf)(CH_3)(CO)(DPP)(I)]	8.81(s; CH), 8.05(s; CH), 7.81(s; CH), 7.50(s; CH), 7.36(s; CH), 2.15(s; NH), 1.60 (s; CH_3)
[Rh(acac)$(CO)_2$]	3.38(d; CH), 2.05(s; CH), 1.54(CH_3; s), 1.21(d;CH_3)
[Rh(acac)(CO)(DPP)]	7.81(d; CH), 7.31(t; CH), 3.38(d; CH), 2.05(s; CH), 1.54(CH_3; s), 1.21(d;CH_3)

Table 4.3: Summary of ^{31}P-NMR data for the different rhodium(I) complexes synthesized.

Complex	**^{1}J(Rh–P)**
[Rh(cupf)(CO)(DPP)]	175.42
[Rh(acac)(CO)(DPP)]	170.19

4.1.7 Discussion

A comparison between the IR spectra of the rhodium dicarbonyl complex and that of the substituted carbonyl complex clearly show the disappearance of one of the carbonyl stretching frequencies confirming the displacement of one of the carbonyl ligands by the phosphine ligand. In both cases the stretching frequency of the mono substituted carbonyl shifted to a lower wavelength. This is in accordance with other complexes[7] indicating an increase in electron density on the metal center which can be attributed to the Lewis basicity of the phosphine and the absence of competition by the other carbonyl ligand. The decrease in ν(CO) indicates an increase in the metal-carbon π-backbonding and a decrease in carbon-oxygen triple bond character. The IR spectra collected during the formation of the oxidative addition product, [Rh(cupf)(CH_3)(CO)(DPP)(I)], clearly show the disappearance of the Rh(I)-carbonyl peak at 1981 cm^{-1} with the formation of a Rh(III)-carbonyl peak at 2060 cm^{-1}. The higher value obtained for the Rh(III)-complex illustrates that there is less metal to carbon electron back donation as is the case for the Rh(I)-complex

Basson and co-workers[8, 9] studied the influence of different phosphine ligands on the electron density of the rhodium atom. The results are summarized in **Table 4.4**[8] to **Table 4.6**[9] for the different complexes that were investigated.

[7] A.M. Trzeciak and J.J. Ziólkowski, *Inorg. Chim. Acta*, **96**, (1985), 15.

[8] S.S. Basson, J.G. Leipoldt, A. Roodt, J.A. Venter and T.J. van der Walt, *Inorg. Chim. Acta*, **119**, (1986), 35.

[9] S.S. Basson, J.G. Leipoldt, A. Roodt and J.A. Venter, *Inorg. Chim. Acta*, **118**, (1986), L45.

Table 4.4: Carbonyl stretching frequencies for [Rh(acac)(CO)(PX_3)] complexes.

PX_3	ν(CO) (cm^{-1})
P(*ρ*-PhCl)$_3$	2056
PPh_3	2060
P(*ρ*-PhOMe)$_3$	2056
DPP	1980*

* This study

Table 4.5: Carbonyl stretching frequencies for [Rh(cupf)(CO)(PX_3)] complexes.

PX_3	ν(CO) (cm^{-1})
DPP	1989*
$PPh_2C_6F_5$	1983
PPh_3	1982
P(*ρ*-ClC_6H_4)$_3$	1977
P(*ρ*-$MeOC_6H_4$)$_3$	1971
P(*ρ*-Tol)$_3$	1971
PCy_3	1959

* This study

Table 4.6: Carbonyl stretching frequencies for [Rh(cupf)(CH_3)(CO)(PX_3)(I)] complexes.

PX_3	ν(CO) (cm^{-1})
P(*ρ*-ClC_6H_4)$_3$	2072
PPh_3	2068
P(*ρ*-$MeOC_6H_4$)$_3$	2066
DPP	2060*
PCy_3	2056

* This study

If the IR data found for the substituted complexes synthesized during the study are compared to those that Basson and co-workers found, it can be concluded that the phosphine under investigation has good electron donating properties to increase the electron density on the rhodium atom and so decrease the ν(CO) (electronic effect). As can be seen in **Table 4.4** to **4.6** the type of β-diketone coordinated to the metal center also has an effect on the ν(CO). In **Table 4.4** the [Rh(acac)(CO)(DPP)] complex has a lower ν(CO) compared to those previously investigated, while in **Table 4.5** and **4.6** the [Rh(cupf)(CO)(DPP)] has a higher ν(CO). This can be explained by the electron withdrawing groups (NH) on the cupferron ligand that decreases the electron density on the metal center which leads to an increase in ν(CO). In the acac complex there are only CH_3 groups that draw electron density away from the metal center. The effect of this increase in electron density on the metal center was kinetically investigated and its effect on oxidative addition will be discussed in **Chapter 5**.

The ^{1}H-NMR results for the mono carbonyl complexes obtained in the current study clearly show an up-field shift of new peaks compared to the dicarbonyl complexes and confirm a change in the chemical environment in the metal complex which correlates with the substitution of one of the carbonyl ligands by a phosphine ligand. The up-field chemical shift also confirms to an increase in electron density around the metal center by the electron donating character of the phosphine ligand. The ^{1}H-NMR spectrum for [Rh(cupf)(CH_3)(CO)(DPP)(I)] shows a down-field shift of a new peak compared to the mono carbonyl complex confirming a change in the chemical environment in the metal complex which correlates with the addition of a methyl group to the corresponding complex. The ^{31}P-NMR data of the synthesized complexes were also compared to other [Rh(LL')(CO)(PX_3)] complexes and are summarized in **Table 4.7**.

Table 4.7: Summary of ^{31}P-NMR data for different [Rh(LL')(CO)(PX_3)] complexes.[10, 11, 12, 13]

LL'	^{1}J(Rh–P)
acac	175.42*
acac	175.7
cupf	171.1
cupf	170.19*
pic	161.9
ox	161.6
hpt	157.1
hacsm	148.9
dmavk	148.0

*This study

As can be seen from **Table 4.7** the ^{1}J(Rh–P) values of 175.42 and 170.19 Hz for the [Rh(acac)(CO)(DPP)] and [Rh(cupf)(CO)(DPP)] respectively, correlated well with those of other complexes found in the literature.

The IR and ^{1}H-NMR data confirmed the forming of the mono substituted and oxidative addition complexes synthesized and correlates well with the values found in the literature.[7, 8, 9]

[10] D.E. Graham, G.J. Lamprecht, I.M. Potgieter, A. Roodt and J.G. Leipoldt, *Trans. Met. Chem*., **16**, (1991), 193.

[11] G.J.J. Steyn, A. Roodt, I. Poletaeva and Y. Varshavsky, *J. Organomet. Chem*., **536**, (1997), 797.

[12] S.S. Basson, J.G. Leipoldt, A. Roodt and H. Preston, *Acta Cryst*., **C47**, (1991), 1961.

[13] G.J.J. Steyn, A. Roodt and J.G. Leipoldt, *Rhodium Ex*., 1, (1993), 25.

4.2 X-ray crystallography

It was decided to include the ground state stereochemistry of the starting complexes in this study. These studies were undertaken to identify the reactants with certainty, as well as to help with the interpretation of kinetic data. All the efforts to recrystallize [Rh(cupf)(CO)(DPP)] resulted in the formation of an oily substance and hence no crystals were obtained to study. However, the crystallization of the [Rh(acac)(CO)(DPP)] complex resulted in the crystallization of the complex in two different space groups when using two different solvents, namely chloroform and diethyl ether. All the bond distances, angles and anistropic thermal parameters are given in **Appendix A**.

4.2.1 Experimental procedure for crystal growth

Monoclinic space group

$[Rh(acac)(CO)_2]$[14] (0.0109 g, 0.042 mmol) was dissolved in methanol (5 cm^{-3}). Diphenyl-2-pyridylphosphine (0.0111 g, 0.042 mmol) was added to this solution. The solution was stirred until a yellow precipitate formed. The product was dissolved in 5 cm^{-3} diethyl ether and filtered. Yellow crystals were obtained after 24 h.

Triclinic space group

$[Rh(acac)(CO)_2]$[14] (0.0109 g, 0.042 mmol) was dissolved in methanol (5 cm^{-3}). Diphenyl-2-pyridylphosphine (0.0111 g, 0.042 mmol) was added to this solution. The solution was stirred until a yellow precipitate formed. The product was dissolved in 5 cm^{-3} chloroform and filtered. Yellow crystals were obtained after 24 h.

[14] J. G. Leipoldt, S. S. Basson, L. D. C. Bok and T. I. A. Gerber, *Inorg. Chim. Acta*, **26**, (1978), L35–L37

4.2.2 Monoclinic space group

The crystal data and refinement parameters for both space groups are summarized in **Table 4.8**. A perspective view of monoclinic [Rh(acac)(CO)(DPP)] is presented in **Figure 4.14** and the most important bond lengths and bond angles are given in **Table 4.9** and **Table 4.10** respectively.

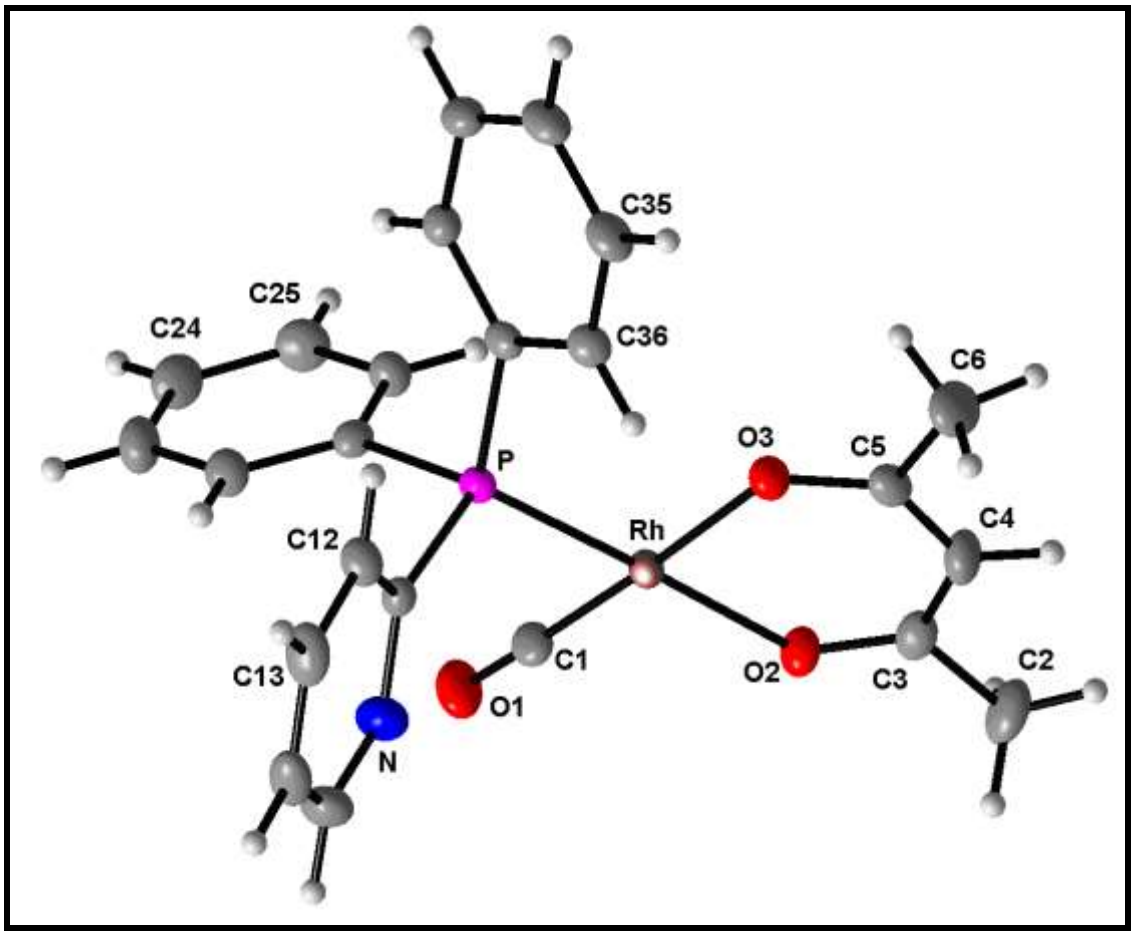

Figure 4.14: The structure of monoclinic [Rh(acac)(CO)(DPP)] showing the atom numbering scheme. Displacement ellipsoids are drawn at the 50% probability level.

Table 4.8: Crystal data and refine parameters for [Rh(acac)(CO)(DPP)].

	Monoclinic	**Triclinic**
Identification code	6imc1_0m	6imc2_0m
Empirical formula	$RhC_{23}H_{21}NO_3P$	$RhC_{23}H_{21}NO_3P$
Formula weight	493.29	493.29
Temperature	293(2) K	293(2) K
Wavelength	0.71069 Å	0.71073 Å
Crystal system	Monoclinic	Triclinic
Space group	$P2_1/n$	$P\bar{1}$
Unit cell dimensions	a = 8.814(5) Å b = 17.756(5) Å c = 13.754(5) Å; α = 90.000(5)° β = 103.170(5)° γ = 90.000(5)°	a = 8.814(5) Å b = 12.793(3) Å c = 18.629(4) Å; α = 104.57(3)° β = 100.06(3)° γ = 106.83(3)°
Volume	2095.9(15) $Å^3$	2145.6(7) $Å^3$
Z	4	4
Density (calculated)	1.563 Mg/m^3	1.527 Mg/m^3
Absorption coefficient	0.915 mm^{-1}	0.894 mm^{-1}
F(000)	1000	1000
Crystal size	0.19 x 0.13 x 0.12 mm^3	0.19 x 0.13 x 0.12 mm^3
Theta range for data collection	2.51 to 28.31°	2.19 to 25.68°
Index ranges	-11<=h<=11, -23<=k<=23, -18<=l<=18	-11<=h<=12, -15<=k<=15, -18<=l<=22
Reflections collected	28772	12389
Independent reflections	5217 [R(int) = 0.0495]	8065 [R(int) = 0.0204]
Completeness to theta	99.9 %	98.9 %
Absorption correction	None	None
Max. and min. transmission	0.8981 and 0.8453	0.8981 and 0.8453
Refinement method	Full-matrix least-squares on F^2	Full-matrix least-squares on F^2
Data / restraints / parameters	5217 / 0 / 264	8065 / 0 / 527
Goodness-of-fit on F^2	1.053	1.020
Final R indices [I>2sigma(I)]	R1 = 0.0281, wR2 = 0.0610	R1 = 0.0308, wR2 = 0.0757
R indices (all data)	R1 = 0.0374, wR2 = 0.0653	R1 = 0.0430, wR2 = 0.0824
Largest diff. peak and hole	0.423 and -0.433 $e.Å^{-3}$	0.388 and -0.433 $e.Å^{-3}$

Table 4.9: Selected bond lengths (Å) for monoclinic [Rh(acac)(CO)(DPP)].

Bond	Length (Å)	Bond	Length (Å)
Rh-C1	1.810(2)	P-C31	1.821(2)
Rh-O3	2.035(2)	P-C21	1.822(2)
Rh-O2	2.070(2)	P-C11	1.839(2)
Rh-P	2.230(1)	O1-C1	1.147(3)
N-C15	1.359(3)	O2-C3	1.274(3)
N-C11	1.362(3)	O3-C5	1.275(3)

Table 4.10: Selected bond angles (°) for monoclinic [Rh(acac)(CO)(DPP)].

Bond	Angle (°)	Bond	Angle (°)
C1-Rh-O3	177.66(8)	N-C11-C12	122.16(2)
C1-Rh-O2	93.63(8)	N-C11-P	114.49(1)
O3-Rh-O2	88.42(6)	C12-C11-P	123.34(2)
C1-Rh-P	85.26(7)	C31-P-C21	104.54(9)
O3-Rh-P	92.71(4)	N-C15-C14	123.13(3)
O2-Rh-P	178.43(4)	C31-P-C11	103.56(9)
C31-P-Rh	116.80(7)	C21-P-C11	103.94(9)
C21-P-Rh	112.61(6)	C22-C21-P	123.18(2)
C11-P-Rh	114.05(6)	C26-C21-P	116.90(2)
C3-O2-Rh	126.64(1)	C15-N-C11	117.22(2)
C5-O3-Rh	127.60(1)	C32-C31-P	121.16(2)
O1-C1-Rh	178.47(2)	C36-C31-P	119.23(2)

The [Rh(acac)(CO)(DPP)] contains a rhodium(I) center which is surrounded by two oxygen atoms of the acac ligand, a carbon atom of the carbonyl ligand and a phosphorus atom of the ligand. The [Rh(acac)(CO)(DPP)] coordination sphere adopts a square-planar geometry with bond angles around the rhodium(I) centre varying between 85.26(7)° and 93.63(8)°. The two phenyl rings and the one pyridine ring of the phosphine ligand are arranged in a face on/edge on orientation, with dihedral angles between the planes formed by these rings ranging between 66.55(7)° and 80.50(7)°. The diphenyl-2-pyridylphosphine ligand is behaving as a monodentate ligand in this complex

although several cases have been reported where it coordinates as a bridging[15] or a bidentate ligand.[16]

4.2.3 Triclinic space group

The crystal data and refinement parameters for both space groups were summarized in **Table 4.8**. A perspective view of triclinic [Rh(acac)(CO)(DPP)] is presented in **Figure 4.15** and the most important bond lengths and bond angles are given in **Table 4.11** and **Table 4.12** respectively.

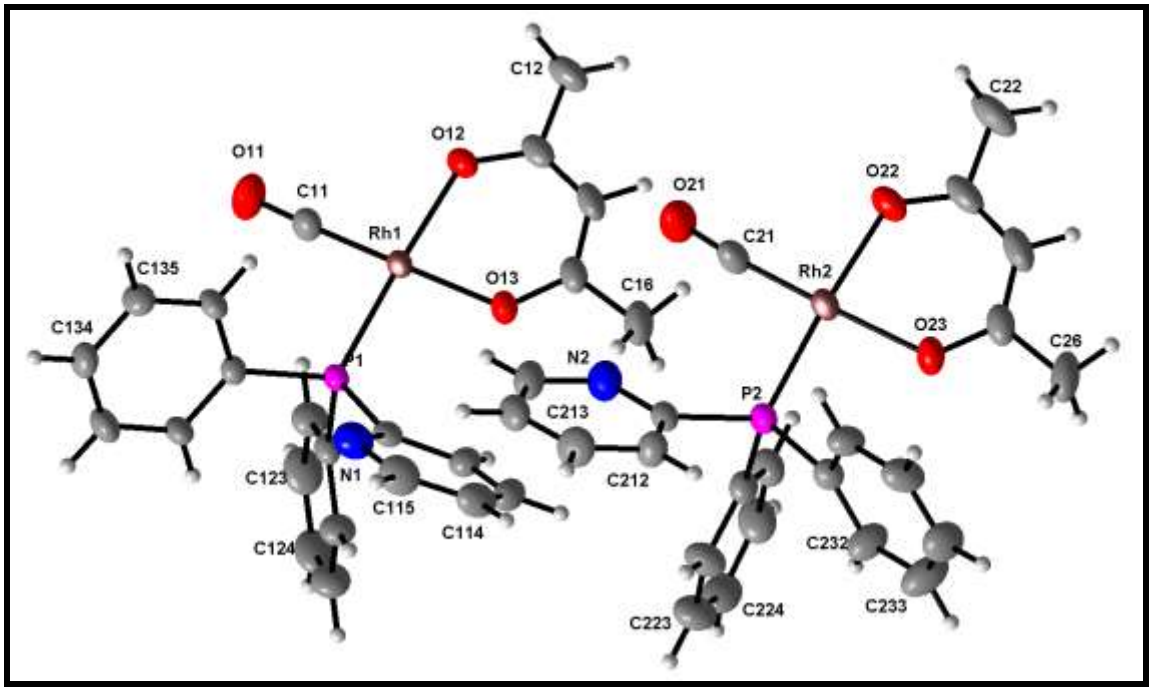

Figure 4.15: The structure of monoclinic [Rh(acac)(CO)(DPP)] showing the atom numbering scheme. Displacement ellipsoids are drawn at the 30% probability level.

[15] J. P. Farr, M. M. Olmstead, F. E. Wood and A. L. Balch, *J. Am. Chem. Soc*., **105**, (1983), 792–798.

[16] M. L. Clarke, A. M. Z. Slawin, M. V. Wheatley and J. D. Woollins, *J. Chem. Soc. Dalton Trans*., (2001), 3421–3423.

Table 4.11: Selected bond lengths (Å) for triclinic [Rh(acac)(CO)(DPP)].

Molecule 1		**Molecule 2**	
Bond	**Length (Å)**	**Bond**	**Length (Å)**
Rh1-C11	1.790(2)	Rh2-C21	1.787(2)
Rh1-O13	2.030(2)	Rh2-O23	2.034(2)
Rh1-O12	2.074(5)	Rh2-O22	2.067(5)
Rh1-P1	2.243(5)	Rh2-P2	2.234(5)
O11-C11	1.150(1)	O21-C21	1.143(2)
P1-C131	1.829(2)	P2-C221	1.826(3)
P1-C111	1.832(4)	P2-C231	1.831(3)
P1-C121	1.835(3)	P2-C211	1.846(1)
N1-C111	1.381(3)	N2-C211	1.361(2)
N1-C115	1.395(2)	N2-C215	1.375(1)

Table 4.12: Selected bond angles (°) for triclinic [Rh(acac)(CO)(DPP)].

Molecule 1		**Molecule 2**	
Bond	**Angle (°)**	**Bond**	**Angle (°)**
C11-Rh1-O13	178.36(1)	C21-Rh2-O23	178.34(1)
C11-Rh1-O12	91.86(2)	C21-Rh2-O22	90.29(2)
O13-Rh1-O12	88.09(9)	O23-Rh2-O22	88.40(1)
C11-Rh1-P1	89.58(1)	C21-Rh2-P2	93.22(1)
O13-Rh1-P1	90.58(7)	O23-Rh2-P2	88.12(9)
O12-Rh1-P1	176.43(7)	O22-Rh2-P2	176.09(7)
C131-P1-Rh1	118.0(1)	C221-P2-Rh2	115.47(1)
C111-P1-Rh1	112.98(1)	C231-P2-Rh2	108.74(1)
C121-P1-Rh1	113.78(1)	C211-P2-Rh2	120.44(1)
C13-O12-Rh1	125.86(2)	C23-O22-Rh2	126.17(2)
C15-O13-Rh1	128.20(2)	C25-O23-Rh2	127.91(2)
O11-C11-Rh1	177.89(3)	O21-C21-Rh2	174.80(4)
C131-P1-C111	102.61(1)	C221-P2-C231	105.03(1)
C131-P1-C121	103.67(1)	C221-P2-C211	101.03(2)
C111-P1-C121	104.24(1)	C231-P2-C211	104.62(2)
C111-N1-C115	117.85(3)	C211-N2-C215	117.27(3)
N1-C111-P1	119.88(2)	N2-C211-P2	115.05(2)

An interesting fact about this structure is that Pī normally requires only two molecules per unit cell which are related normally by a center of symmetry. The fact that four molecules crystallize per unit cell in the current study suggests that the orientation of the two sets of molecules should differ substantially within the cell.

A comparison between the molecules situated in the triclinic space group reveal subtle differences in bond distances and angles. The Rh-CO and Rh-O (*trans* to carbonyl) bond distances are almost identical with a slight difference in the Rh-P (2.243(5) vs 2.234(5) Å) and Rh-O (*cis* to carbonyl) bond distances (2.074(5) vs 2.076(5) Å). The *trans* O-Rh-CO bond angle changes from 89.58(1)° in the one isomer to 93.22(1)° in the other isomer.

Comparing the molecule in the monoclinic space group also demonstrate small changes in bond angles and lengths with the largest difference in the Rh-O (trans to carbonyl) bond length. The bond lengths and angles are almost equal to each other, with the only difference in the position of the nitrogen on the pyridine ring. The nitrogen of the phosphine ligand in the monoclinic and the one in the triclinic space group bonded towards the Rh-CO bond while the other molecule in the triclinic space group bonded away from the Rh-CO bond.

The rhodium bond lengths and angles found for both the mono and triclinic space groups were compared with those found for other [Rh(LL')(CO)(PX_3)] complexes and are summarised in **Table 4.13** and **Table 4.14**. [14, 17, 18]

[17] D. Lamprecht, G. J. Lamprecht, J. M. Botha , K. Umakoshi and Y.Sasaki, Acta Cryst**., C53**, (1997), 1403.

[18] J.G. Leipoldt, L.D.C. Bok, S.S. Basson and H. Meyer, *Inorg. Chim. Acta*., **42**, (1980), 105.

Table 4.13: Selected rhodium bond distances of [Rh(LL')(CO)(PX_3)] complexes.[14, 17, 18]

Complex	Rh-CO (Å)	Rh-P (Å)	Rh-L (*trans*) (Å)	Rh-L' (*cis*) (Å)	CO (Å)
[Rh(cupf)(CO)(PPh_3)]	1.78(1)	2.232(3)	2.063(6)	2.024(6)	1.17(1)
[Rh(acac)(CO)(DPP)]	1.790(2)*	2.230(1)*	2.035(2)*	2.070(2)*	1.147(3)
[Rh(neocupf)(CO)(PPh_3)]	1.802(5)	2.227(1)	2.081(3)	2.025(3)	1.139(5)
[Rh(cupf)(CO){$P(OCH_2)_3CCH_3$}]	1.772(9)	2.156(2)	2.026(5)	2.059(4)	1.155(9)
[Rh(tfdmaa)(CO)(PPh_3)]	1.781(9)	2.239(2)	2.089(4)	2.057(6)	1.159(1)
[Rh(acac)(CO)(PPh_3)]	1.801(8)	2.244(4)	2.087(4)	2.029(5)	1.153(1)
[Rh(dmavk)(CO)(PPh_3)]	1.784(5)	2.275(1)	2.045(4)	2.044(3)	1.142(6)

*This study

(cupf LL' = O,O; acac LL' = O,O; neocupf LL' = O,O; tfdmaa LL' = O,O and dmavk LL' = N,O)

Table 4.14: Selected rhodium bond angles of [Rh(LL')(CO)(PX_3)] complexes.[14, 17, 18]

Complex	Rh-C-O (°)	L-Rh-P (*trans*) (°)	L'-Rh-P (*cis*) (°)	L-Rh-C (*cis*) (°)	L'-Rh-C (*trans*) (°)
[Rh(cupf)(CO)(PPh_3)]	176.3(9)	172.6(2)	96.8(2)	98.1(4)	172.8(3)
[Rh(acac)(CO)(DPP)]	178.47(2)*	178.43(4)*	92.71(4)*	93.63(8)*	177.66(8)*
[Rh(neocupf)(CO)(PPh_3)]	177.3(5)	168.16(9)	90.95(8)	100.5(2)	175.8(2)
[Rh(cupf)(CO){$P(OCH_2)_3CCH_3$}]	174.4(1)	170.8(1)	94.8(1)	99.9(3)	175.6(3)
[Rh(tfdmaa)(CO)(PPh_3)]	178.2(7)	93.7(1)	87.2(2)	87.5(2)	91.7(3)
[Rh(acac)(CO)(PPh_3)]	176.8(9)	92.0(1)	87.8(2)	92.4(2)	128.7(5)
[Rh(dmavk)(CO)(PPh_3)]	177.9(5)	179.3(2)	89.69(1)	87.43(2)	177.9(5)

*This study

As can be seen from **Table 4.13** the Rh-O (*cis* to the carbonyl) distance is longer than the Rh-O (*trans* to the carbonyl) distance and can be explained by the large *trans*-influence of the phosphine ligand under investigation, compared to the carbonyl ligand. The bond angles of 93.63(8)° and 177.66(8) for the *cis* and *trans* O-Rh-C bonds respectively, deviated sightly from the normal expected values for square planar complexes as can be seen in **Table 4.14**. Larger deviations were observed for cupf and neocupf complexes where ring strain due to smaller bite angle of the bidentate ligand dominates. There is also a significant shortening of the Rh-P bond distance due to the steric effect of the DPP ligand (bulky phosphine) and a significant increase in back

donation to the phosphorus atom from the electron rich rhodium center. The Rh-P bond distance and angles are further influenced by the coordinated bidentate ligand. According to published findings[10, 19], the trans influence of the bidentate ligand can be summarised as follows, sulphur > nitrogen > oxygen, and can be explained by the π- and σ-trans-influence.[19] The sulphur atom can form a π-bond with the rhodium atom (greater π-trans-influence), while the nitrogen is less electronegative than the oxygen atom, is a better σ-donor and exert a larger σ-trans-influence. The electronic and the steric effect with regards to the ring size of the bidentate ligand also has an effect on the coordination ability of the coordinatively unsaturated square-planar rhodium complexes under investigation. The ability of the Rh(I) complex to accomadate an increase in coordination number increases with a decrease in bite angle of the bidentate ligand.

The Rh-C-O angle is almost linear (**Table 4.13**) and the Rh-CO bond distance correlated well with those found for similar complexes (**Table 4.12**). The higher electron density on the rhodium center resulted in a stronger Rh-CO bond due to more π back bonding to the π*-orbitals of the carbon atom. This leads to a weaker C-O bond and a decrease in ν(CO).

The bond angles and bond distances of [Rh(acac)(CO)(DPP)] were compared to other [Rh(acac)(CO)(PX_3)][14] complexes and it was found that the bond angles around the rhodium center of between 85.28(7)° and 93.59(8)° and the bond distances for Rh-CO and Rh-P of 1.790 and 2.230 Å respectively, correlated well with those found in the literature.[14, 17, 18]

To summarise, both electronic as well as the steric parameters played a vital role in the substitution of one of the carbonyl groups for the phosphine ligand. The [Rh(acac)(CO)(DPP)], [Rh(cupf)(CO)(DPP)] and [Rh(cupf)(CH_3)(CO)(DPP)(I)] complexes were successfully synthesized and characterized by means of IR, NMR and X-ray crystallography.

[19] C.H. Langford and H.B. Gray, *Ligand Substitution Processes, Benjamin, New York* (1966).

Chapter 5

Oxidative addition of methyl iodide to [Rh(cupf)(CO)(DPP)] complex

The oxidative addition of methyl iodide to rhodium(I) complexes is a key step in the carbonylation of methanol to acetic acid as was discussed in detail in **Chapter 2**. Previous work done by our group was concerned with the mechanistic study of the oxidative addition as well as CO-insertion reaction of Rh(I) complexes.[1, 2, 3, 4] Results obtained from these studies indicated that these reactions follow an ionic S_N2 two step mechanism. The results further showed a *trans*-geometry towards the alkyl halide addition, as was observed for the [Rh(ox)(CO)(CH_3)(I)(PPh_3)] complex.[5] In the case of [Rh(cupf)(CO)(CH_3)(I)(PPh_3)][6] an unusual *cis*-addition was observed during the reaction with methyl iodide. The above-mentioned is also in contrast with the results found for the oxidative addition of methyl iodide to [Rh(sacac)(CO)(PX_3)][7] which led to the formation of an acyl product in the final step of the reaction. The different results for the oxidative addition for these reactions led to a closer investigation into the mechanisms of these types of reaction. As a further extension on the research done by our group, the PPh_3 ligand was substituted by a more electron donating phosphine ligand, namely diphenyl-2-pyridyl phosphine (DPP), in order to determine the electronic and steric effect on the oxidative addition of methyl iodide to the [Rh(cupf)(CO)(PX_3)] complex. The *trans*-influence exerted by the bidentate ligand (cupf) will also play a vital role in die oxidative addition reaction.

[1] A. Roodt and G.J.J. Steyn, *Resent Res. Devel. Inorg. Chem*., **2**, (2000), 1.

[2] G.J.J. Steyn, A. Roodt and J.G. Leipoldt, *Inorg. Chem*., 31, (1992), 3477.

[3] D.M.C. Smit, S.S. Basson and E.C. Steynberg, *Rhodium Ex*., **7**-**8**, (1994), 12.

[4] S.S. Basson, J.G. Leipoldt and J.T. Nel, *Inorg. Chim. Acta*., **84**, (1984), 167.

[5] K.G. van Aswegen, J.G. Leipoldt, I.M. Potgieter, G.J. Lamprecht, A. Roodt and G.J. van Zyl, *Trans. Met. Chem*., **16**, (1991), 369.

[6] S.S. Basson, J.G. Leipoldt, A. Roodt and J.A. Venter, *Inorg. Chim. Acta*., **128**, (1987), 31.

[7] J.G. Leipoldt, S.S. Basson and L.J. Botha, *Inorg. Chim. Acta*., **168**, (1990), 215.

After taking all the possible factors into account, a possible mechanism for the reaction will be concluded. A generalized reaction scheme for the oxidative addition to [Rh(L,L')(CO)(PX_3)] complexes is given in **Scheme 5.1**. In the case of [Rh(cupf)(CO)(PPh_3)][6] substantial solvent interaction was observed while the solvent pathway was absent for the [Rh(sacac)(CO)(PPh_3)][7] complex.

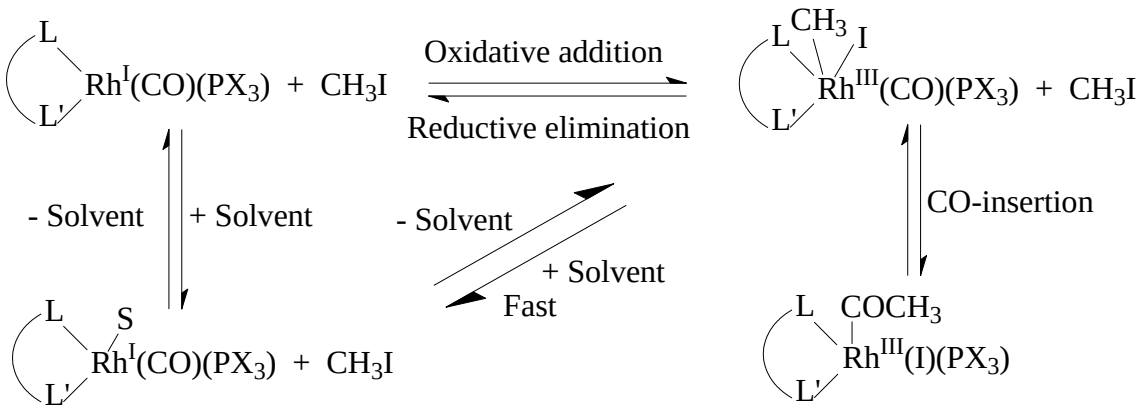

Scheme 5.1: Methyl iodide oxidative addition to [Rh(L,L')(CO)(PX_3)] complexes.[6]

5.1 Experimental procedure

The [Rh(cupf)(CO)(DPP)] complex was prepared according to **Paragraph 4.3** in **Chapter 4**. All chemicals used during the kinetic study were of reagent grade and were used without further purification. Solvents were purified and dried (**Appendix C**) prior to use by standard procedure.[8]

[8] A.J. Gordon and R.A. Ford, *The Chemist Companion: A Handbook of Practical Data, Techniques and References, John Wiley and Sons, New York*, (1972).

The CH_3I (carcinogenic and volatile) used during the study was purchased from Merck and stabilized with silver. The CH_3I was only used in well ventilated areas. IR kinetic studies were recorded with a Digilab FTS 2000 series spectrophotometer while the UV/visible measurements was monitored with a Varian Cary 50 spectrophotometer and both were equipped with a temperature controlled cell changer (accuracy ± 0.1°C). A NaCl cell was used during the IR study while a multi cell changer was used with the UV/visible measurements. All the reactions were followed under pseudo-first-order conditions. Typical complex concentrations were 2.5×10^{-4} for the visible and 0.02 M for the IR kinetic measurements with the methyl iodide concentration varied between 0.1 and 1.0 M. The temperature as well as the solvents was varied during the study to determine the activation entropy and enthalpy.

The kinetic data was processed by means of the Scientist[9] (least square fit) software. The observed pseudo-first-order rate constant, k_{obs}, was calculated from the absorption-time-data by means of **Equation 5.1**.

$$A = A_\infty - (A_\infty - A_0)e^{k_{obs}t} \qquad \textbf{5.1}$$

where A = absorption of solution

A_0 = absorption at t_0

t = reaction time

A_∞ = absorption at t_∞

k_{obs} = observed rate constant

The activation parameters, ΔH^* and ΔS^*, were determined by the Eyring equation (**Equation 5.2**).

$$\ln\left(\frac{k}{T}\right) = \ln\left(\frac{k_b}{h}\right) + \frac{\Delta S^*}{R} - \frac{\Delta H^*}{RT} \qquad \textbf{5.2}$$

[9] Micromath Scientist for Windows, Version 2.0, 1986-2995.

---

where k = rate constant
k_b = Boltzman constant
ΔS^* = activation entropy
ΔH^* = activation entropy
T = absolute temperature
h = Planck constant
R = universal gas constant

The standard free energy change, ΔG^0, was determined by **Equation 5.3**.

$$\Delta G^0 = -RT \ln K \qquad \textbf{5.3}$$

where ΔG^0 = standard free energy change
T = absolute temperature
R = universal gas constant
K = equilibrium constant

The experimental values in the figures are represented by points while the lines represent the computer calculated values. The standard deviation for all the calculated values is reported in brackets.

5.2 Kinetic study of the oxidative addition of methyl iodide to [Rh(cupf)(CO)(DPP)]

The reaction between CH_3I and [Rh(cupf)(CO)(DPP)] can be presented as follows:

$$[Rh(cupf)(CO)(DPP)] + CH_3I \longrightarrow \text{product}$$

The oxidative addition of CH_3I to [Rh(cupf)(CO)(DPP)] was studied in four different solvents to determine the influence of these solvents on the rate and type of reaction that takes place.

The addition of CH_3I to an acetonitrile solution containing [Rh(cupf)(CO)(DPP)] resulted in a change in the UV/visible spectra. The results in **Figure 5.1** clearly show an initial rapid absorption increase and then a slower decrease in absorption with the formation of an isosbestic point at 420 nm, indicating the presence of two possible reactions. A time scan of the same reaction as seen in **Figure 5.2** illustrates the presence of the two distinguishable reactions even more clearly. The initial reaction resulted in an absorption increase with a $t_{½}$ of 110 s^{-1} while the second slower reaction resulted in an absorption decrease with $t_{½}$ of approximately 1432 s^{-1}. A time scan separation of the reaction in **Figure 5.2** resulted in two distinguishable pseudo-first-order reactions as indicated in **Figure 5.3 and 5.4**. Similar results were obtained in different solvents as seen in **Figures 5.5** to **5.8**. Isosbestic points were also observed for chloroform and ethyl acetate at 350.0 nm. The absorption change spectra for the reaction in ethyl acetate as seen in **Figure 5.11** showed only one reaction (time for completion of reaction > 500 minutes) accompanied by decomposition of the complex with time. The dielectric constants[10] and donocity[10] for the four different solvents and the specific wavelength at which the reactions were followed are summarized in **Table 5.1**. Supplementary data of the observed rate constants is given in **Appendix E**.

Table 5.1: Dielectric constants, donocity and experimental wavelengths for the oxidative addition of CH_3I with [Rh(cupf)(CO)(DPP)] in different solvents.

Solvent	**Dielectric constant**	**Dn**	**Wavelength (λ_{exp}) (nm)**
Acetonitrile	38.0	14.1	380.0, 420.0
Acetone	20.7	4.0	380.0
Chloroform	4.8	17.1	380.0
Ethyl acetate	6.0	17.1	380.0

[10] V. Gutmann, *Angew. Chem. Int. Ed*., **11**, (1970), 843.

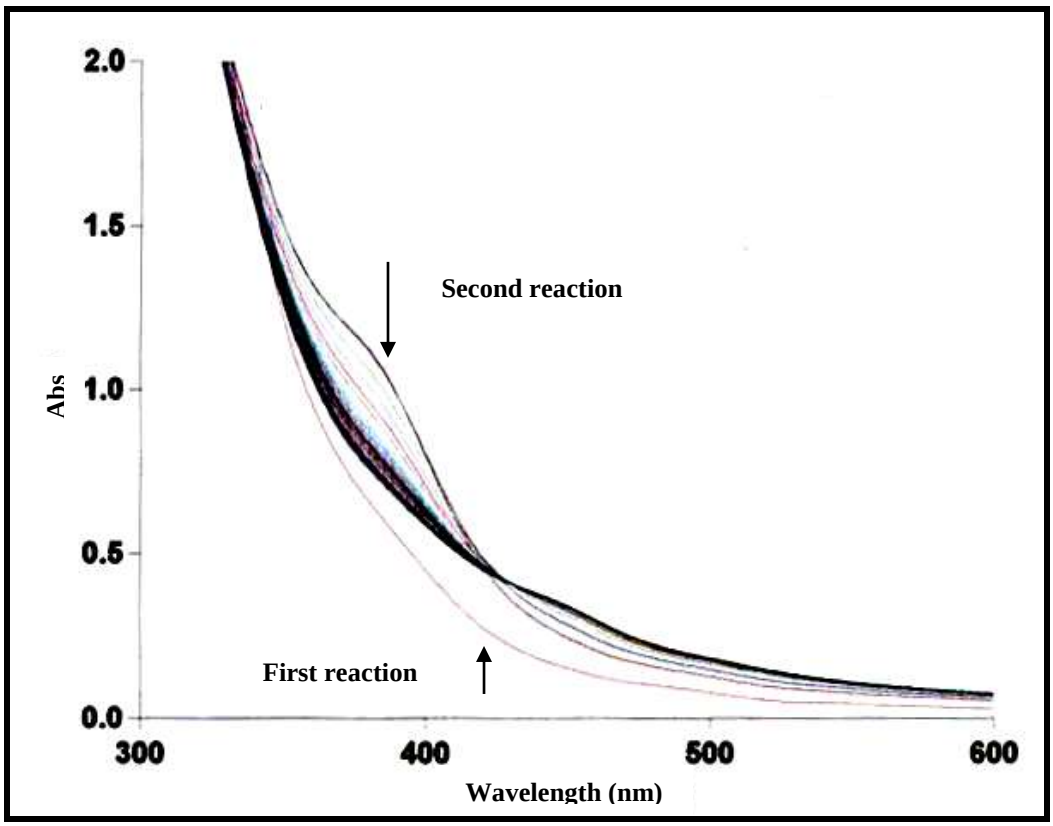

Figure 5.1: Oxidative addition reaction of CH_3I (0.5 M) with [Rh(cupf)(CO)(DPP)] (2.5 x 10^{-4} M) in acetonitrile (2 min intervals, 25.0°C).

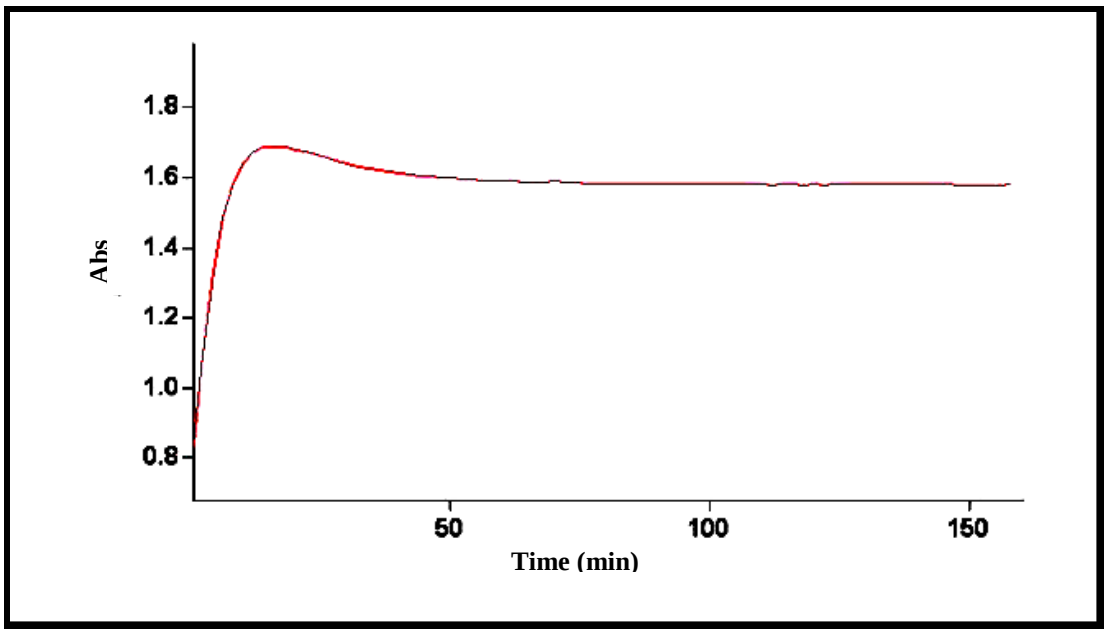

Figure 5.2: Absorption vs time spectrum of CH_3I (0.5 M) with [Rh(cupf)(CO)(DPP)] (2.5 x 10^{-4} M) in acetonitrile at 380 nm (2 min intervals, 25.0°C).

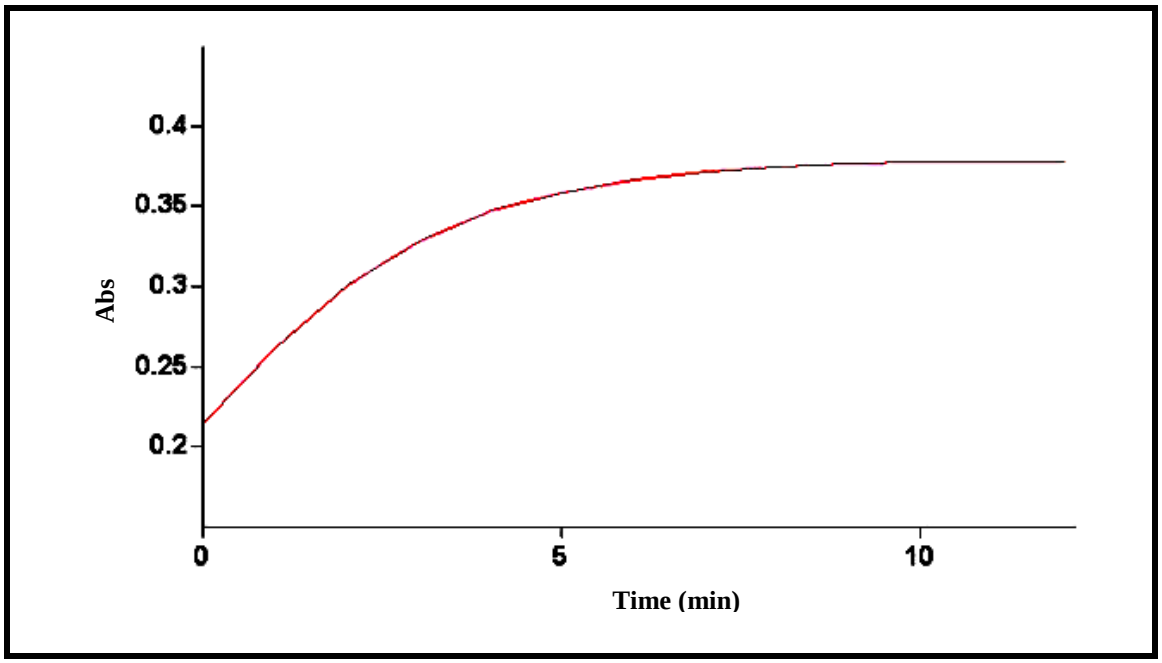

Figure 5.3: Absorption vs time spectrum of CH_3I (0.5 M) with [Rh(cupf)(CO)(DPP)] (2.5 x 10^{-4} M) in acetonitrile at 420 nm (2 min intervals, 25.0°C).

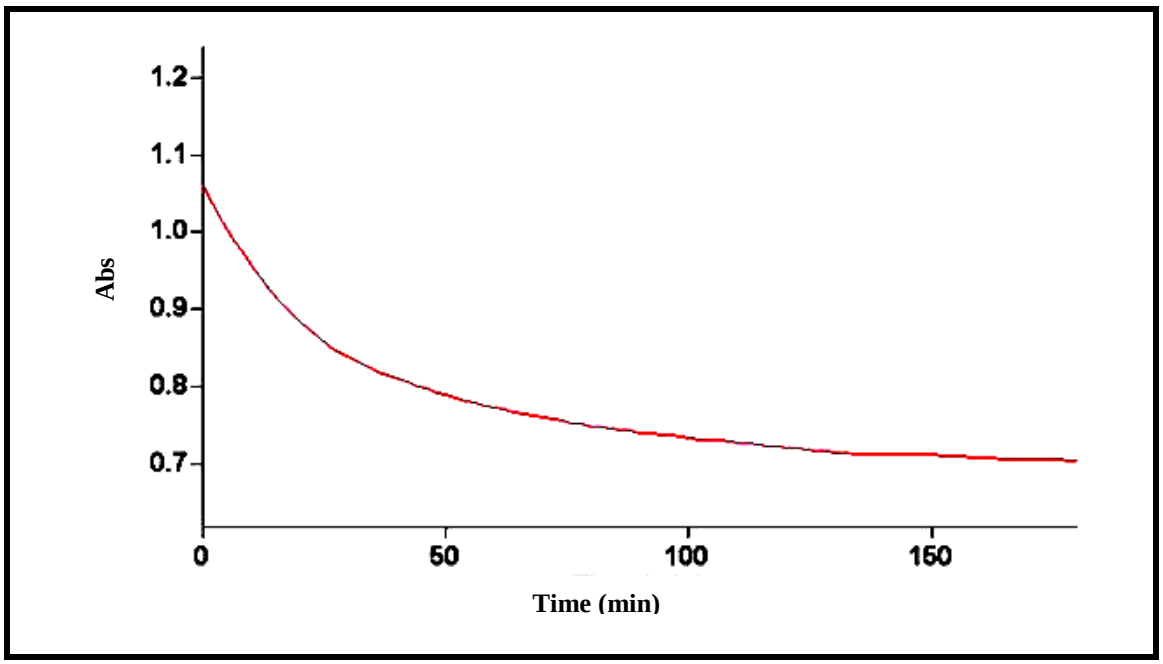

Figure 5.4: Absorption vs time spectrum of CH_3I (0.5 M) with [Rh(cupf)(CO)(DPP)] (2.5 x 10^{-4} M) in acetonitrile at 380 nm (2 min intervals, 25.0°C).

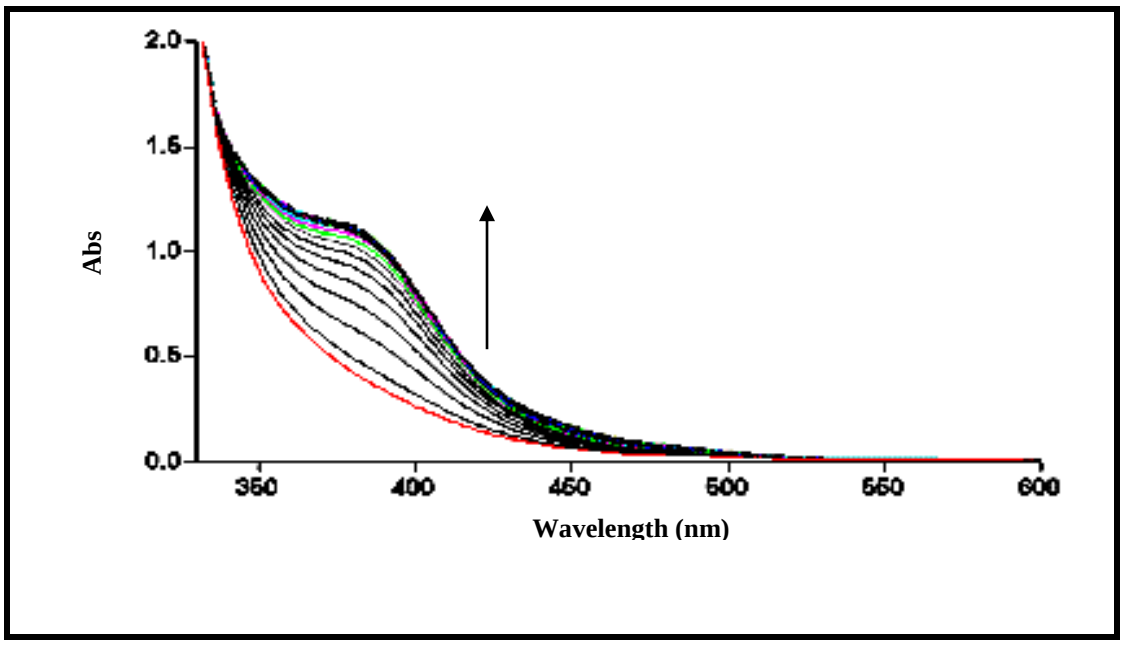

Figure 5.5: Oxidative addition reaction of CH_3I (0.5 M) with [Rh(cupf)(CO)(DPP)] (2.5×10^{-4} M) in acetone (2 min intervals, 25.0°C).

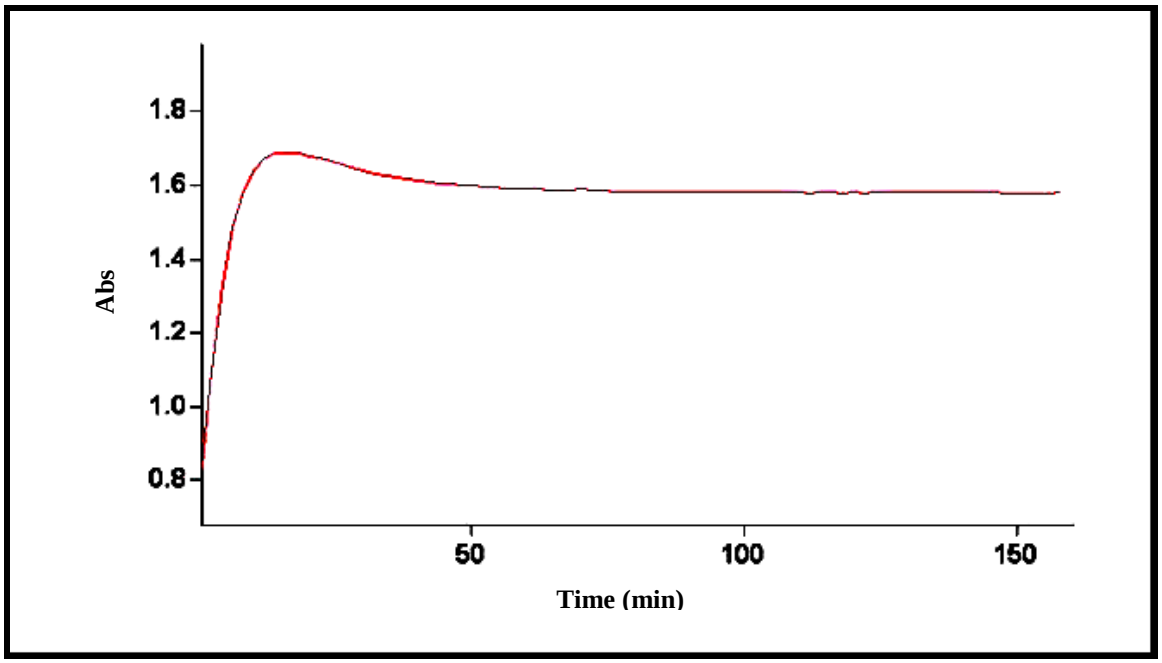

Figure 5.6: Absorption vs time spectrum of CH_3I (0.5 M) with [Rh(cupf)(CO)(DPP)] (2.5×10^{-4} M) in acetone at 380 nm (2 min intervals, 25.0°C).

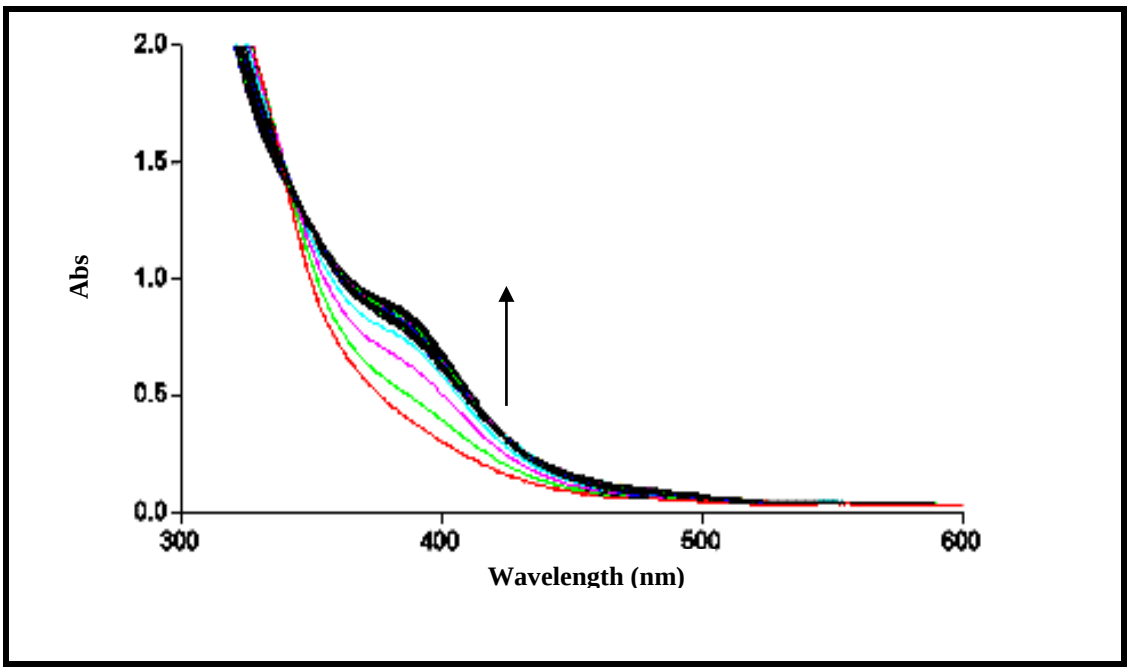

Figure 5.7: Oxidative addition reaction of CH_3I (0.5 M) with [Rh(cupf)(CO)(DPP)] (2.5×10^{-4} M) in chloroform (2 min intervals, 25.0°C).

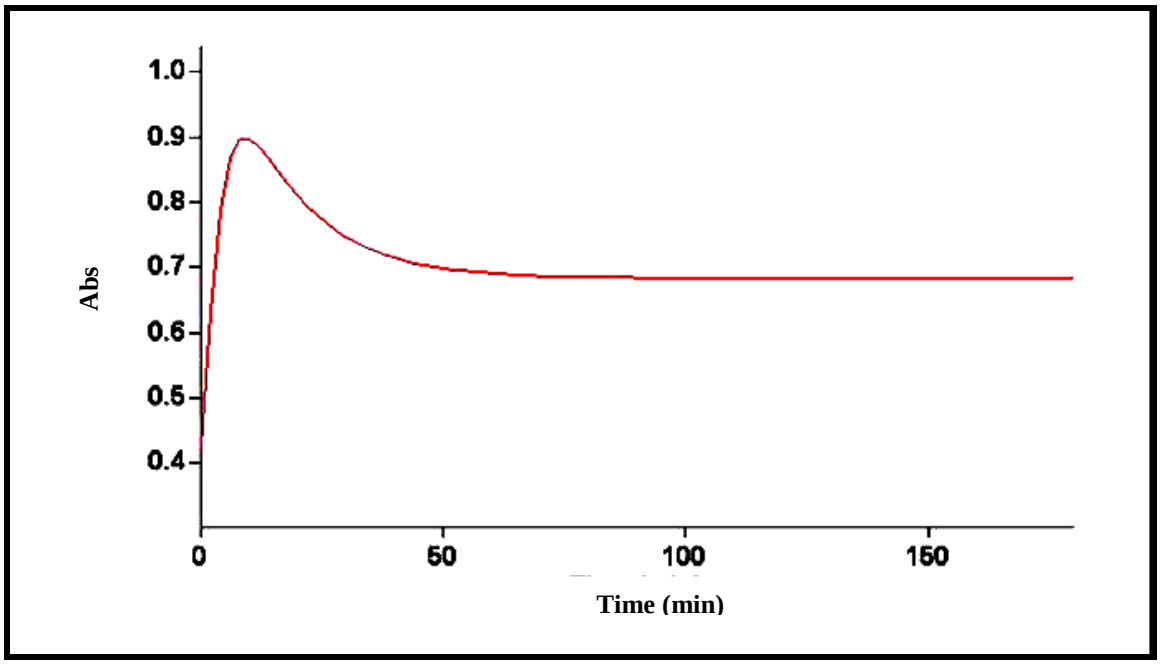

Figure 5.8: Absorption vs time spectrum of CH_3I (0.5 M) with [Rh(cupf)(CO)(DPP)] (2.5×10^{-4} M) in chloroform at 380 nm (2 min intervals, 25.0°C).

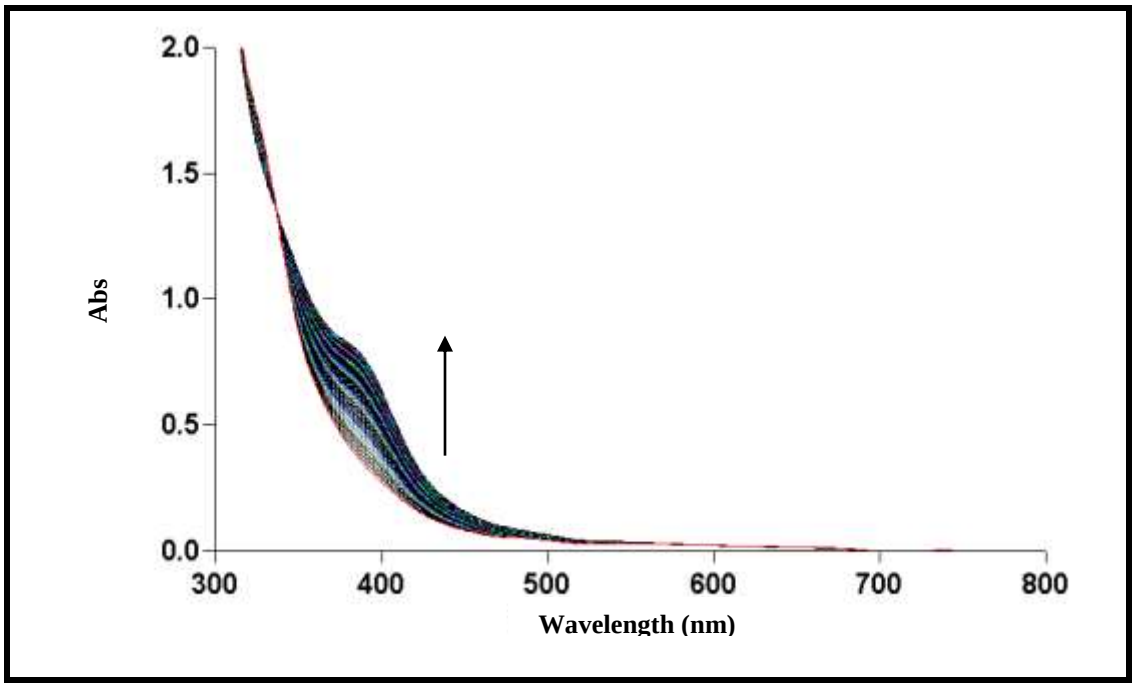

Figure 5.9: Oxidative addition reaction of CH_3I (0.5 M) with [Rh(cupf)(CO)(DPP)] (2.5 x 10^{-4} M) in ethyl acetate (2 min intervals, 25.0°C).

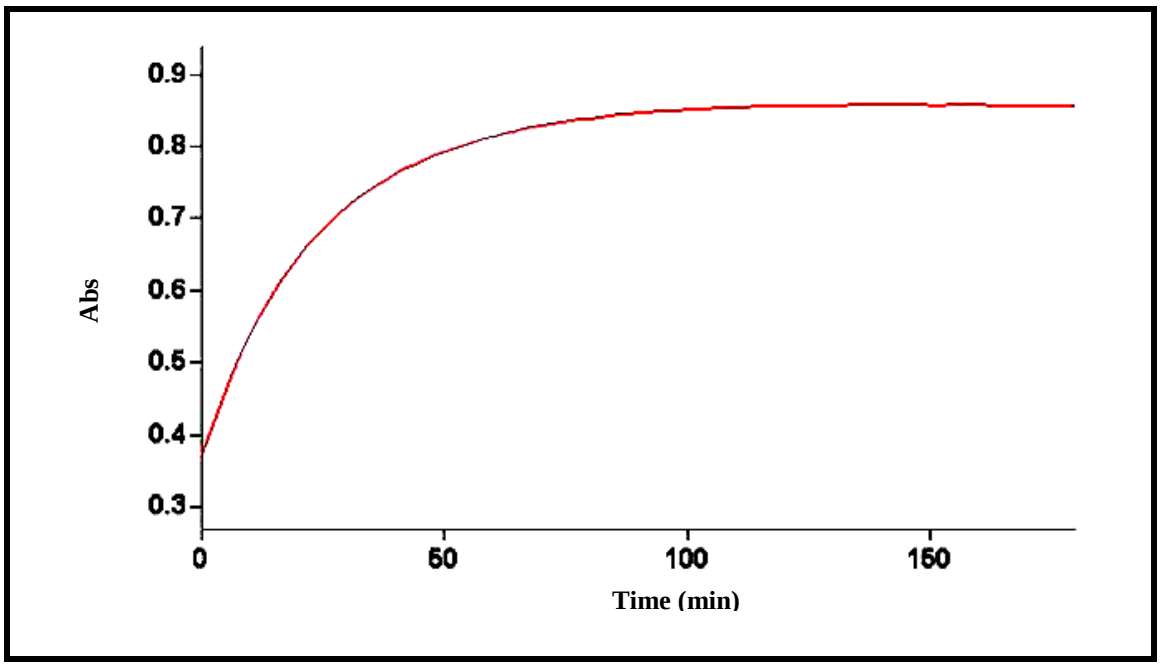

Figure 5.10: Absorption vs time spectrum of CH_3I (0.5 M) with [Rh(cupf)(CO)(DPP)] (2.5 x 10^{-4} M) in ethyl acetate at 380 nm (2 min intervals, 25.0°C).

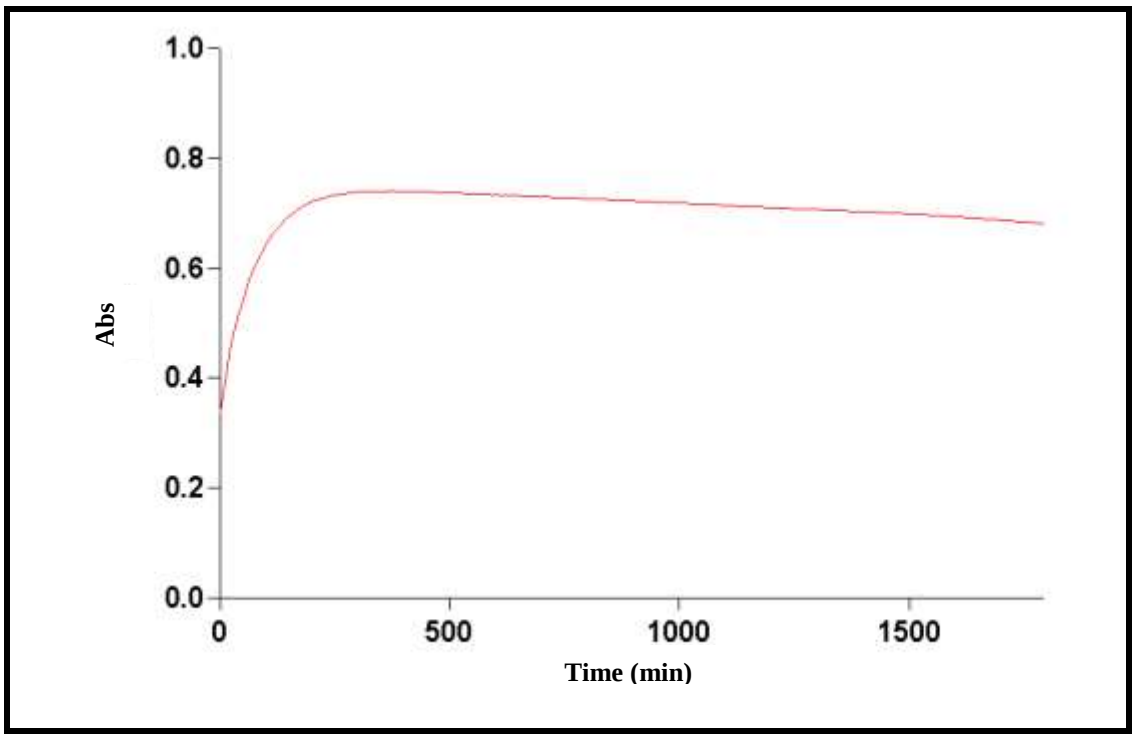

Figure 5.11: Absorption vs time spectrum of CH_3I (0.5 M) with [Rh(cupf)(CO)(DPP)] (2.5 x 10^{-4} M) in ethyl acetate at 380 nm (2 min intervals, 25.0°C).

An IR study (see **Figure 5.12**) of the oxidative addition reaction between CH_3I and [Rh(cupf)(CO)(DPP)] in acetonitrile shows a rapid disappearance of the Rh(I)-CO stretching frequency at 1980 cm^{-1} with the simultaneous appearance of the Rh(III)–CO carbonyl stretching frequency at 2064 cm^{-1}. The same spectrum shows the slow appearance of the rhodium acyl peak at 1688 cm^{-1}. Spectra obtained for the same reaction in chloroform show similar behavior, namely the rapid formation of the Rh(III)-alkyl intermediate and the subsequent slow carbonyl insertion, resulting in the formation of the Rh(III)-acyl product. Large absorption maxima at 1700 cm^{-1} for acetone and ethyl acetate however prevented the possible observation of acyl formation for these two solvents. A comparison of the IR spectra however show a substantial slower alkyl formation reaction in ethyl acetate as solvent (**Figure 5.15**), predicting major solvent interaction or participation in the formation of the final product. Another important aspect of the results obtained with the IR spectra is the complete disappearance of the Rh(I)-CO peak, but no significant disappearance of the Rh(III)-CO peak (alkyl product)

during the formation of the Rh(III) acyl product, indicating the existence of an equilibrium between the alkyl and acyl products.

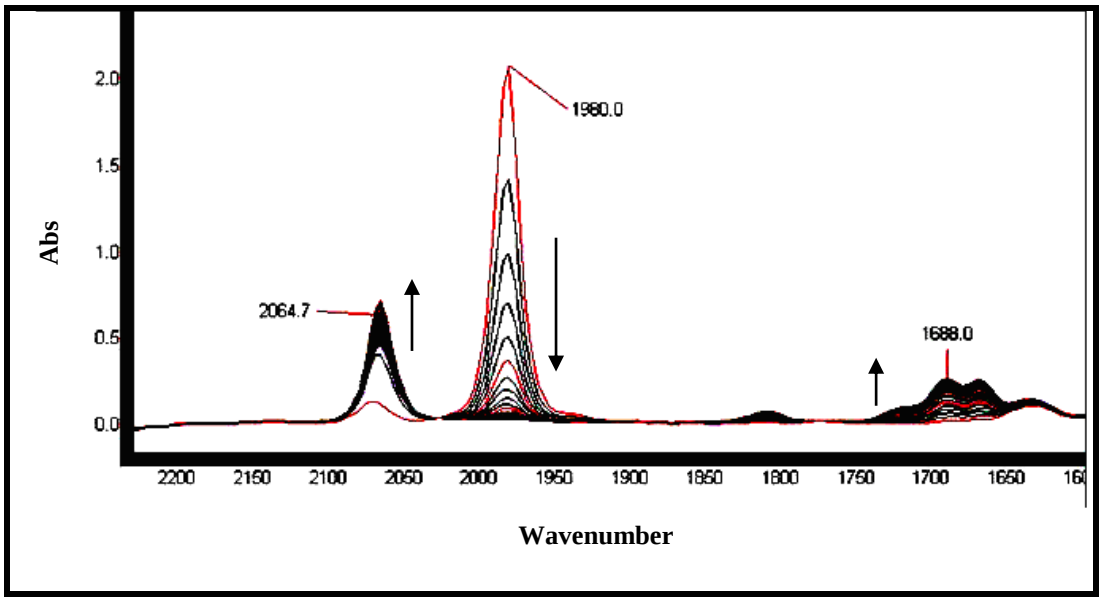

Figure 5.12: IR spectra for the reaction of CH_3I (0.2 M) with [Rh(cupf)(CO)(DPP)] (2.0×10^{-2} M) in acetonitrile (2 min intervals, 25.0°C).

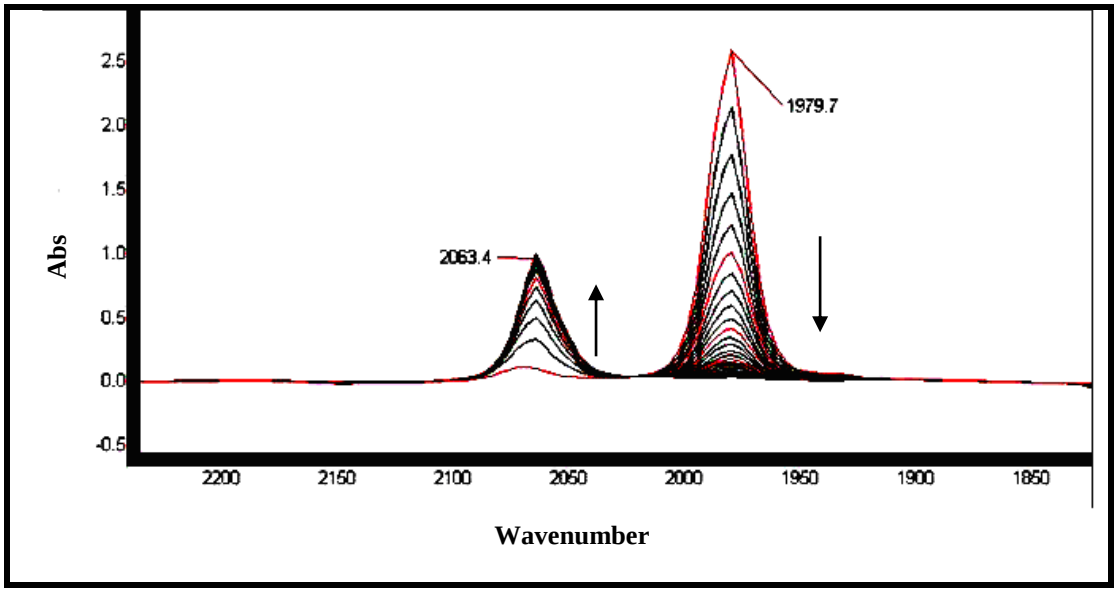

Figure 5.13: IR spectra for the reaction of CH_3I (0.2 M) with [Rh(cupf)(CO)(DPP)] (2.0×10^{-2} M) in acetone (2 min intervals, 25.0°C).

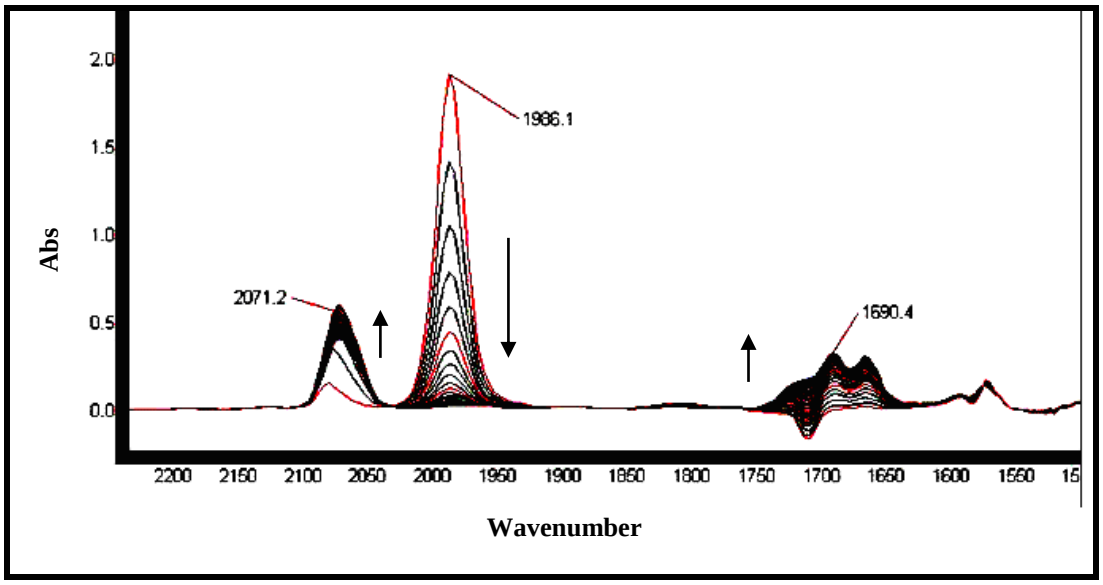

Figure 5.14: IR spectra for the reaction of CH_3I (0.2 M) with [Rh(cupf)(CO)(DPP)] (2.0×10^{-2} M) in chloroform (2 min intervals, 25.0°C).

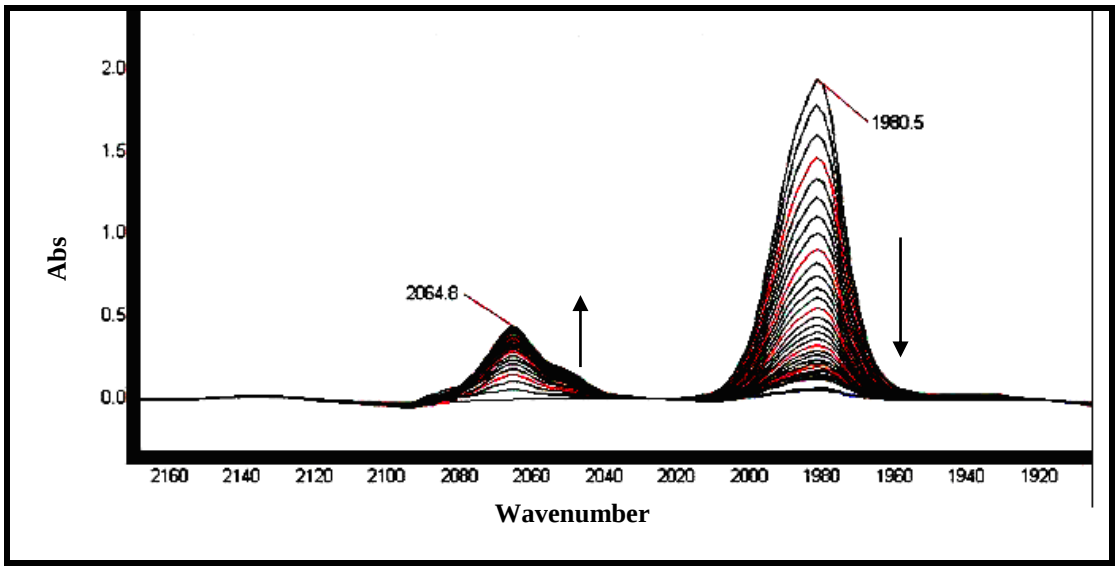

Figure 5.15: IR spectra for the reaction of CH_3I (0.2 M) with [Rh(cupf)(CO)(DPP)] (2.0×10^{-2} M) in ethyl acetate (2 min intervals, 25.0°C).

5.2.1 Rate laws and mechanism for the methyl iodide oxidative addition to [Rh(cupf)(CO)(DPP)]

An important result obtained from the initial IR study is the observed rate for the disappearance of the Rh(I) complex ($t_{½}$ ~ 232 s^{-1}) and the appearance of the Rh(III)-alkyl complex ($t_{½}$ ~ 224 s^{-1}) are within experimental error the same, while the appearance of the Rh(III)-acyl is much slower with $t_{½}$ ~ 1136 s^{-1}. These results indicate that the rate of the disappearance of the Rh(I) is the same as the rate of Rh(III)-alkyl formation, while the Rh(III)-acyl formation is much slower confirming the results that were discussed in the previous paragraph.

The reaction between CH_3I and [Rh(cupf)(CO)(DPP] was also studied under similar conditions using UV/visible and IR in acetonitrile to try and identify or allocate the two UV/visible reactions to different species formed in solution. The disappearance of the Rh(I) complex was followed by means of IR (see **Figure 5.16**) and compared to the fast reaction followed by means of UV/visible (see **Figure 5.3**). The observed rate for the two reactions are 2.98 x 10^{-3} s^{-1} and 3.45 x 10^{-3} s^{-1} respectively, indicating that the fast reaction which are observed by the UV/visible spectra is indeed the disappearance of the Rh(I) complex or the formation of Rh(III)-alkyl complex. A complete [CH_3I] variation was studied with IR (see **Figure 5.17**) in acetone and the results showed non-linear kinetics. The pseudo-first-order rate constants in **Table 5.2** also confirm the excellent correlation between the fast reaction in UV/visible and the disappearance of the Rh(I) complex or the Rh(III)-alkyl formation, followed in IR.

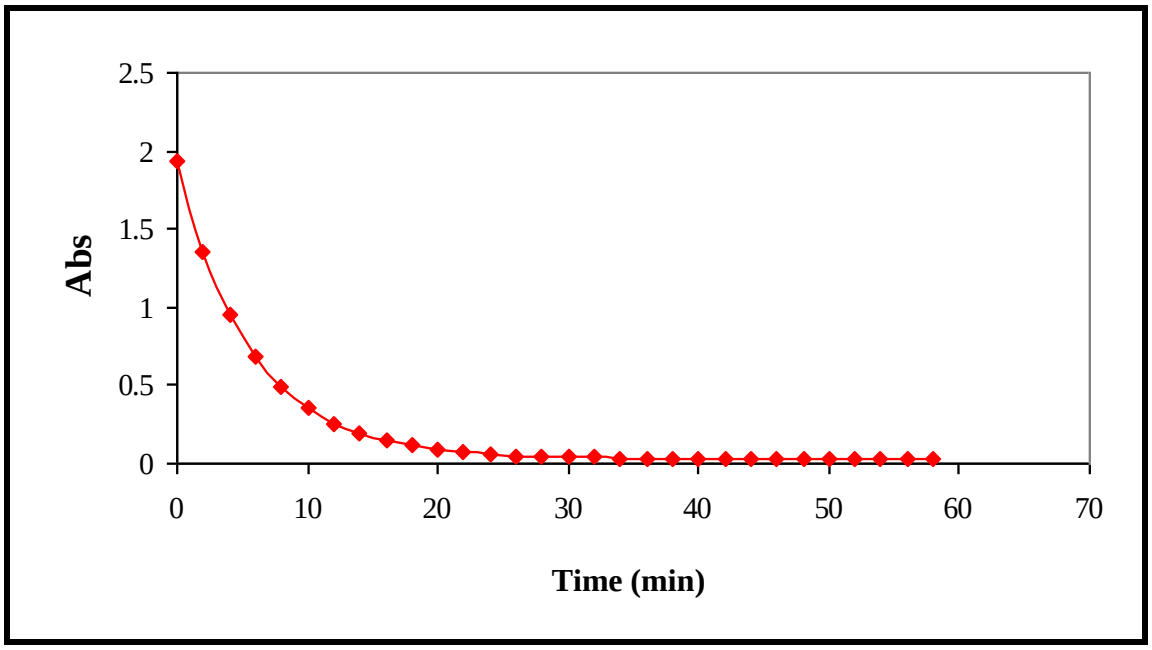

Figure 5.16: Disappearance of the Rh(I) complex in acetonitrile at 25°C (IR data).

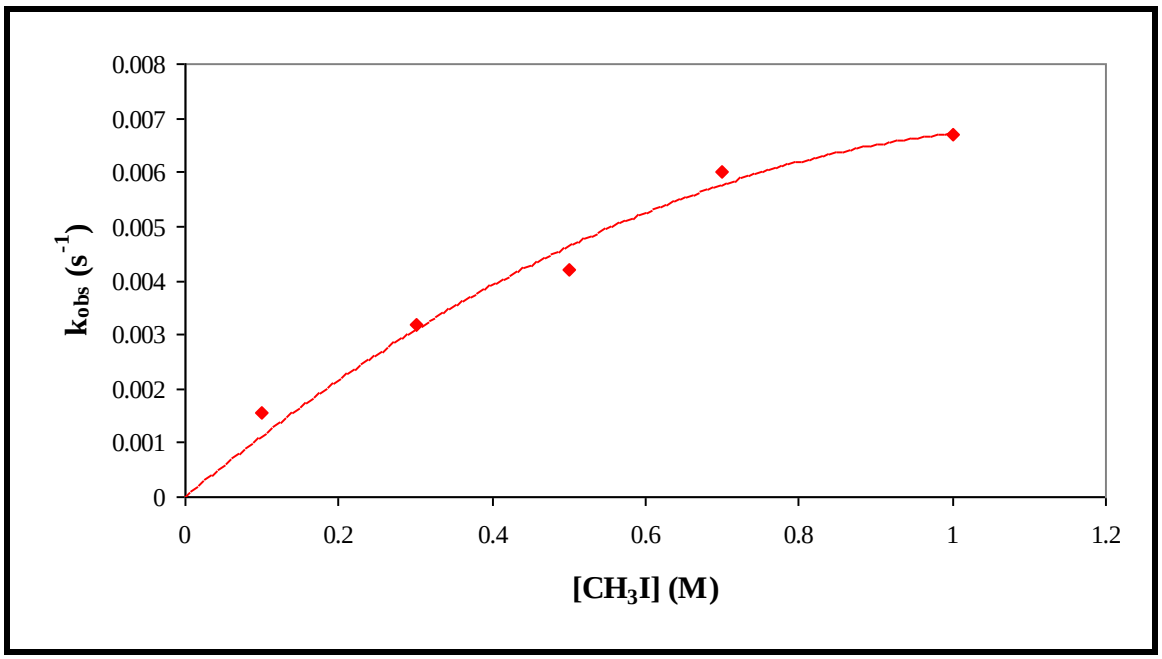

Figure 5.17: IR data for k_{obs} against [CH_3I] for oxidative addition (alkyl formation) of CH_3I to [Rh(cupf)(CO)(DPP)] in acetone at 25°C.

Table 5.2: Comparative data for the UV and IR study for the oxidative addition reaction of CH_3I to [Rh(cupf)(CO)(DPP)] in acetone at 25°C

[CH_3I] (M)	**UV** **10^3 k_{obs} (s^{-1})** **(Rh(III)-alkyl formation)**	**IR** **10^3 k_{obs} (s^{-1})** **(Rh(I) disapparance)**
0.1012	2.5(5)	1.57(6)
0.3021	3.6(8)	3.17(6)
0.5011	4.7(5)	4.2(5)
0.7013	5.9(5)	6.0(5)
1.016	6.3(4)	6.7(5)

The [CH_3I] variation at different temperatures (see **Figure 5.18**) for acetonitrile also indicated non-linear kinetics. Similar results were obtained for acetone and chloroform (see **Figure 5.19** and **5.20**). In contrast to the above-mentioned, ethyl acetate showed a linear correlation (see **Figure 5.21**) between k_{obs} and [CH_3I] at different temperatures.

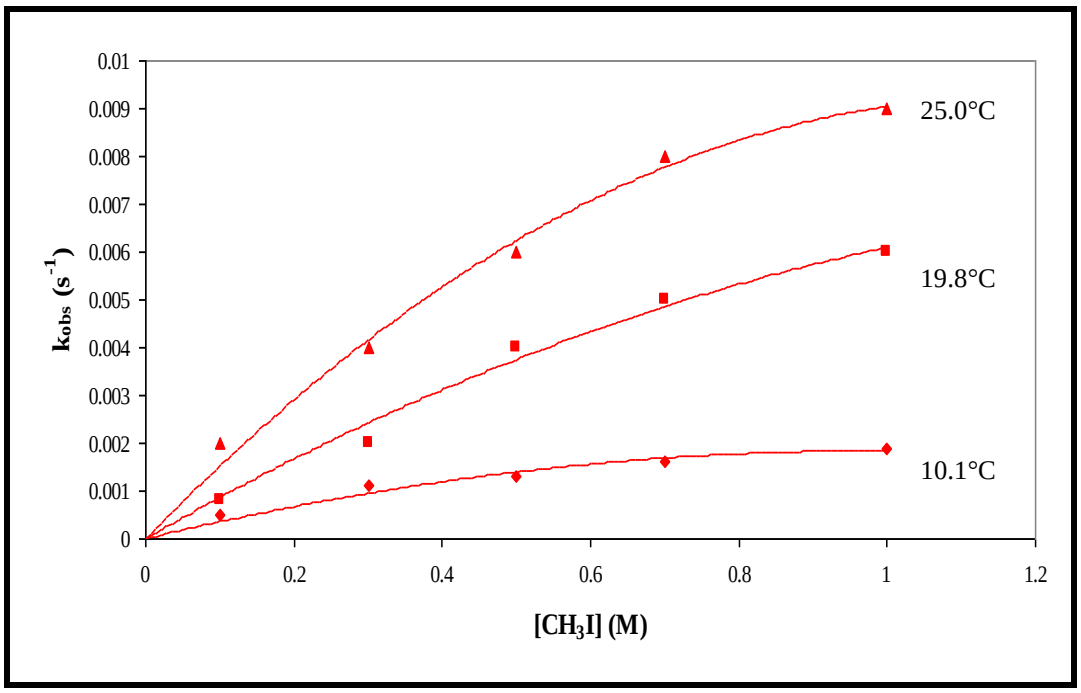

Figure 5.18: k_{obs} against [CH_3I] for oxidative addition (alkyl formation) of CH_3I to [Rh(cupf)(CO)(DPP)] in acetonitrile at different temperatures.

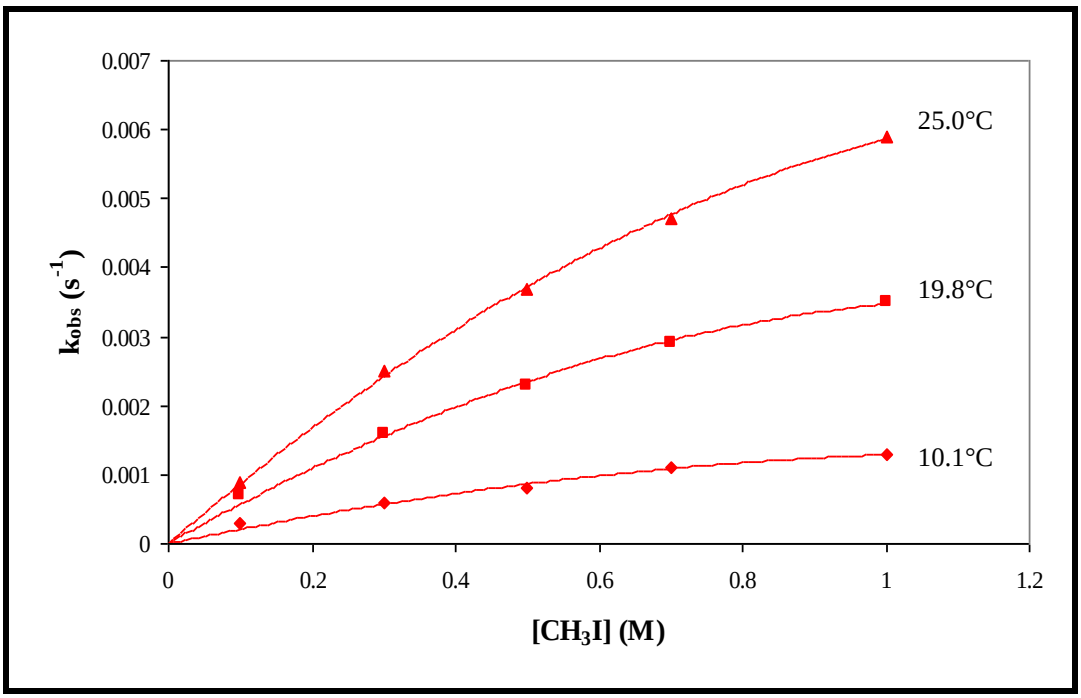

Figure 5.19: k_{obs} against $[CH_3I]$ for oxidative addition (alkyl formation) of CH_3I to [Rh(cupf)(CO)(DPP)] in acetone at different temperatures.

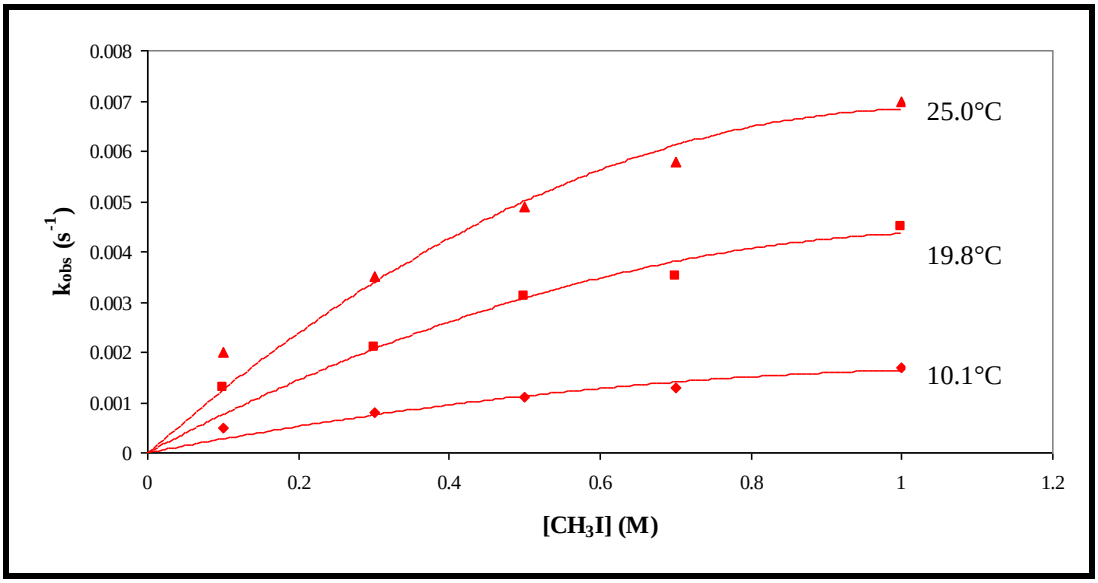

Figure 5.20: k_{obs} against $[CH_3I]$ for oxidative addition (alkyl formation) of CH_3I to [Rh(cupf)(CO)(DPP)] in chloroform at different temperatures.

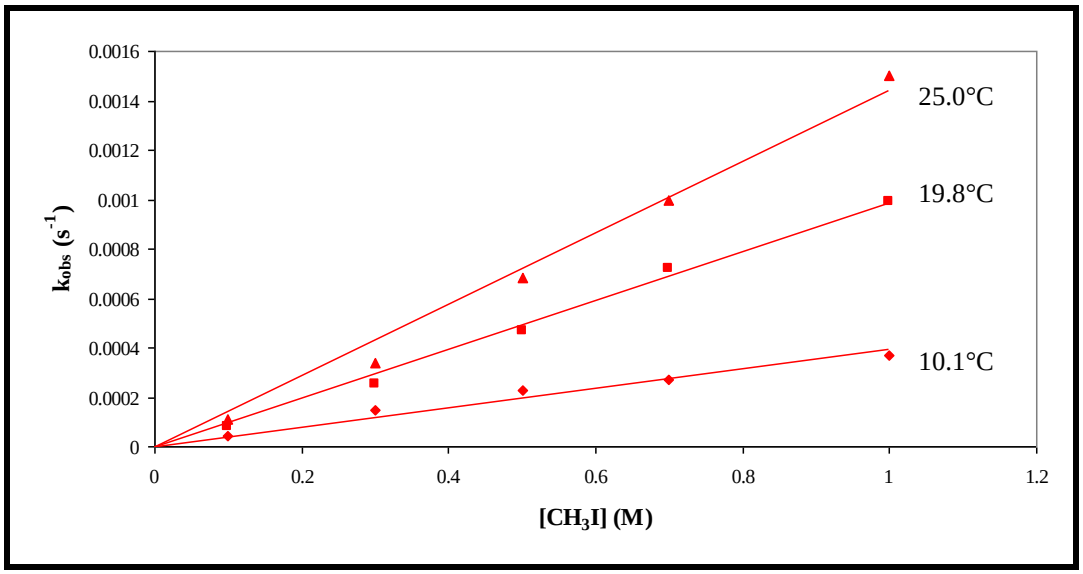

Figure 5.21: k_{obs} against $[CH_3I]$ for oxidative addition (alkyl formation) of CH_3I to [Rh(cupf)(CO)(DPP)] in ethyl acetate different temperatures.

A study of the Rh(III)-acyl formation with $[CH_3I]$ variation at different temperatures indicated a reaction which is independent of $[CH_3I]$ (see **Figure 5.22**). Similar results were obtained for acetone and chloroform as solvents (see **Figure 5.23** and **5.24**).

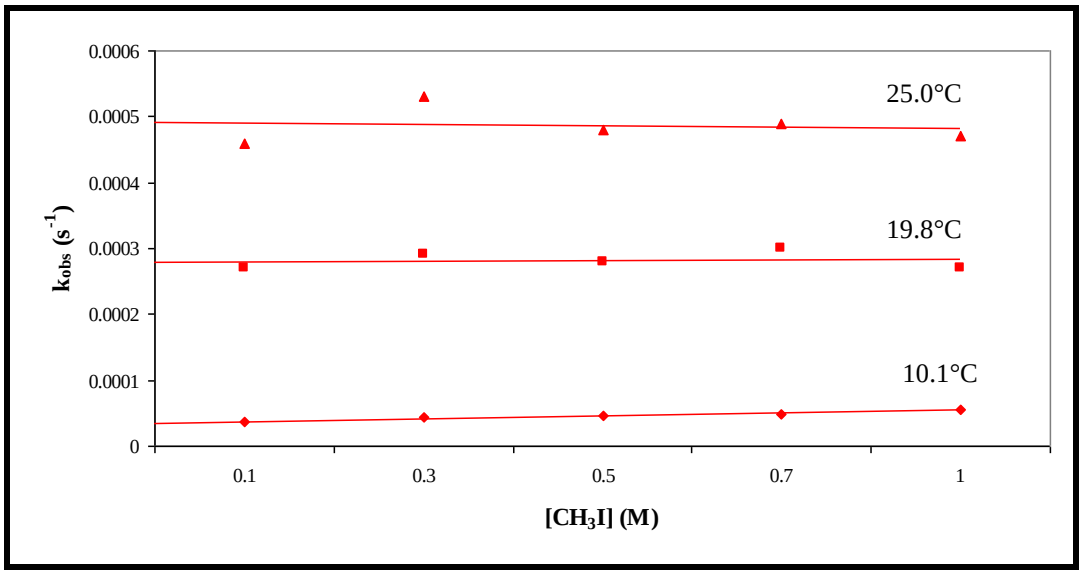

Figure 5.22: k_{obs} against $[CH_3I]$ for insertion reaction (acyl formation) in acetonitrile at different temperatures.

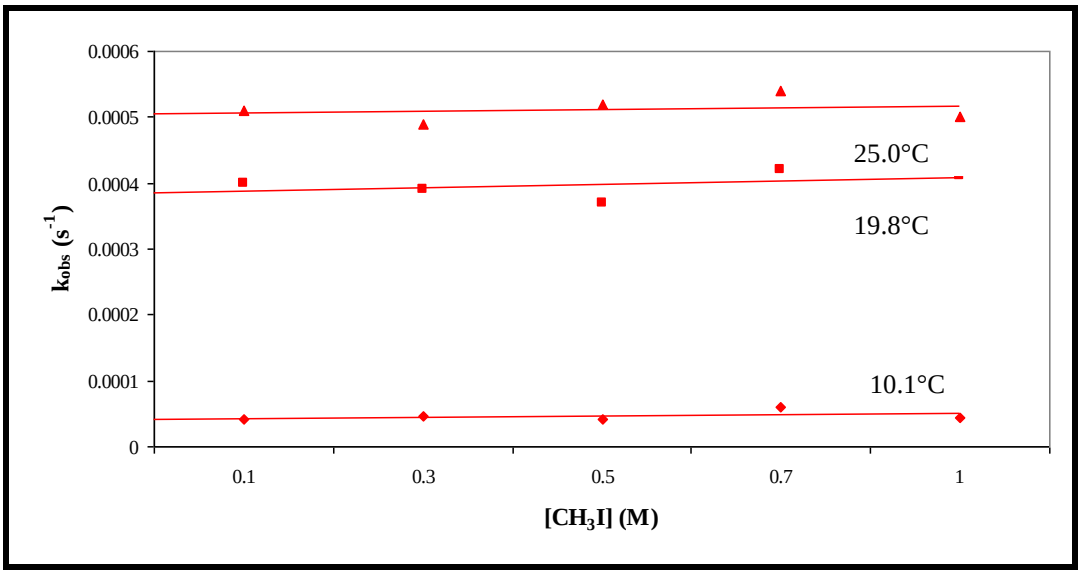

Figure 5.23: k_{obs} against $[CH_3I]$ for insertion reaction (acyl formation) in acetone at different temperatures.

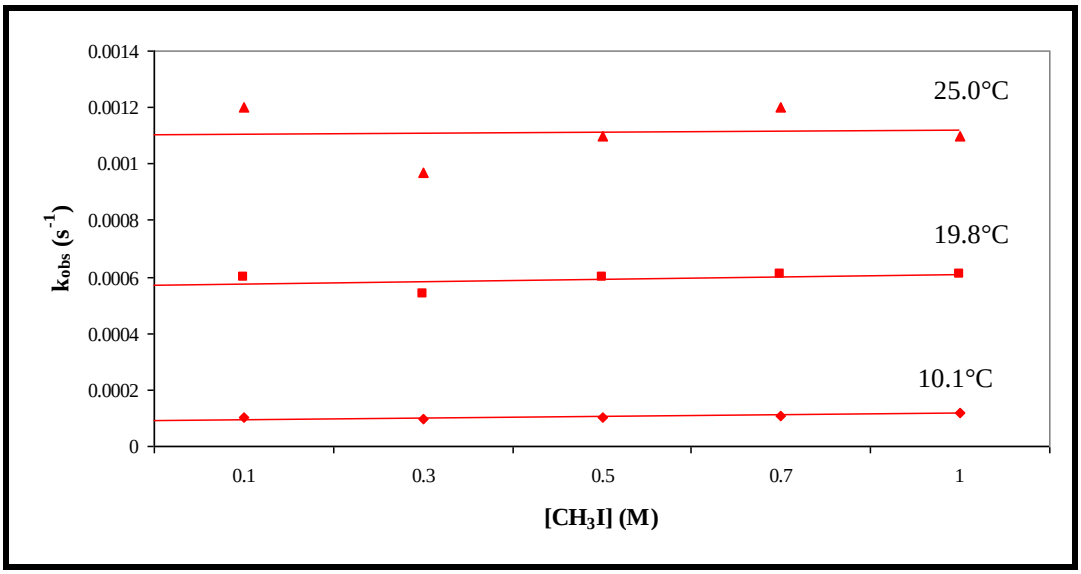

Figure 5.24: k_{obs} against $[CH_3I]$ for insertion reaction (acyl formation) in chloroform at different temperatures.

These results indicate that the oxidative addition reaction between CH_3I and [Rh(cupf)(CO)(DPP)] follows the same reaction mechanism for acetonitrile, acetone and chloroform but a different one (as evident also in the absence of acyl formation) in ethyl

acetate. A possible mechanism complying with the observed non-linear kinetics (see **Scheme 5.2**) can be postulated for the oxidative addition reaction.

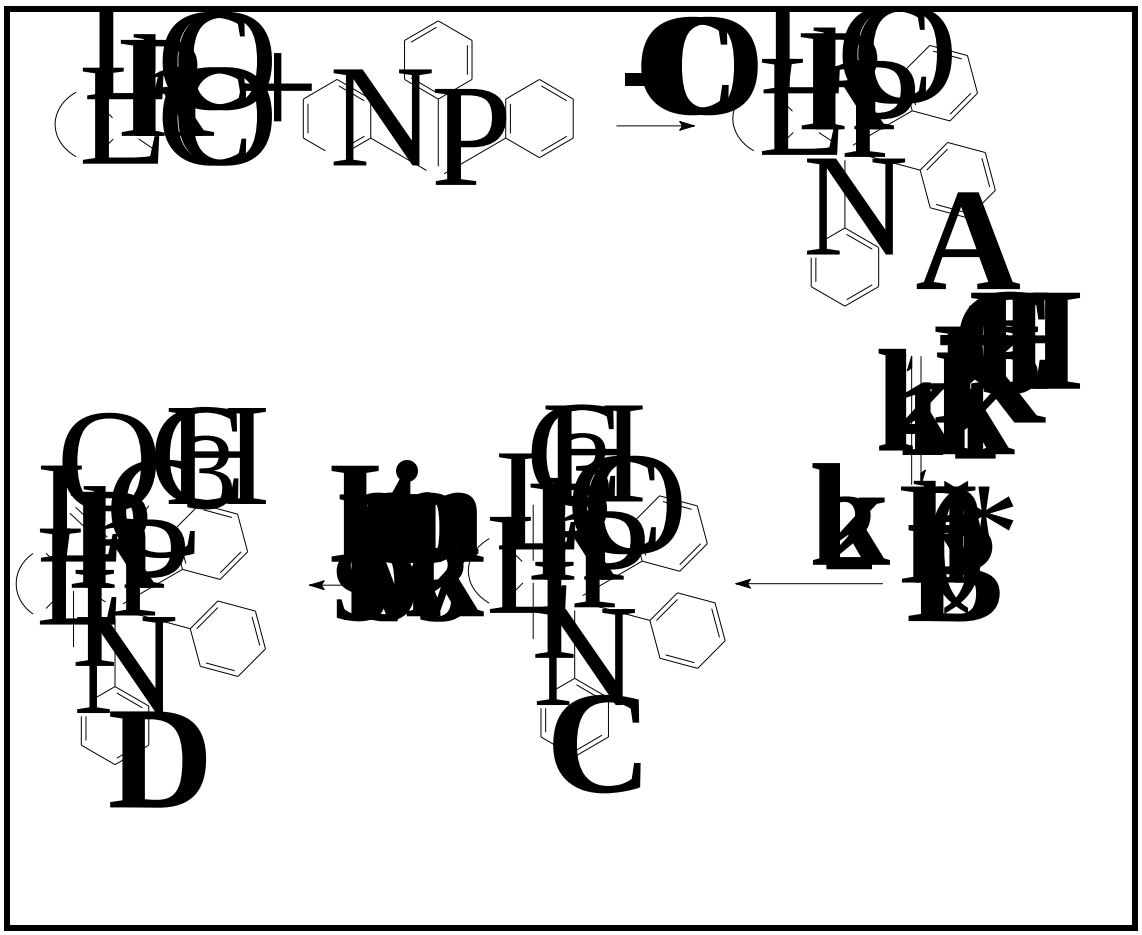

Scheme 5.2: Reaction mechanism for the methyl iodide oxidative addition to [Rh(cupf)(CO)(DPP)] in acetonitrile, acetone and chloroform.

Using all of the above-mentioned information the following rate law can be deducted for the oxidative addition of CH_3I to [Rh(cupf)(CO)(DPP)] in these solvents.

$$\frac{d[Rh(I)]^*}{dt} = k_1[Rh(I)][CH_3I] - k_{-1}[Rh(I)^*] - k_2[Rh(III)alkyl] \qquad \textbf{5.4}$$

where [Rh(I)]* = structure B (**Scheme 5.2**)

[Rh(I)] = structure A (**Scheme 5.2**)

[Rh(III)alkyl] = structure C (**Scheme 5.2**)

The pseudo-first order rate constant ([CH_3I] >> [Rh(I)] for the alkyl formation can be presented by the following:

$$k_{obs} = \frac{k_2 K[CH_3I]}{1 + K[CH_3I]} \qquad \textbf{5.5}$$

See **Appendix D** for the full derivation of **Equation 5.5** from **Equation 5.4**.

This corresponds to a mechanism which consists of a very fast equilibrium reaction (formation of Rh(I)*) followed by a second reaction to form the Rh(alkyl) product.

The rate law for the formation of the acyl product from the reaction scheme (**Scheme 5.2**; structure D) can be presented in the following way:

$$\frac{d[Rh(III)alkyl]}{dt} = k_2[Rh(I)^*] - k_3[Rh(III)acyl] \qquad \textbf{5.6}$$

The formation of the intermediate, Rh(I)*, can be represented by the following:

$$\frac{d[Rh(I)^*]}{dt} = k_1[Rh(I)][CH_3I] - k_{-1}[Rh(I)^*] \sim 0 \qquad \textbf{5.7}$$

If the intermediate attains equilibrium with the reactants (pre-equilibrium), **Equation 5.7** simplifies to:

$$[Rh(I)^*] = \frac{k_1}{k_{-1}}[Rh(I)][CH_3I] = K[Rh(I)][CH_3I] \qquad \textbf{5.8}$$

Substitution of **Equation 5.8** into **Equation 5.6** and under pseudo-first-order conditions:

$$k_{obs} = k_2 K[CH_3I] + k_3 \qquad \textbf{5.9}$$

If the reaction is independent of the [CH_3I]:

$$k_{obs} = k_3 \qquad \textbf{5.10}$$

See **Appendix D** for the full derivation of **Equation 5.10**

These experimental data for acetonitrile, acetone and chloroform (see **Appendix E**) were fitted to **Equation 5.5** and **5.10** and the calculated constants for the reactions at different temperatures and in different solvents are given in **Table 5.3**.

Table 5.3: Summary for the oxidative addition of CH_3I to [Rh(cupf)(CO)(DPP)] at different temperatures in acetonitrile, acetone and chloroform.

Solvent	Temperature (ºC)	10^3 k_2 (alkyl) ($M^{-1}s^{-1}$)	10^3 k_3(acyl) (s^{-1})	K (M^{-1})	ΔH* ($kJ.mol^{-1}$)	ΔS* ($J.K^{-1}.mol^{-1}$)
Acetonitrile	10.1	5.0(1)	0.043(5)	1.99(1)	48(9)	-214(7)
	19.8	7.0(2)	0.29(6)	0.2(1)		
	25.0	17(6)	0.49(6)	0.9(1)		
Acetone	10.1	3.0(2)	0.044(5)	1.7(4)	34(8)	-209(6)
	19.8	8.0(2)	0.039(6)	1.4(1)		
	25.0	9.0(1)	1.1(5)	0.5(1)		
Chloroform	10.1	1.4(4)	0.11(7)	0.39(2)	12(9)	-173(7)
	19.8	20(2)	0.59(6)	4.6(9)		
	25.0	20(3)	1.1(5)	2.6(4)		

The fact that the oxidative addition reaction between CH_3I and [Rh(cupf)(CO)(DPP)] in ethyl acetate showed different kinetic behavior, a different mechanism was postulated (see **Scheme 5.3**).

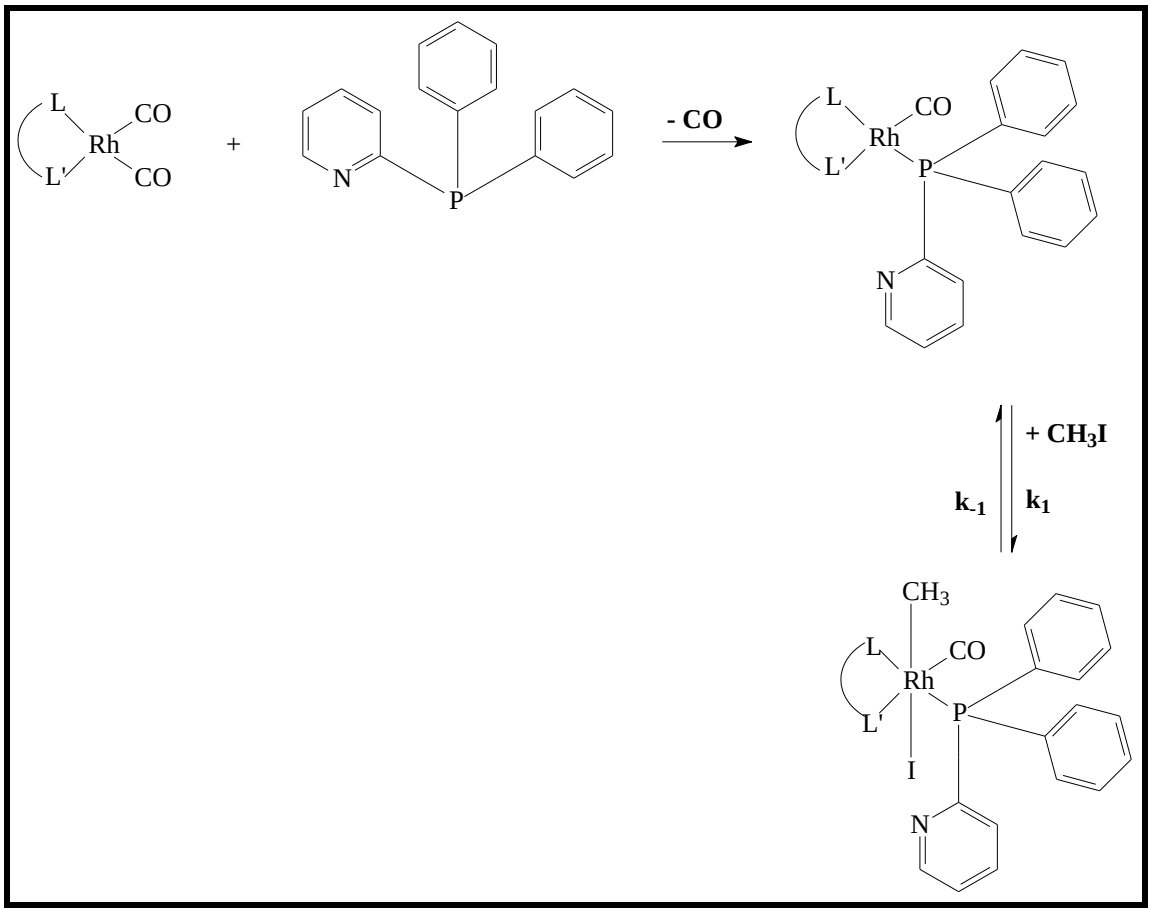

Scheme 5.3: Reaction mechanism for the methyl iodide oxidative addition to [Rh(cupf)(CO)(DPP)] in ethyl acetate.

$$\frac{d[Rh(I)]}{dt} = k_1[Rh(I)][CH_3I] + k_{-1}[Rh(III)alkyl] \qquad \textbf{5.11}$$

Under pseudo-first-order conditions ([CH_3I] >> [Rh(I)]):

$$k_{obs} = k_1[CH_3I] + k_{-1} \qquad \textbf{5.12}$$

See **Appendix D** for the full derivation of **Equation 5.12**

The experimental data for ethyl acetate (see **Appendix E**) was fitted to **Equation 5.12** and the calculated constants for the reaction at different temperatures and in different solvents are given in **Table 5.4**.

Table 5.4: Summary for the oxidative addition of CH_3I to [Rh(cupf)(CO)(DPP)] at different temperatures in ethyl acetate.

Temperature (°C)	10^3 k_1 ($M^{-1}s^{-1}$)	10^4 k_{-1} (s^{-1})	K (M^{-1})	ΔH* ($kJ.mol^{-1}$)	ΔS* ($J.K^{-1}.mol^{-1}$)
10.1	0.12(2)	0.60(1)	2.0(2)	19(9)	-238(8)
19.8	1.03(3)	0.39(2)	2.64(1)		
25.0	1.59(7)	0.98(4)	1.62(2)		

5.3 Discussion

The IR study of the reaction of CH_3I to [Rh(cupf)(CO)(DPP)] in acetonitrile, acetone and chloroform showed a rapid disappearance of the Rh(I)-CO stretching frequency with the simultaneous appearance of the Rh(III)-CO carbonyl stretching frequency. Comparing the fast reaction of the UV/visible study to the IR study revealed that the observed rate for the two reactions were almost of the same magnitude indicating that the fast reaction is indeed the disappearance of the Rh(I) complex and the simultaneous formation of Rh(III)-alkyl complex. Acetonitrile, acetone and chloroform showed a non-linear correlation with variation in [CH_3I] at 25°C with a linear correlation for ethyl acetate (**Figure 5.25**).

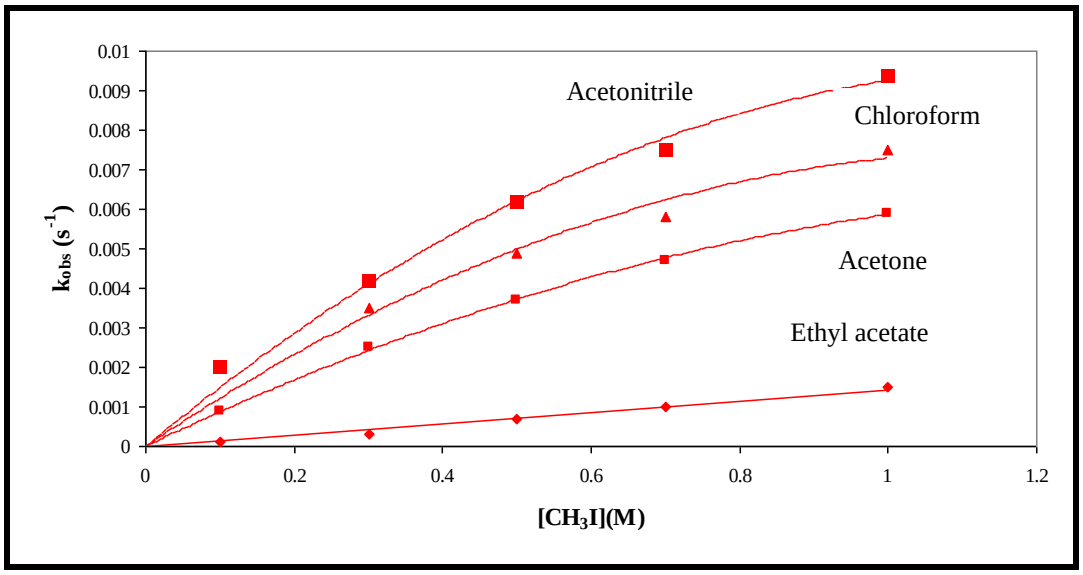

Figure 5.25: k_{obs} against [CH_3I] for oxidative addition (alkyl formation) of CH_3I to [Rh(cupf)(CO)(DPP)] in different solvents at 25°C.

The IR study in acetonitrile and chloroform also showed the formation of a Rh(III)-acyl complex which correlates well with the observed rate constants obtained for the UV/visible study. As was previously mentioned, the large absorption maxima at approximately 1700 cm^{-1} for acetone and ethyl acetate prevented the possible observation of the Rh(III)-acyl complex formation.

The absence of acyl formation and the difference in mechanism for ethyl acetate compared to the other solvents investigated is interesting and unexpected. Normally, the more polar solvent or better donor solvent molecule accelerates the rate of oxidative addition but from this comparative set of kinetic data the effect seems to be much smaller than expected from the polarity and donocity values (see **Table 5.1**). A possible reason for the difference in mechanism which was obtained for the two sets of solvents (acetonitrile, acetone and chloroform *vs* ethyl acetate) may be due to the difference in geometry of the oxidative addition product as indicated in **Figure 5.26**.

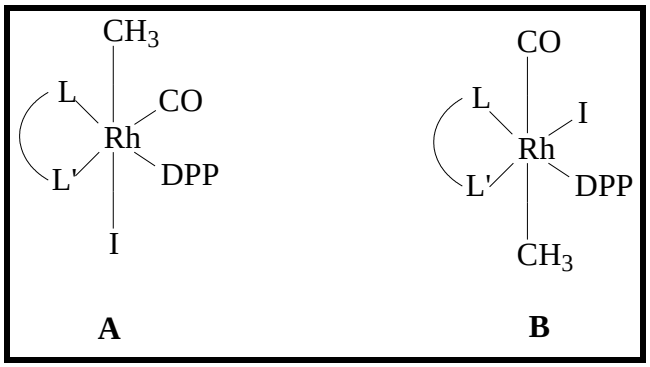

Figure 5.26: Geometry of oxidative addition product.

In structure **A** the CH_3 and CO ligands are situated *cis* towards each other allowing the migration of the CO group much easier compared to structure **B** were the two ligands are situated *trans* with respect to each other making the distance much longer with the route possible obstructed by the phosphine and iodide ligands.

The kinetic data showed that the oxidative addition of CH_3I to [Rh(cupf)(CO)(DPP)] in three of the four solvents investigated proceeds *via* the rapid formation of a reactive Rh(I)*-intermediate followed by the formation of a Rh(III)-alkyl complex and finally the formation of a Rh(III)-acyl complex which is a much slower reaction.

It is clear from the kinetics that the establishment of the equilibrium in the initial reaction is much faster than the rate of alkyl formation as illustrated by the almost identical rate constants for the Rh(I) disappearance and the Rh(III)-alkyl formation. The K values of approximately one is also large enough to ensure a constant (therefore a pre-equilibrium approximation in the rate law) supply of intermediate to ensure the complete disappearance of the Rh(I) complex as indicated by **Figure 5.12-5.14**.

A possible structure of the Rh(I)*-intermediate is given in **Figure 5.27**. Transition state **C** represents a S_N2 mechanism and **D** a concerted three-centered mechanism.

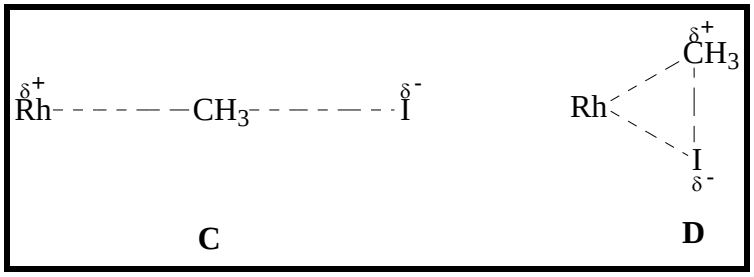

Figure 5.27: Possible structure of the Rh(I)*-intermediate.

The nature of the intermediate, as suggested by the reaction scheme is also very interesting. The clear movement in reaction from Rh(I) to Rh(III), as suggested by the IR spectrum, with no indication of a Rh(I) carbonyl stretching frequency shift indicate a more loose interaction between the Rh(I) center and the CH_3I molecule rather than a formal bond formation reaction. The formation of this intermediate seems to be a very important step in the formation of the Rh(III)-acyl product as is evident from the difference in mechanism for the two sets of solvents that were used in this study. The absence of any shoulders or new peaks with the formation of the Rh(III)-alkyl product in the IR study (see **Figure 5.12-5.14**) suggests the formation of only one Rh(III)-alkyl

isomer during the first step of the reaction. The reaction in acetonitrile (most polar solvent), acetone and chloroform would rather proceed according to **C**, which involves a two centered transition state that normally results in large charge transfer and can also lead to stereochemical inversion at the carbon center of the alkyl group. The reaction according to **D** is more likely to take place in ethyl acetate (less charge transfer) with retention or inversion of configuration at carbon. Both pathways however can disintegrate into either *cis* or *trans* adducts. The activation enthalpy and entropy values for various oxidative addition reactions have indicated that a clear distinction cannot be made between two- and three-centered transition states.

The kinetic data in **Table 5.3** shows that there is an increase in reaction rate for the oxidative addition and CO insertion reactions with an increase in temperature as expected. There is also a slight difference in reaction rate for each solvent used during the study. Comparison of the rate constants with the dielectric constants and donocity values of the solvents showed that more polar solvents, like acetonitrile, accelerated the reaction. The role of the polarity of the solvent can be seen for the values obtained for k_2 which indicate an increase in reaction rate with a increase in dielectric constant as was observed for acetonitrile, acetone and chloroform. In the case of ethyl acetate a negligible contribution was observed and can be seen in the slower rate observed. The k_{-1} values obtained were considered to be approximately zero within experimental fault. The values obtained for ΔH^* and ΔS^* were calculated from data points obtained at only three temperatures with a narrow 15°C variation. The values for the activation parameters obtained during the study were compared to values obtained for [Rh(cupf)(CO)(PPh_3)] in acetonitrile, acetone and chloroform and are summarized in **Table 5.5**.

Table 5.5: Activation parameters for the oxidative addition of CH_3I to [Rh(cupf)(CO)(PPh_3)] and [Rh(cupf)(CO)(DPP)] in acetonitrile, acetone and chloroform.

Complex	Solvent	ΔH*(kJ.mol^{-1})	ΔS*(J.K^{-1}.mol^{-1})
[Rh(cupf)(CO)(PPh_3)]	Acetonitrile	42(1)	-144(1)
	Acetone	36(1)	-180(5)
	Chloroform	33(3)	-180(9)
[Rh(cupf)(CO)(DPP)]#	Acetonitrile	48(9)	-214(7)
	Acetone	34(8)	-209(6)
	Chloroform	12(9)	-173(7)

#This study

As can been seen from **Table 5.5**, the values obtained during this study differ slightly from those found for the [Rh(cupf)(CO)(PPh_3)] complex with slightly higher ΔH* values and slightly lower ΔS* values. The relatively small ΔH* values, along with the large negative ΔS* values, indicates a possible nucleophilic attack on carbon which leads to a linear S_N2-displacement at carbon, so that the transition state can be represented by **C**. This is indicative of an assosiative mechanism which involves bond forming and /or charge transfer during the formation of the transition state.

The results for the alkyl and acyl formation was compared to other [Rh(cupf)(CO)(PX_3] complexes and are summarized in **Table 5.6**. This comparative study allows for the isolation of the steric or the electronic influence of the different phosphine ligands on the rate of alkyl and acyl formation.

Table 5.6: Rate constants for the oxidative addition of CH_3I to $[Rh(cupf)(CO)(PX_3)]$[11] in acetone at 25°C.

PX_3	θ	υ (cm^{-1})	pK_a	10^3k (alkyl) ($M^{-1}s^{-1}$)	10^3k (acyl) (s^{-1})
	Cone angle[12]	Tolman electronic parameter[12]			
P(*p*-$ClC_6H_4)_3$	145	2072.8	1.03	0.193(8)	0.14(6)
PPh_3	145	2068.9	2.73	1.22(2)	0.31(1)
P(*p*-$MeOC_6H_4)_3$	145	2066.1	4.57	4.20(8)	0.20(5)
DPP*	~145			9.0(1)	1.1(5)
PCy_3	170	2056.4	9.65	1.94(3)	0.24(2)

*This study

For this comparison, the cone angle for the DPP ligand was estimated to be the same as for PPh_3, as the only difference between the two ligands is the nitrogen situated on the benzene ring in the case of DPP. The results in **Table 5.6** clearly indicate that the cone angle for the first four phosphine ligands are the same but an increase of 50 times was observed for the Rh(III)-alkyl formation and 8 times increase in Rh(III)-acyl formation with the fastest reaction that of the electron rich DPP phosphine ligand. It is anticipated that the Tolman electronic parameter of DPP will be lower than that of P(*p*-$MeOC_6H_4)_3$ and the pK_a higher than the 4.57 of the same phosphine ligand due to the additional electron density that is centered in the DPP phosphine ligand. It is thus clear that the substantial increase in oxidative addition rate as well as acyl formation can be attributed to the electronic parameter or property of the DPP phosphine ligand. The additional electron density of the phosphine ligand increases the nucleophilicity of the rhodium metal center which then increases the reaction rate with the CH_3I molecule.

[11] D.E. Graham, G.J. Lamprecht, I.M. Potgieter, A. Roodt and J.G. Leipoldt, *Transition Met. Chem*., **16**, (1991), 193.

[12] C.A. Tolman, *Chem. Rev*., **77**, (1977), 313.

These results correlate also very well with those obtained in the IR study as discussed in **Chapter 4**, **Paragraph 4.6**. The carbonyl stretching frequency for the [Rh(cupf)(CO)(DPP)] complex is the highest for all the phoshines discussed due to a possible interaction between the phosphine's nitrogen and the carbonyl, resulting in a weaker Rh-CO bond. This can then lead to easier CO migration the Rh(III)-acyl formation reaction.

5.4 Conclusion

In conclusion, the kinetic study of the oxidative addition of CH_3I to the [Rh(cupf)(CO)(DPP)] complex demonstrated very interesting kinetics. Not only were two different mechanisms obtained for the different solvents, but also different products were obtained under these conditions. The [Rh(cupf)(CO)(DPP)] undergoes oxidative addition by methyl iodide, forming a Rh(I)*-intermediate species *via* a very fast equilibrium, followed by the formation of a Rh(III)-alkyl species and finally the formation of a Rh(III)-acyl species as was observed for acetonitrile, acetone and chloroform. Only one reaction was observed for ethyl acetate. The results obtained during the study show that more electron back donation from the phosphine ligand to the metal center led to a more rapid reaction between CH_3I and the [Rh(cupf)(CO)(DPP)] complex by increasing the nucleophilicity of the metal center.

Chapter 6

Evaluation of this study

The success and relevance of this study is outlined in this chapter with respect to the aims depicted in **Chapter 1**. Lastly, some future research aspects are also given.

6.1 Success and relevance

Firstly, the aim of this study was to synthesize and characterize different [Rh(LL')(CO)(DPP)] complexes [LL' = cupf (N-Phenyl-N-nitrosohydroxylamine ammonium salt, acac (2,4-pentadione) and DPP (diphenyl-2-pyridylphosphine)]. The above-mentioned complexes was successfully synthesized and characterized by means of IR and NMR (**Chapter 4**). We were also successful in the isolation of [Rh(acac)(CO)(DPP)] which crystallizes in two different space groups. The oxidative addition products for [Rh(cupf)(CO)(DPP)] were also isolated and characterized by means of IR and NMR.

The second aim was to study kinetically the oxidative addition between methyl iodide and [Rh(cupf)(CO)(DPP)] in different solvents and at different temperatures to determine the rates of this reaction as well as to obtain a possible mechanism for the reaction. Both the formation of the Rh(III) alkyl and Rh(III) acyl compounds were kinetically observed and studied. The oxidative addition reaction in acetonitrile, acetone and chloroform as solvents showed the rapid formation of the Rh(III)-alkyl with the subsequent slow formation of the Rh(III)-acyl complex. The same reaction in ethyl acetate only produced the Rh(III)-alkyl complex as final product. A comparative study indicated that the DPP phosphine ligand increases the rate of oxidative addition by a factor of 50 while acyl formation increased by a factor 7 as a result of the added electron density of the nitrogen within the phosphine ligand.

It is clear from these results that the main objectives, as set out in **Chapter 1**, has all successfully been achieved and it's our opinion that this study was great success.

This study again underlines the importance of the manipulation of the reactivity of rhodium complexes by means of the variation of phosphine ligands or bidentate ligands to influence the rate of oxidative addition and also the type of final product that is obtained from the reaction. These results not only increase our understanding of the catalytic involvement of rhodium complexes in, for example the Monsanto process, but also enable us to suggest possible changes to the catalyst to decrease the harshness of the reaction conditions, eliminate or decrease side-reactions or increase yield in future.

6.2 Future research

The mechanism for the oxidative addition of methyl iodide to [Rh(cupf)(CO)(DPP)] is discussed in detail in **Chapter 5**, but information about the intermediate formed during the first step is sketchy and mainly unknown, and a high pressure kinetic study may improve our knowledge on the type of intermediate as well as its importance in the production or formation of the final acyl product. In **Chapter 4** the [Rh(acac)(CO)(DPP)] complex was successfully synthesized and characterized by means of IR, NMR and crystallographic data. The next step will be to investigate the oxidative addition of the above-mentioned complex to learn more about the type of mechanisms the complex follows and if there is any correlation between the [Rh(acac)(CO)(DPP)] and [Rh(cupf)(CO)(DPP)] complexes during the oxidative addition reaction. The study can be further extended to other bidentate ligands to see the effect different donor atoms have on oxidative addition. The study can even be extended to a variation in the type of metal center used. By substituting rhodium for iridium, the effect on the oxidative addition can be observed and compared to other iridium and rhodium complexes to see what effect the phophine ligand under investigation has on the nucleophilicity of the metal centre.

Finally, the DPP phoshine ligand can act as a mono as well as a bidentate ligand as indicated by previous studies. UV radiation of the [Rh(L,L')(CO)(DPP)] complex can possibly lead to the formation of a five-coordinated complex which can also undergo oxidative addition. This in itself will open a new and exciting new angle to the oxidative addition reactions of rhodium and iridium complexes.

Appendix A

Crystal Data

Supplementary data for the structures discussed in **Chapter 4**, is given in this section. The three tables for each complex is given under a heading consisting of the formula of the complex studied containing: (1) a table containing all the bond angles, (2) a table containing all the bond distances and (3) a table containing the anisotropic thermal parameters.

Appendix A

Monoclinic [Rh(acac)(CO)(DPP)], paragraph 4.2.2

Table 1: Interatomic bond distances (Å) for monoclinic [Rh(acac)(CO)(DPP)].

Rh—C1	1.810(2)	C11—C12	1.386(3)
Rh—O3	2.035(2)	C12—C13	1.385(4)
Rh—O2	2.070(2)	C13—C14	1.377(4)
Rh—P1	2.230(1)	C14—C15	1.378(4)
P—C31	1.821(2)	C21—C22	1.387(3)
P—C21	1.822(2)	C21—C26	1.387(3)
P—C11	1.839(2)	C22—C23	1.390(3)
O1—C1	1.147(3)	C23—C24	1.380(4)
O2—C3	1.274(3)	C24—C25	1.386(4)
O3—C5	1.275(3)	C25—C26	1.371(3)
N—C15	1.359(3)	C31—C32	1.390(3)
N—C11	1.362(3)	C31—C36	1.396(3)
C2—C3	1.510(3)	C32—C33	1.385(3)
C3—C4	1.389(3)	C33—C34	1.374(3)
C4—C5	1.394(3)	C34—C35	1.391(3)
C5—C6	1.502(4)	C35—C36	1.384(3)

Table 2: Interatomic bond angles (°) for monoclinic [Rh(acac)(CO)(DPP)].

C1—Rh—O3	177.66(8)	N—C11—C12	122.16(2)
C1—Rh—O2	93.63(8)	N—C11—P	114.49(1)
O3—Rh—O2	88.42(6)	C12—C11—P	123.34(2)
C1—Rh—P	85.26(7)	C11—C12—C13	119.29(2)
O3—Rh—P	92.71(4)	C14—C13—C12	119.21(2)
O2—Rh—P	178.43(4)	C13—C14—C15	118.98(3)
C31—P—C21	104.54(9)	N—C15—C14	123.13(3)
C31—P—C11	103.56(9)	C22—C21—C26	119.78(2)
C21—P—C11	103.94(9)	C22—C21—P	123.18(2)
C31—P—Rh	116.80(7)	C26—C21—P	116.90(2)
C21—P—Rh	112.61(6)	C21—C22—C23	119.73(2)
C11—P—Rh	114.05(6)	C24—C23—C22	120.21(2)
C3—O2—Rh	126.64(1)	C23—C24—C25	119.58(3)
C5—O3—Rh	127.60(1)	C26—C25—C24	120.55(2)
C15—N—C11	117.22(2)	C25—C26—C21	120.12(2)
O1—C1—Rh	178.47(2)	C32—C31—C36	119.61(2)
O2—C3—C4	125.73(2)	C32—C31—P	121.16(2)
O2—C3—C2	114.68(2)	C36—C31—P	119.23(2)
C4—C3—C2	119.58(2)	C33—C32—C31	119.90(2)
C3—C4—C5	125.94(2)	C34—C33—C32	120.70(2)
O3—C5—C4	125.64(2)	C33—C34—C35	119.72(2)
O3—C5—C6	114.93(2)	C36—C35—C34	120.26(2)
C4—C5—C6	119.43(2)	C35—C36—C31	119.81(2)

Appendix A

Table 3: Anisotropic displacement parameters (in Å ^{2}) for monoclinic [Rh(acac)(CO)(DPP)].

Atom	U_{11}	U_{22}	U_{33}	U_{12}	U_{13}	U_{23}
Rh	0.01686(8)	0.01676(8)	0.01774(8)	-0.00021(6)	0.00598(6)	-0.00119(6)
P	0.0141(2)	0.0158(2)	0.0174(2)	0.00127(2)	0.00381(2)	-0.00040(2)
O1	0.0435(1)	0.0230(8)	0.0357(9)	-0.0073(7)	0.0185(8)	-0.0026(7)
O2	0.0303(8)	0.0234(8)	0.0216(7)	0.0005(7)	0.0107(6)	-0.0030(6)
O3	0.0252(8)	0.0230(8)	0.0225(7)	-0.0038(6)	0.0065(6)	0.0010(6)
N	0.0226(1)	0.0404(1)	0.0335(1)	-0.0032(9)	0.0045(8)	-0.0052(9)
C1	0.0253(1)	0.0223(1)	0.0224(1)	-0.0012(9)	0.0092(9)	-0.0074(8)
C2	0.0483(2)	0.0414(2)	0.0224(1)	0.0113(1)	0.0139(1)	-0.0014(1)
C3	0.0232(1)	0.0316(1)	0.0205(1)	0.0081(9)	0.0058(8)	0.0016(9)
C4	0.0332(1)	0.0358(1)	0.0211(1)	0.0019(1)	0.0111(9)	0.0067(9)
C5	0.0192(1)	0.0295(1)	0.0237(1)	-0.0011(9)	0.0021(8)	0.0076(9)
C6	0.0445(2)	0.0348(1)	0.0331(1)	-0.0096(1)	0.0075(1)	0.0100(1)
C11	0.0154(9)	0.0229(1)	0.0152(8)	0.0030(8)	0.0041(7)	0.0020(7)
C12	0.0225(1)	0.0238(1)	0.0268(1)	0.0035(9)	0.0092(9)	0.0020(9)
C13	0.0309(1)	0.0353(1)	0.0329(1)	0.0154(1)	0.0154(1)	0.0079(1)
C14	0.0178(1)	0.0611(2)	0.0275(1)	0.0097(1)	0.0072(9)	0.0127(1)
C15	0.0214(1)	0.0534(2)	0.0319(1)	-0.0075(1)	0.0015(1)	-0.0032(1)
C21	0.0194(1)	0.0172(1)	0.0174(9)	0.0007(8)	0.0018(8)	-0.0006(7)
C22	0.0236(1)	0.0233(1)	0.0252(1)	0.0041(9)	0.0074(9)	0.0010(8)
C23	0.0347(1)	0.0337(1)	0.0264(1)	0.0015(1)	0.0125(1)	0.0059(1)
C24	0.0354(1)	0.0289(1)	0.0299(1)	0.0039(1)	0.0042(1)	0.0093(1)
C25	0.0264(1)	0.0311(1)	0.0345(1)	0.0088(1)	0.0031(1)	0.0048(1)
C26	0.0193(1)	0.0274(1)	0.0236(1)	0.0035(9)	0.0054(8)	0.0035(9)
C31	0.0144(9)	0.0185(1)	0.0216(9)	0.0005(7)	0.0068(7)	-0.0034(8)
C32	0.0199(1)	0.023(1)	0.0202(9)	0.0001(8)	0.0067(8)	-0.0012(8)
C33	0.0222(1)	0.0315(1)	0.0236(1)	-0.0044(9)	0.0054(9)	-0.0068(9)
C34	0.0253(1)	0.0251(1)	0.0355(1)	-0.0067(9)	0.0113(1)	-0.0093(9)
C35	0.0271(1)	0.0196(1)	0.0346(1)	-0.0022(9)	0.0106(9)	0.0013(9)
C36	0.0194(1)	0.0223(1)	0.0257(1)	0.0014(8)	0.0056(8)	0.0001(8)

Triclinic [Rh(acac)(CO)(DPP)], paragraph 4.2.3

Table 1: Interatomic bond distances (Å) for triclinic [Rh(acac)(CO)(DPP)].

Rh1—C11	1.790(2)	C111—C112	1.385(2)
Rh1—O13	2.030(2)	C112—C113	1.385(2)
Rh1—O12	2.074(5)	C113—C114	1.361(3)
Rh1—P1	2.243(5)	C114—C115	1.364(2)
Rh2—C21	1.787(2)	C121—C122	1.369(4)
Rh2—O23	2.034(2)	C121—C126	1.373(3)
Rh2—O22	2.067(5)	C122—C123	1.38(2)
Rh2—P2	2.234(5)	C123—C124	1.362(3)
P1—C131	1.829(2)	C124—C125	1.359(4)
P1—C111	1.832(4)	C125—C126	1.379(2)
P1—C121	1.835(3)	C131—C132	1.366(2)
P2—C221	1.826(3)	C131—C136	1.371(1)
P2—C231	1.831(3)	C132—C133	1.367(1)
P2—C211	1.846(1)	C133—C134	1.374(2)
N1—C111	1.381(3)	C134—C135	1.364(2)
N1—C115	1.395(2)	C135—C136	1.378(1)
N2—C211	1.361(2)	C211—C212	1.349(4)
N2—C215	1.375(1)	C212—C213	1.379(1)
O11—C11	1.150(1)	C213—C214	1.349(2)
O12—C13	1.278(2)	C214—C215	1.368(4)
O13—C15	1.276(2)	C221—C222	1.383(3)
O21—C21	1.143(2)	C221—C226	1.385(3)
O22—C23	1.272(2)	C222—C223	1.388(2)
O23—C25	1.272(2)	C223—C224	1.367(3)
C12—C13	1.508(4)	C224—C225	1.367(3)
C13—C14	1.372(2)	C225—C226	1.381(2)
C14—C15	1.379(4)	C231—C232	1.361(2)
C15—C16	1.505(2)	C231—C236	1.376(2)
C22—C23	1.509(4)	C232—C233	1.380()
C23—C24	1.384(2)	C233—C234	1.363(2)
C24—C25	1.381(4)	C234—C235	1.359(2)
C25—C26	1.502(2)	C235—C236	1.375(2)

Appendix A

Table 2: Interatomic bond angles (°) for triclinic [Rh(acac)(CO)(DPP)].

C11—Rh1—O13	178.36(1)	N1—C111—C112	120.42(3)
C11—Rh1—O12	91.86(2)	N1—C111—P1	119.88(2)
O13—Rh1—O12	88.09(9)	C112—C111—P1	119.30(2)
C11—Rh1—P1	89.58(1)	C113—C112—C111	119.90(3)
O13—Rh1—P1	90.58(7)	C114—C113—C112	120.23(3)
O12—Rh1—P1	176.43(7)	C113—C114—C115	119.66(5)
C21—Rh2—O23	178.34(1)	C114—C115—N1	121.87(3)
C21—Rh2—O22	90.29(2)	C122—C121—C126	119.85(3)
O23—Rh2—O22	88.40(1)	C122—C121—P1	118.00(3)
C21—Rh2—P2	93.22(1)	C126—C121—P1	122.15(3)
O23—Rh2—P2	88.12(9)	C121—C122—C123	119.62(3)
O22—Rh2—P2	176.09(7)	C124—C123—C122	120.66(5)
C131—P1—C111	102.61(1)	C125—C124—C123	119.57(5)
C131—P1—C121	103.67(1)	C124—C125—C126	120.62(5)
C111—P1—C121	104.24(1)	C121—C126—C125	119.68(4)
C131—P1—Rh1	118.0(1)	C132—C131—C136	120.25(3)
C111—P1—Rh1	112.98(1)	C132—C131—P1	121.48(2)
C121—P1—Rh1	113.78(1)	C136—C131—P1	118.18(2)
C221—P2—C231	105.03(1)	C131—C132—C133	119.56(3)
C221—P2—C211	101.03(2)	C132—C133—C134	120.79(4)
C231—P2—C211	104.62(2)	C135—C134—C133	119.45(4)
C221—P2—Rh2	115.47(1)	C134—C135—C136	120.15(3)
C231—P2—Rh2	108.74(1)	C131—C136—C135	119.76(3)
C211—P2—Rh2	120.44(1)	C212—C211—N2	122.55(3)
C111—N1—C115	117.85(3)	C212—C211—P2	122.38(2)
C211—N2—C215	117.27(3)	N2—C211—P2	115.05(2)
C13—O12—Rh1	125.86(2)	C211—C212—C213	118.65(3)
C15—O13—Rh1	128.20(2)	C214—C213—C212	120.91(4)
C23—O22—Rh2	126.17(2)	C213—C214—C215	118.89(3)
C25—O23—Rh2	127.91(2)	C214—C215—N2	121.72(4)
O11—C11—Rh1	177.89(3)	C222—C221—C226	119.05(3)
O12—C13—C14	126.25(3)	C222—C221—P2	121.34(3)
O12—C13—C12	114.30(3)	C226—C221—P2	119.60(3)
C14—C13—C12	119.45(3)	C221—C222—C223	120.17(4)
C13—C14—C15	126.59(3)	C224—C223—C222	119.99(4)
O13—C15—C14	124.98(4)	C225—C224—C223	120.29(4)
O13—C15—C16	114.58(3)	C224—C225—C226	120.30(5)
C14—C15—C16	120.44(3)	C225—C226—C221	120.11(3)
O21—C21—Rh2	174.80(4)	C232—C231—C236	119.36(3)
O22—C23—C24	125.75(3)	C232—C231—P2	121.80(3)
O22—C23—C22	113.69(4)	C236—C231—P2	118.34(2)
C24—C23—C22	120.56(4)	C231—C232—C233	119.93(4)
C25—C24—C23	126.86(4)	C234—C233—C232	120.63(3)
O23—C25—C24	124.85(4)	C235—C234—C233	119.48(5)
O23—C25—C26	114.36(3)	C234—C235—C236	120.33(4)
C24—C25—C26	120.77(4)	C235—C236—C231	120.23(3)

Table 3: Anisotropic displacement parameters (in Å ^{2}) for triclinic [Rh(acac)(CO)(DPP)].

Atom	U_{11}	U_{22}	U_{33}	U_{12}	U_{13}	U_{23}
Rh1	0.03822(1)	0.03623(1)	0.04664(1)	0.01024(1)	0.01306(1)	0.01791(1)
Rh2	0.04791(2)	0.04337(1)	0.04705(2)	0.00777(1)	0.01479(1)	0.01674(1)
P1	0.0370(4)	0.0356(3)	0.0413(4)	0.0123(3)	0.0134(3)	0.0155(3)
P2	0.0466(4)	0.0389(4)	0.0436(4)	0.0103(3)	0.0117(3)	0.0149(3)
N1	0.068(2)	0.072(2)	0.066(2)	0.0181(2)	0.0188(2)	0.0138(2)
N2	0.082(2)	0.0634(2)	0.0653(2)	0.0209(2)	0.0169(2)	0.0240(2)
O11	0.107(2)	0.099(2)	0.0692(2)	0.0129(2)	-0.0055(2)	0.0470(2)
O12	0.0427(1)	0.0440(1)	0.0647(1)	0.0090(9)	0.0154(1)	0.0201(1)
O13	0.0554(1)	0.0528(1)	0.0570(1)	0.0135(1)	0.0162(1)	0.0302(1)
O21	0.086(2)	0.181(4)	0.101(2)	-0.001(2)	-0.0080(2)	0.094(3)
O22	0.0539(1)	0.0523(1)	0.0644(1)	0.0018(1)	0.0217(1)	0.0133(1)
O23	0.0739(2)	0.0618(1)	0.0636(2)	0.0153(1)	0.0182(1)	0.0361(1)
C11	0.0531(2)	0.0510(2)	0.061(2)	0.0048(2)	0.0075(2)	0.0254(2)
C12	0.056(2)	0.056(2)	0.102(3)	0.0054(2)	0.032(2)	0.024(2)
C13	0.0512(2)	0.0357(2)	0.076(2)	0.0153(1)	0.0314(2)	0.0164(2)
C14	0.070(2)	0.0509(2)	0.076(2)	0.0226(2)	0.043(2)	0.0334(2)
C15	0.066(2)	0.0441(2)	0.062(2)	0.0218(2)	0.0297(2)	0.0258(2)
C16	0.101(3)	0.078(3)	0.069(2)	0.027(2)	0.030(2)	0.044(2)
C21	0.052(2)	0.084(3)	0.062(2)	-0.0014(2)	0.0095(2)	0.035(2)
C22	0.075(3)	0.072(3)	0.118(4)	-0.005(2)	0.047(3)	0.019(3)
C23	0.065(2)	0.0432(2)	0.084(3)	0.0085(2)	0.045(2)	0.0104(2)
C24	0.092(3)	0.051(2)	0.082(3)	0.020(2)	0.051(2)	0.030(2)
C25	0.087(3)	0.0526(2)	0.070(2)	0.028(2)	0.037(2)	0.0319(2)
C26	0.136(4)	0.094(3)	0.091(3)	0.056(3)	0.051(3)	0.065(3)
C111	0.0345(1)	0.0468(2)	0.0421(2)	0.0124(1)	0.0129(1)	0.0132(1)
C112	0.0481(2)	0.0606(2)	0.0558(2)	0.0221(2)	0.0118(2)	0.0242(2)
C113	0.058(2)	0.089(3)	0.057(2)	0.027(2)	0.0124(2)	0.038(2)
C114	0.060(2)	0.100(3)	0.0426(2)	0.015(2)	0.0107(2)	0.017(2)
C115	0.079(3)	0.070(2)	0.051(2)	0.014(2)	0.0154(2)	0.0011(2)
C121	0.0503(2)	0.0385(2)	0.0518(2)	0.0183(1)	0.0232(1)	0.0207(1)
C122	0.062(2)	0.064(2)	0.0534(2)	0.0251(2)	0.0208(2)	0.0123(2)
C123	0.114(4)	0.075(3)	0.063(2)	0.039(3)	0.045(2)	0.013(2)
C124	0.099(3)	0.084(3)	0.102(3)	0.058(3)	0.065(3)	0.042(3)
C125	0.068(2)	0.091(3)	0.096(3)	0.045(2)	0.037(2)	0.040(3)
C126	0.053(2)	0.064(2)	0.065(2)	0.0279(2)	0.0221(2)	0.0200(2)
C131	0.0434(2)	0.0344(1)	0.0365(1)	0.0107(1)	0.0110(1)	0.0131(1)
C132	0.0401(2)	0.0467(2)	0.0649(2)	0.0167(1)	0.0216(1)	0.0259(2)
C133	0.057(2)	0.059(2)	0.080(2)	0.0127(2)	0.0303(2)	0.0366(2)
C134	0.065(2)	0.0412(2)	0.062(2)	0.0139(2)	0.0154(2)	0.0259(2)
C135	0.0552(2)	0.0469(2)	0.071(2)	0.0231(2)	0.0193(2)	0.0220(2)
C136	0.0433(2)	0.0420(2)	0.0594(2)	0.0138(1)	0.0238(1)	0.0209(1)
C211	0.0452(2)	0.0412(2)	0.0506(2)	0.0138(1)	0.0168(1)	0.0195(1)
C212	0.066(2)	0.0440(2)	0.0490(2)	0.0112(2)	0.0033(2)	0.0141(2)
C213	0.082(3)	0.0430(2)	0.073(3)	0.0127(2)	0.009(2)	0.0083(2)
C214	0.067(2)	0.0491(2)	0.084(3)	0.0216(2)	0.025(2)	0.0326(2)
C215	0.079(3)	0.068(2)	0.064(2)	0.027(2)	0.0215(2)	0.034(2)
C221	0.0562(2)	0.0488(2)	0.0435(2)	0.0188(2)	0.0147(1)	0.0183(1)
C222	0.055(2)	0.065(2)	0.071(2)	0.0103(2)	0.0199(2)	0.0077(2)
C223	0.062(2)	0.104(3)	0.082(3)	0.029(2)	0.029(2)	0.027(3)
C224	0.088(3)	0.102(3)	0.078(3)	0.057(3)	0.040(2)	0.036(3)
C225	0.105(3)	0.061(2)	0.081(3)	0.040(2)	0.041(2)	0.020(2)
C226	0.070(2)	0.0474(2)	0.064(2)	0.0156(2)	0.0223(2)	0.0174(2)
C231	0.0484(2)	0.0500(2)	0.0457(2)	0.0095(1)	0.0084(1)	0.0151(1)
C232	0.082(3)	0.079(2)	0.053(2)	0.045(2)	0.0085(2)	0.0142(2)
C233	0.104(4)	0.119(4)	0.069(3)	0.063(3)	0.001(2)	0.024(3)
C234	0.085(3)	0.107(3)	0.051(2)	0.029(3)	0.006(2)	0.023(2)
C235	0.058(2)	0.097(3)	0.053(2)	0.019(2)	0.0146(2)	0.010(2)
C236	0.0488(2)	0.077(2)	0.0514(2)	0.0215(2)	0.0099(2)	0.0155(2)

Appendix B

Material Safety Data Sheets

Safety data for acetonitrile

General

Synonyms: cyanomethane, ethyl nitrile, methanecarbonitrile, methyl cyanide, ethanenitrile, USAF EK-488, NCI-C60822, NA 1648.

Molecular formula: C_2H_3N

CAS No: 75-05-8

EC No: 200-835-2

Annex I Index No: 608-001-00-3

Physical data

Appearance: colourless liquid with ether-like odour

Melting point: -46 °C

Boiling point: 80 °C

Vapour density: 1.41

Vapour pressure: 72.8 mm Hg at 20 °C

Specific gravity: 0.786

Flash point: 6 °C

Explosion limits: 4.4% - 16%

Autoignition temperature: 973 F

Critical temperature: 275 °C

Stability

Unstable. Incompatible with alkali metals, acids, bases, reducing agents and oxidizing agents. Highly flammable.

Toxicology

Toxic by inhalation, ingestion or skin absorption. Irritant. Typical STEL 60 ppm. Typical OEL 30 ppm. May cause serious damage to the eyes. Possible teratogen.

Personal protection

Safety glasses. Good ventilation.

Safety data for Acetone

General

Synonyms: dimethyl ketone, methyl ketone, 2-propanone, beta-ketopropane, acetone, dimethylketal, pyroacetic acid, dimethylformaldehyde, pyroacetic ether

Molecular formula: $(CH_3)_2CO$

CAS No: 67-64-1

EC No: 200-662-2

Annex I Index No: 606-001-00-8

Physical data

Appearance: colourless liquid with a fragrant, sweet odour

Melting point: -95 °C

Boiling point: 56 °C

Vapour density: 2.0

Vapour pressure: 181 mm Hg at 20 °C

Specific gravity: 0.79

Flash point: -18 C

Explosion limits: 2.6% - 13.0%

Autoignition temperature: 538 °C

Stability

Stable. Incompatible with halogen acids and halogen compounds, strong bases, strong oxidizing agents, caustics, amines and ammonia, chlorine and chlorine compounds, strong acids, nitrosyl compounds. Highly flammable. Readily forms explosive mixtures with air.

Toxicology

May be harmful by inhalation, ingestion or skin absorption. Irritant. Liquid may cause permanent eye damage (corneal clouding). Contact with skin may cause defatting, leading to irritation. Long-term exposure may cause liver damage. Typical TLV 750 ppm. Typical OEL 250 ppm.

Environmental information

Biological degradability: good. Aquatic toxicity: low. Bioaccumulation potential: low. Fish toxicity LC50 (*L. macrochirus*) 8300 mg/l/96h.

Personal protection

Safety glasses. Good ventilation. Remove sources of ignition from the working area. Butyl rubber gloves.

Safety data for chloroform

General

Synonyms: trichloromethane, methyl trichloride, formyl trichloride, methane trichloride, trichloroform, methenyl trichloride, trichlormethan

Molecular formula: $CHCl_3$

CAS No: 67-66-3

EC No: 200-663-8

Annex I Index No: 602-006-00-4

Physical data

Appearance: clear colourless liquid with a sweet odour

Melting point: -63 °C

Boiling point: 61 °C

Vapour density: 4.1

Vapour pressure: 159 mm Hg at 20 °C

Specific gravity: 1.48 g/cm^3

Flash point: none

Explosion limits:

Autoignition temperature:

Water solubility: 8 g/l at 20 °C

Refractive index: 1.4459 at 20 °C, 589 nm

Stability

Stable. May decompose on exposure to light. Incompatible with a wide variety of materials, including peroxy compounds, alkali amides, strong bases, alkali metals, magnesium, aluminium, strong oxidizing agents.

Toxicology

This material causes cancer in laboratory animals, and is IARC listed as a probable human carcinogen. Inhalation and ingestion are harmful and may be fatal. May cause reproductive damage. Irritant. Exposure to alcohol may increase toxic effects. Prolonged or repeated skin contact may cause dermatitis. Typical TLV 50 ppm.

Personal protection

Safety glasses and gloves. Good ventilation.

Safety data for dimethylformamide

General

Synonyms: N,N-dimethylformamide, dimethyl formamide, N-formyldimethylamine, DMF, U-4224, DMFA, NSC 5356

Molecular formula: $HCON(CH_3)_2$

CAS No: 68-12-2

EC No: 200-679-5

Annex I Index No: 616-001-00-X

Physical data

Appearance: colourless liquid with slight ammonia odour

Melting point: -61 °C

Boiling point: 153 °C

Vapour density: 2.5

Vapour pressure: 2.6 mm Hg at 20 °C

Specific gravity: 0.95

Flash point: 58 °C

Explosion limits: 2.2% - 15.2%

Autoignition temperature: 445 °C

Stability

Stable. Incompatible with strong oxidizing agents, halogenated hydrocarbons, chloroformates, active halogen compounds, strong acids, strong reducing agents, rubber, leather.

Toxicology

Harmful by inhalation, ingestion or skin contact. May act as a carcinogen. Ingestion or absorption through skin may be fatal. Exposure may result in foetal death. Long-term exposure may result in kidney or liver damage. Irritant.

Personal protection

Safety glasses. Good ventilation.

Safety data for ethyl acetate

General

Synonyms: acetic ether, acetoxyethane, ethyl ethanoate, acetic acid ethyl ester, ethanoic acid ethyl ester, ethyl acetic ester, acetidin, vinegar naphtha

Molecular formula: $CH_3COOC_2H_5$

CAS No: 141-78-6

EC No: 205-500-4

Annex I Index No: 607-022-00-5

Physical data

Appearance: colourless liquid with fruit-like odour

Melting point: -84 C

Boiling point: 77 C

Vapour density: 3.04

Vapour pressure: 100 mm Hg at 27 C

Specific gravity: 0.9

Flash point: -4 C

Explosion limits: 2.2 - 11%

Autoignition temperature:

Stability

Stable. Incompatible with various plastics, strong oxidizing agents. Highly flammable. Vapour/air mixtures explosive. May be moisture sensitive.

Toxicology

Harmful if swallowed in quantity. Vapours may cause drowsiness. Irritant. Typical PEL 400 ppm.

Personal protection

Safety glasses, adequate ventilation.

Safety data for celite

General

Synonyms: infusorial earth, amorphous silica, diatomaceous silica, kieselgur, various trade names

Molecular formula: SiO_2

CAS No: 61790-53-2

EINECS No: 212-293-4

Physical data

Appearance: tan powder

Melting point:

Boiling point:

Vapour density:

Vapour pressure:

Density (g cm^{-3}):

Flash point:

Explosion limits:

Autoignition temperature:

Stability

Stable. Incompatible with strong acids

Toxicology

Harmful if inhaled; may be harmful if ingested in quantity. Eye, skin and respiratory irritant.

Personal protection

Safety glasses, adequate ventilation.

Safety data for cupferron

General

Synonyms: N-Hydroxy-N-nitrosobenzenamine ammonium salt; N-Nitroso-N-phenylhydroxyamine ammonium salt.

Molecular formula: $C_6H_9N_3O_2$

CAS No: AC195770000

Physical data

Appearance: white yellow - brown - beige - light buff, with an ammonia-like odour

Melting point: 153 - 163 °C

Boiling point:

Vapour density:

Vapour pressure:

Density (g cm^{-3}):

Flash point:

Explosion limits:

Autoignition temperature:

Water solubility:

Stability

Air sensitive. Light sensitive. Hygroscopic: absorbs moisture or water from the air.

Toxicology

Toxic if swallowed. Suspect cancer hazard. May cause cancer. Causes eye, skin, and respiratory tract irritation.

Personal protection

Safety glasses, gloves, good ventilation.

Safety data for diphenyl-2-pyridylphosphine

General

Molecular formula: $C_{17}H_{14}NP$

CAS No: 37943-90-1

Physical data

Appearance: orange-yellow powder

Melting point: 82-85 °C

Boiling point:

Vapour density:

Vapour pressure:

Density (g cm^{-3}):

Flash point:

Explosion limits:

Autoignition temperature:

Stability

Unstable. May decompose if exposed to light.

Toxicology

Irritating to eyes, respiratory system and skin

Personal protection

Safety glasses, adequate ventilation.

Safety data for Rhodium trichloride hydrate

General

Molecular formula: $RhCl_3.xH_2O$

CAS No: 20765-98-4

Physical data

Appearance: dark red solid

Melting point: 187 °C

Boiling point:

Vapour density:

Vapour pressure:

Specific gravity:

Flash point:

Explosion limits:

Autoignition temperature:

Stability

Stable. May decompose on exposure to light**.**

Toxicology

Irritating to eyes, respiratory system and skin

Personal protection

Safety glasses, gloves, good ventilation.

Safety data for 2,4-pentadione

General

Synonyms: acetylacetone, acetyl-2-propanone, diacetylmethane

Molecular formula: $C_5H_8O_2$

CAS No: 123-54-6

EINECS No: 204-634-0

Physical data

Appearance: colourless liquid with an unpleasant smell

Melting point: -23 °C

Boiling point: 140 °C

Vapour density: 3.5 (air = 1)

Vapour pressure:

Density (g cm^{-3}): 0.98

Flash point: 41 °C (closed cup)

Explosion limits: 2.4 – 11.6%

Autoignition temperature:

Water solubility: appreciably

Stability

Stable. Combustible. Incompatible with strong oxidizing agents. May discolour in light

Toxicology

Harmful if inhaled or swallowed. Possible teratogen; may cause harm to the unborn child. Irritant.

Personal protection

Safety glasses, adequate ventilation.

Safety data for phosphorus pentoxide

General

Synonyms: diphosphorus pentoxide, phosphorus (V) oxide, phosphorus pentaoxide, phosphorus oxide, phosphoric anhydride

Molecular formula: P_4O_{10}

CAS No: 1314-56-3

EINECS No: 215-236-1

Annex I Index No: 015-010-00-0

Physical data

Appearance: white powder or crystals with a sharp, irritating odour

Melting point: 360 °C

Boiling point:

Vapour density: 4.9 (air = 1)

Vapour pressure: 10 mm Hg at 238 °C

Density (g cm^{-3}): 2.38

Flash point:

Explosion limits:

Autoignition temperature:

Water solubility:

Stability

Stable, but reacts violently with water, alcohols, metals, sodium, potassium, ammonia, oxidizing agents, HF, peroxides, magnesium, strong bases.

Toxicology

Toxic if inhaled. Harmful if swallowed or absorbed through the skin. Very destructive of mucous membranes. Eye contact may lead to serious permanent eye damage. Corrosive - causes burns.

Personal protection

Safety glasses, gloves, good ventilation.

Appendix C

Purification of solvents[1]

Several precautions have to be considered before the handling and purification of the solvent:

a) Never use sodium, active metals or metal hydrides to dry acidic or halogenated liquids or compounds that may act as oxidizing agents.
b) Pre-dry first with ordinary agents (Na_2SO_4, e.g.) before using powerful drying agents (Na, CaH, $LiAlH_4$, H_2SO_4 or P_2O_5).
c) First test for and destroy peroxides in ethers or other solvents before distillation and/or drying.
d) Most solvents are toxic; avoid inhalation of vapours. Also avoid flames.
e) Highly purified solvents must be stored in a sealed container under inert atmosphere.

[1] A.J. Gordon and R.A. Ford, *The Chemist Companion: A Handbook of Practical Data, Techniques and References, John Wiley and Sons, New York*, (1972).

Appendix C

Acetone

Acetone reacts with most of the usual drying agents ($MgSO_4$) and this makes it difficult dry. The analytical pure acetone was saturated with dry NaI at 25-30 °C. The solution was decanted and cooled to -10 °C. The resulting crystals of the NaI complex that formed was filtered and heated to 30 °C. The resulting liquid was finally distilled.

Acetonitrile

Analytical grade acetonitrile was pre-dried and stirred with CaH until gas evolution ceased. The solution was distilled from P_2O_5 in an all glass apparatus. The distillate was refluxed over CaH for 1 hour and then distilled slowly, discarding the first 5 and last 10% of the distillate.

Chloroform

Most analytical grade chloroform contains about 1 % ethanol to stabilize air oxidation to phosgene. Purification can be done by the following procedures followed by storage under N_2 atmosphere in the dark.

a) The solvent was shaking with concentrated H_2SO_4, washed with water, dried over $CaCl_2$ or K_2CO_3 and finally distilled.
b) The solvent can also be passed through a column of Grade I activated alumina (25 g/500 ml $CHCl_3$).
c) Finally the solvent can be shaking several times with one-half its volume of water, dried with $CaCl_2$ and then distilled from P_2O_5.

Ethyl Acetate

Water, ethanol and acid impurities were removed by washing the solvent with 5% aqueous sodium carbonate. The resulting solution was then saturated with $CaCl_2$, dried over anhydrous potassium carbonate and finally distilled from P_2O_5.

Appendix D

Theoretical aspect of kinetics

Reaction kinetics is the study of the rate of a chemical reaction as well as the mechanism by which it takes place. Various factors influence the rate of the reaction like, concentration of the reagents and products, temperature and the reaction medium (solvent). The results obtained give insight into the type of mechanism by which the reaction takes place.

Rate law and rate constants[1]

The rate of a reaction is defined by the rate by which the concentration of any of the reagents involved changes.

$$A + B \longrightarrow C \qquad \textbf{1}$$

The rate of the reaction can be expressed in terms of the disappearance of A or B or the formation of C.

$$Rate = -\frac{d[A]}{dt} = -\frac{d[B]}{dt} = \frac{d[C]}{dt} \qquad \textbf{2}$$

The rate of **Equation 1** can be given in terms of A and B. A typical rate law for the reaction is given in **Equation 3.**

$$\text{Rate} = k[A]^a[B]^b \qquad \textbf{3}$$

k = rate constant, a and b = order of reaction with regards to [A] and [B]

[1] R.G. Wilkins, *The study of kinetics and mechanism of reactions of transition metal complexes*., Allyn and Bacon Incorporated: Boston, 1974.

Appendix D

Pseudo-first-order reactions[2]

The chemical reaction in **Equation 4** can be illustrated by the second-order rate law in **Equation 5**.

$$A + B \xrightarrow{k} C \qquad \textbf{4}$$

$$R = k[A][B] \qquad \textbf{5}$$

The rate law can be simplified by increasing the concentration of one of the reagents. If it is found that the reaction is first-order with regards to the reagents with the lowest concentration, then the reaction proceeds under pseudo-first-order conditions. If the [B] >> [A], then the [B] is constant during the reaction and the rate law can be simplified to the following (Equation 6):

$$R = k_{obs}[A] \qquad \textbf{6}$$

where

$$k_{obs} = k[B] \qquad \textbf{7}$$

k_{obs} is the observed pseudo-first-order rate constant for the reaction. The value of k_{obs} is calculated at different concentrations. The graph of k_{obs} against [B] will be linear with gradient equal to k and the intercept equal to zero if the reaction is first-order in [B]. If the graph shows a non-zero intercept, there can be a second reaction taking place that is independent of [B]. This can be illustrated by **Equation 8**:

$$k_{obs} = k_1[B] + k_2 \qquad \textbf{8}$$

The intercept of the graph represents the value of k_2

[2] S.W. Benson, *The foundation of chemical kinetics*., McGraw-Hill book company: New York, 1960.

Mathematical derivation of Equation 5.5 in Chapter 5

Consider the following reaction, a very important reaction in chemistry:[3]

$$A + B \underset{k_{-1}}{\overset{K_1,\, k_1}{\rightleftharpoons}} C \xrightarrow{k_2} D \qquad \textbf{9}$$

The first reaction (formation of C) is very fast so that the equilibrium is kept the whole time during the reaction between the reagents A and B and the product C. The equilibrium constant, K_1, is presented by the following:

$$K_1 = \frac{k_1}{k_{-1}} = \frac{[C]}{[A][B]} \qquad \textbf{10}$$

The reaction is followed by the disappearance of both A and C or the formation of D.

$$\frac{d[D]}{dt} = k([A]+[C]) = k_2[C] \qquad \textbf{11}$$

With substitution of [C] from **Equation 10**:

$$k_{obs} = \frac{k_2 K_1 [A][B]}{[A]+[C]} \qquad \textbf{12}$$

With substitution of [A] from **Equation 10**:

$$k_{obs} = \frac{k_2 K_1 [A][B]}{\frac{[C]}{K_1[B]}+[C]} = \frac{[A]k_2 K_1 [B]}{[C]\left[\frac{1}{K_1[B]}+1\right]} \qquad \textbf{13}$$

[3] F.M. Beringer and E.M Findler, *J. Am. Chem. Soc*. **77**, (1955), 3200.

Further, from **Equation 10** $\frac{[A]}{[C]} = \frac{1}{K_1[B]}$

$$k_{obs} = \frac{k_2 K_1[B]}{1 + K_1[B]} \quad \textbf{14}$$

Equation 14 is the rate law for the saturation kinetics and gives a hyperbola for k_{obs} against [B]. At low concentrations of B, **Equation 14** simplifies to:

$$k_{obs} = k_2 K_1[B] \quad \textbf{15}$$

The graph of for k_{obs} against [B] is linear with a zero intercept and gradient k_2K_1

At high concentrations of B, **Equation 14** simplifies to:

$$k_{obs} = k_2 \quad \textbf{16}$$

The graph of for k_{obs} against [B] is linear with a zero gradient.

Mathematical derivation of Equation 5.10 in Chapter 5

Consider the following reaction:

$$A + B \underset{k_{-1}}{\overset{k_1, K_1}{\rightleftharpoons}} C \xrightarrow{k_2} D \xrightarrow{k_3} E \quad \textbf{17}$$

The first reaction (formation of C) is very fast so that the equilibrium is kept the whole time during the reaction between the reagents A and B and the product C.

The rate law for the formation of D can be presented by the following:

$$\frac{d[D]}{dt} = k_2[C] - k_3[E] \quad \textbf{18}$$

The rate law formation of C can be presented by the following:

$$\frac{d[C]}{dt} = k_1[A][B] - k_{-1}[C] \quad \textbf{19}$$

Equation 19 simplifies to:

$$[C] = \frac{k_1}{k_{-1}}[A][B] = K[A][B] \quad \textbf{20}$$

Substitution of **Equation 20** in **Equation 18**

$$\frac{d[D]}{dt} = k_2K[A][B] - k_3[E] \quad \textbf{21}$$

Under pseudo-first-order conditions and integration:

$$k_{obs} = k_2K[B] + k_3 \quad \textbf{22}$$

If the reaction is independent of [B]:

$$k_{obs} = k_3 \quad \textbf{23}$$

Mathematical derivation of Equation 5.12 in Chapter 5

Consider the following equilibrium reaction:

$$A + B \underset{k_{-1}}{\overset{k_1}{\rightleftharpoons}} C \quad \textbf{24}$$

Appendix D

The reaction rate can be illustrated as follows:

$$\frac{-d[A]}{dt} = k_1[A][B] + k_{-1}[C] \qquad \textbf{25}$$

If the reaction proceeds under pseudo-first-order conditions ([B] >> [A]) the quantity of k_1[B] can be considered as a constant k_1. From this assumption **Equation 25** simplifies to:

$$\frac{-d[A]}{dt} = k_1[A] + k_{-1}[C] \qquad \textbf{26}$$

The sum of the rate constants k_1 and k_{-1} is given by k_{obs}.

$$k_{obs} = k_1 + k_{-1} \qquad \textbf{27}$$

Under pseudo-first-order conditions **Equation 26** simplifies to:

$$k_{obs} = k_1[B] + k_{-1} \qquad \textbf{28}$$

A graph of k_{obs} against [CH3I] will give a straight line with gradient k_1 and intercept k_{-1}.

Activation parameters, ΔH* and ΔS*[1]

The activation parameters, ΔH* and ΔS*, can be determined from the relationship between the physical characteristics like temperature and the reaction rate. Calculations of the activation parameters from kinetic results give insight about the type of mechanism for a specific reaction. Values of ΔH* does not give must insight about the mechanism of a reaction while values obtained for ΔS* will give much more insight about the type of mechanism.

Negative values for ΔS* suggest a associative (bond formation) mechanism while positive values suggest a dissociative (bond breaking) mechanism. The activation parameters are calculated by the transition state theory.[4] The transition state theory postulates that the transition state (AB)*, is in equilibrium with the reagents A and B and that the reaction rate observed is the dissociation of the transition state.

$$A + B \underset{}{\overset{K^*}{\rightleftharpoons}} (AB)^* \xrightarrow{k^*} \text{Product} \qquad \textbf{29}$$

where K* = equilibrium constant

For **Equation 29**:

$$K^* = \frac{[(AB)^*]}{[A][B]} \qquad \textbf{30}$$

$$k = K^* k^* \qquad \textbf{31}$$

Eyering[4] showed that the rate constant, k*, can be given by **Equation 32**.

$$k^* = \frac{k_b T}{h} \qquad \textbf{32}$$

where k_b = Boltzman constant

h = Planck constant

T = temperature in Kelvin

Substitution of **Equation 32** into **Equation 31**

$$k = \left[\frac{k_b T}{h}\right] K^* \qquad \textbf{33}$$

[4] H. Eyering, *J. Chem. Phys*., **3**, (1953), 107.

Appendix D

From thermodynamic principles, can the Gibbs free energy of activation, ΔG*, be given by **Equation 34**.

$$\Delta G^* = -RT\ln K^* \qquad \textbf{34}$$

where R = universal gas constant

ΔG* can also be expressed by the activation enthalpy and entropy.

$$\Delta G^* = \Delta H^* - T\Delta S^* \qquad \textbf{35}$$

From **Equation 32** and **Equation 33**.

$$K^* = e^{\left[\frac{-\Delta H^*}{RT}+\frac{\Delta S^*}{R}\right]} \qquad \textbf{36}$$

Substitution of **Equation 36** into **Equation 33**.

$$k = \frac{k_b T}{h} e^{\left[\frac{-\Delta H^*}{RT}+\frac{\Delta S^*}{R}\right]} \qquad \textbf{37}$$

With rearrangement of **Equation 37**.

$$\ln\left(\frac{k}{T}\right) = \ln\left(\frac{k_b}{h}\right) + \frac{\Delta S^*}{R} - \frac{\Delta H^*}{RT} \qquad \textbf{38}$$

Values for ΔH* and ΔS* can be determined experimentally from a graph of $\ln\frac{k}{T}$ against $\frac{1}{T}$. The value for ΔH* can be calculated from the gradient $\left(-\frac{\Delta H^*}{R}\right)$ and ΔS* from the intercept $\left(\ln\left(\frac{k_b}{h}\right)+\frac{\Delta S^*}{R}\right)$.

Appendix E

Kinetic Data

Tables in this section give the k_{obs} values for the pseudo-first-order rate constants for the oxidative addition and CO-insertion reactions described in **Chapter 5**.

Table 1: UV/visible kinetic data for the [CH_3I] dependence for the rate constant for the formation of [Rh(cupf)(CH3)(CO)(DPP)(I)] in acetonitrile at different temperatures and 420 nm ([Rh(I)] = 2.5×10^{-4} M).

Temperature (°C)	[CH_3I] (M)	10^3 k_{obs} (s^{-1})
10.1	0.1012	0.46(5)
	0.3021	1.05(5)
	0.5011	1.34(5)
	0.7013	1.58(5)
	1.016	1.78(5)
19.8	0.1012	0.76(1)
	0.3021	2.28(2)
	0.5011	3.62(2)
	0.7013	4.61(4)
	1.016	5.72(5)
25.0	0.1012	2.20(5)
	0.3021	4.20(5)
	0.5011	6.30(2)
	0.7013	7.51(2)
	1.016	9.40(4)

Table 2: IR kinetic data for the rate constant for the formation of [Rh(cupf)(CH3)(CO)(DPP)(I)] in acetonitrile at different temperatures and 1980 nm ([Rh(I)] = 2.5×10^{-2} M, [CH_3I] = 0.2 M).

Temperature (°C)	10^3 k_{obs} (s^{-1})
10.1	1.43(4)
19.8	1.70(5)
25.0	2.98(1)

Appendix E

Table 3: UV/visible kinetic data for the [CH_3I] dependence for the rate constant for the formation of [Rh(cupf)(CH3)(CO)(DPP)(I)] in acetone at different temperatures and 380 nm ([Rh(I)] = $2.5x10^{-4}$ M).

Temperature (°C)	**[CH_3I] (M)**	**10^3 k_{obs} (s^{-1})**
10.1	0.1012	0.27(6)
	0.3021	0.57(5)
	0.5011	0.83(5)
	0.7013	1.05(5)
	1.016	1.30(5)
19.8	0.1012	0.71(6)
	0.3021	1.64(5)
	0.5011	2.34(1)
	0.7013	2.92(2)
	1.016	3.51(3)
25.0	0.1012	0.89(3)
	0.3021	2.52(8)
	0.5011	3.67(2)
	0.7013	4.66(4)
	1.016	5.89(6)

Table 4: IR kinetic data for the [CH_3I] dependence for the rate constant for the formation of [Rh(cupf)(CH3)(CO)(DPP)(I)] in acetone at 25°C and 1980 nm ([Rh(I)] = $2.5x10^{-2}$ M).

[CH_3I] (M)	**10^3 k_{obs} (s^{-1})**
0.1012	1.57(6)
0.3021	3.17(6)
0.5011	4.25(5)
0.7013	5.07(5)
1.016	6.71(5)

Table 5: UV/visible kinetic data for the [CH_3I] dependence for the rate constant for the formation of [Rh(cupf)(CH3)(CO)(DPP)(I)] in chloroform at different temperatures and 380 nm ([Rh(I)] = $2.5x10^{-4}$ M).

Temperature (°C)	**[CH_3I] (M)**	**10^3 k_{obs} (s^{-1})**
10.1	0.1012	0.47(1)
	0.3021	0.75(3)
	0.5011	1.07(7)
	0.7013	1.27(9)
	1.016	1.73(2)
19.8	0.1012	1.27(6)
	0.3021	2.10(2)
	0.5011	3.06(3)
	0.7013	3.45(4)
	1.016	3.61(6)
25.0	0.1012	1.97(9)
	0.3021	3.47(4)
	0.5011	4.92(7)
	0.7013	5.82(9)
	1.016	6.22(1)

Table 6: IR kinetic data for the [CH_3I] dependence for the rate constant for the formation of [Rh(cupf)(CH3)(CO)(DPP)(I)] in chloroform at 25°C and 1980 nm ([Rh(I)] = $2.5x10^{-2}$ M).

[CH_3I] (M)	**10^3 k_{obs} (s^{-1})**
0.1012	1.47(1)
0.3021	2.51(7)
0.5011	5.16(1)
0.7013	7.61(2)
1.016	9.58(2)

Appendix E

Table 7: UV/visible kinetic data for the [CH_3I] dependence for the rate constant for the formation of [Rh(cupf)(CH3)(CO)(DPP)(I)] in ethyl acetate at different temperatures and 380 nm ([Rh(I)] = $2.5x10^{-4}$ M).

Temperature (°C)	**[CH_3I] (M)**	**10^3 k_{obs} (s^{-1})**
10.1	0.1012	0.044(1)
	0.3021	0.15(5)
	0.5011	0.23(2)
	0.7013	0.27(4)
	1.016	0.37(7)
19.8	0.1012	0.079(4)
	0.3021	0.25(1)
	0.5011	0.47(2)
	0.7013	0.72(5)
	1.016	0.99(2)
25.0	0.1012	0.22(1)
	0.3021	0.46(8)
	0.5011	0.73(3)
	0.7013	0.80(7)
	1.016	0.94(1)

Table 8: IR kinetic data for the [CH_3I] dependence for the rate constant for the formation of [Rh(cupf)(CH3)(CO)(DPP)(I)] in ethyl acetate at 25°C and 1980 nm ([Rh(I)] = $2.5x10^{-2}$ M).

[CH_3I] (M)	**10^3 k_{obs} (s^{-1})**
0.1012	0.14(2)
0.3021	0.31(2)
0.5011	0.48(3)
0.7013	0.67(5)
1.016	0.71(3)